Frustrated Magnets: A Monte Carlo Study of Stiffness, Vorticity and Topological Excitations

by

Amra Peles, B.Sc., M.Sc.

A Thesis
Submitted to the Faculty of Graduate Studies
in Partial Fulfillment of the Requirements
for the Degree of

DOCTOR OF PHILOSOPHY

Department of Physics and Astronomy
University of Manitoba
Winnipeg, Manitoba

THE UNIVERSITY OF MANITOBA

FACULTY OF GRADUATE STUDIES

*****

COPYRIGHT PERMISSION

Frustrated Magnets: A Monte Carlo Study of Stiffness, Vorticity and Topological Excitations

BY

Amra Peles, B.Sc., M.Sc.

A Thesis/Practicum submitted to the Faculty of Graduate Studies of The University of Manitoba in partial fulfillment of the requirement of the degree

Of

DOCTOR OF PHILOSOPHY

TABLE OF CONTENTS

LIST OF FIGURES

LIST OF TABLES

GLOSSARY

- **STA** Antiferromagnetic spin model with continuous symmetry defined on a stacked triangular (simple hexagonal) lattice. This model is geometrically frustrated.

- **STAR** STA model with an additional constraint that the vector sum of the spins on disconnected plaquettes is rigidly set to zero.

- **XY model** Classical model for vectors with O(2) symmetry where spin degrees of freedom are constrained to lie in the plane.

- **Ising model** Discrete model of one dimensional vectors. Spin 1/2 model has Z_2 symmetry.

- **O(n) symmetry** Symmetry exhibited by vectors on the surface of the unit sphere in n dimensions. Physical realizations include the vectors of the Heisenberg model O(3) and the vectors of the XY model O(2).

- **NLσ** Non-linear sigma model: perturbative renormalization group approach to O(n) model in $d = 2 + \epsilon$ dimensions involving a low temperature expansion.

- **LGW** Landau-Ginzburg-Wilson coarse grained Hamiltonian in terms of continuous spin variables.

- **KT transition** Kosterlitz-Thouless vortex unbinding phase transition in $2d$ XY spin model from a phase with non-zero rigidity (spin stiffness) characterized by

power law decaying correlations to the phase with zero rigidity and exponentially decaying correlations.

- $\mathbf{Z_2}$ Discrete group symmetry consisting of only two elements.

- **homotopy** Explicit construction of a continuous deformation between two homotopic mappings. Specifying the order parameter along a contour in real space (lattice) determines a mapping of that contour into the order parameter space. Two such mappings are homotopic if they can be continuously changed from one to the other.

- **homotopy group** Defects are in the same homotopy class if all contours enclosing them are homotopic, i.e. can be continuously changed from one to another. The group associated with a particular homotopy class and used to classify different types of defects is called a homotopy group.

- **order parameter space V** The space consisting of all possible realizations of an order parameter

- $\mathbf{S_{n-1}}$ describes the order parameter space of models with O(n) symmetry. In the O(2) case it is a unit circle S_1 and in the O(3) case it is a unit sphere S_2.

- **FSS** Finite size scaling theory.

- **RG** Renormalization group is a transformation involving a coarse graining of the degrees of freedom preserving the important symmetries of the problem.

- **NPRG** Non perturbative renormalization group approach based on the concept of block spins.

- **n-vector model** The model in which the order parameter is an n dimensional vector.

- **universality class** Systems whose properties at a second order phase transition are controlled by the same renormalization group fixed point are in the same universality class. The universality class is typically determined by the spatial dimension, the symmetry of the order parameter and the range of the interaction potential.

- **SO(3)** Special orthogonal group of rotations in $3d$.

- $\mathbf{P_3(SO(3))}$ Order parameter space of the order parameter with SO(3) symmetry. It represents a unit sphere with the two antipodal points identified.

ACKNOWLEDGMENTS

I wish to express my deepest appreciation to my advisor, Dr. Byron Southern for his permanent guidance, counsel and support during the course of this work. As well, I would like to thank my committee members, Dr. R. Roshko, Dr. G. Tabisz and Dr. G. Bridges of the University of Manitoba and Dr. B. Gaulin of McMaster University. I want to thank the Head of our department Dr. G. Williams for his continued support and encouragement. I wish to thank our collaborators, Dr. M. Tissier of Université Paris Sud and Dr. B. Delamotte and Dr. D. Mouhanna of Université Paris VI, for fruitful collaborations and many useful discussions and advice. I would like to thank Dr. Mei Yin Chou of Georgia Institute of Technology for the hospitality and providing me with a dynamic and stimulating working environment. I also thank Dr. S. Bekhechi and Dr. A. Alford for useful comments and advice. I would like to thank our secretaries Wanda Klassen and Marilyn Shantz their help and assistance. I thank Ivor for insightful astounding comments and most importantly I thank Slaven for endless support and love. I am truly thankful to my family and friends for their support, acceptance, encouragement and humour. I would also like to acknowledge support from the National Science and Engineering Research Council of Canada (NSERC) graduate scholarship support, the University of Manitoba graduate fellowship support and the Dean of Graduate studies and the Dean of Science graduate scholarship support. I also acknowledge the high performance computational facilities at the University of Manitoba and at Queen's University.

ABSTRACT

The role of topological excitations in frustrated Heisenberg antiferromagnets between two and three spatial dimensions is studied as well as the controversial issue of the order of the phase transition of Heisenberg and XY frustrated antiferromagnets in $3d$. The antiferromagnetic Heisenberg model on a stacked triangular geometry with a finite number of layers is studied using Monte Carlo methods. The symmetry of the ordered phase of this model admits the existence of the same type of topological defect as in the superfluid B phase of He^3. A phase transition which is purely topological in nature occurs at finite temperature for all film thicknesses. The results indicate that topological excitations are important for a complete understanding of the critical properties of the model between two and and three dimensions. The rigidity properties of the stacked triangular Heisenberg antiferromagnet are studied in $3d$ using both a heat bath and a broad histogram Monte Carlo method. The results are consistent with a continuous transition and a direct estimate of the correlation length critical exponent ν from the spin stiffness yields the value $\nu = 0.59$ in agreement with a newly proposed 'chiral' universality class. A generalized model for the XY antiferromagnet is introduced and studied in $3d$ using heat bath Monte Carlo methods. The model can be continuously tuned from a region of first order transitions to the usual XY model without changing its symmetry properties. The results unambiguously show that the phase transition in XY frustrated antiferromagnets in $3d$ is weakly first order. Further work is needed in $3d$ to clarify the order of the transition in the Heisenberg case and the role played by topological excitations.

Chapter 1

INTRODUCTION AND OVERVIEW

1.1 Frustrated Magnets

Magnetic systems exhibit various types of ordering depending upon the temperature T and external magnetic field H. The ordered state at low temperatures is usually described in terms of an **order parameter**. In systems which favour parallel alignment (**ferromagnetic**) of the magnetic moments, or spins, the ordered state can be described in terms of a **vector** which is fixed in direction and whose magnitude varies with temperature. This vector is the total magnetization of the system. Other systems have no net magnetization but are ordered such that neighbouring spins are anti-parallel (**anti-ferromagnetic**). Here again some direction in spin space is selected in the ordered phase and the order parameter is one of the two sub-lattice magnetization vectors that are anti-parallel. In general, the interactions between spins are not completely isotropic and the anisotropies can favour either preferred crystalline axes or planes. Thus in general, the order parameter is a vector with a variable number of components n. Three simple models used to describe ferromagnetic systems are the Ising model($n = 1$), the planar or XY model($n = 2$) and the Heisenberg model($n = 3$). The *order parameter is an n-component vector* and the critical behaviour of these systems can be classified into universality classes[64] according to the value of n and the spatial dimension d. This is the $O(n)$ model.

However, the behaviour of antiferromagnetic models can also depend upon the detailed lattice geometry. An example of a lattice which does not accomodate both

ferromagnetic and anti-ferromagnetic ordering is the triangular lattice in $d = 2$. The three spins on each elementary triangle can all be parallel but they cannot all be anti-parallel and the system is said to be **frustrated**. The spin $\frac{1}{2}$ Ising model ($n = 1$) is completely frustrated and has a non-zero entropy at zero temperature whereas both the XY ($n = 2$) and the Heisenberg ($n = 3$) models have a unique, but non-collinear, ground state. This non-collinear ground state has the three spins oriented in a plane at an angle of 120^0 to one another and requires *more than one vector* to describe it. Thus frustration can change the symmetry of the order parameter and hence the nature of the phase transition.

The low energy excitations in the low temperature ordered phases of these systems correspond to long wavelength deformations, or twists, of the order parameter in spin space. Such twists cost energy and the ordered phase exhibits a **stiffness** to their excitation in much the same way that an elastic solid resists deformations. As the temperature increases, the stiffness can disappear and the system disorders. If the spatial dimension d is low enough, then these excitations can in fact destroy the ordered phase at all finite temperatures.

In addition to these long wavelength deformations, the ordered system can also have other types of excitations. These excitations are **defects** which can take the form of points, lines or walls. The form depends upon the symmetry of the order parameter. For example, in the Ising model($n = 1$) , the order parameter is a scalar. There is only a discrete symmetry and continuous deformations do not exist. The low energy excitations are domain walls separating regions of opposite spin orientations. The free energy cost associated with these defects can vanish as the temperature increases due to the competition between energy and entropy and the ordered phase will be destroyed. The $d = 2$ ferromagnetic XY model($n = 2$) is another example where defects destroy order. In this latter case the defects are vortex excitations which exist as bound pairs at low temperatures but unbind at a well defined critical temperature referred to as the Kosterlitz-Thouless transition. The low temperature

phase does not have a non-zero magnetization but the spin-spin correlations decay algebraically in this phase. In the high temperature phase they decay exponentially. There is a stiffness against free vortex excitations at low temperatures which vanishes in the high temperature phase and the phase transition corresponds to a melting of defects.

It is of great importance in condensed matter theory/ statistical mechanics to clarify the role of topological defects on the thermodynamic behaviour of frustrated magnetic systems. This is a very difficult problem from the theoretical viewpoint due to (i) the intrinsic nonlinearity of the problem even in the absence of defects and also (ii) the non-separable nature of the defect/spin wave interactions. For this reason, renormalization group treatments of the Landau-Ginzburg-Wilson (LGW) model near $d = 4$ and the nonlinear sigma model (NLσ) near $d = 2$ have generally neglected the contributions from topological defects. The primary aim of this research is to understand the role of such excitations in frustrated magnets. The results could also have important implications for superfluids, type II superconductors and smectic-A liquid crystals.

1.2 Recent Studies in $d = 2$

The classical Heisenberg model on the two dimensional triangular lattice with antiferromagnetic nearest neighbour coupling is the simplest model of a geometrically frustrated system with a noncollinear order parameter. Kawamura and Miyashita[1, ?] have studied the possibility of a Kosterlitz-Thouless[29, 30] type of transition in this system using Monte Carlo methods and obtained evidence for a finite temperature transition driven by the dissociation of vortices. However, a transition at finite temperature is considered by many to be unlikely for the Heisenberg model in two dimensions. Dombre and Read[21] mapped the continuum version of the model onto a non-linear sigma model (NLσ) and Azaria et. al.[31, 32, 7] used renormalization

group (RG) techniques to study the correlation length and effective long-wavelength spin stiffness of this NLσ at low temperatures. Their results were consistent with a phase transition at $T_c = 0$ with an enlarged SO(3) symmetry. Indeed, Monte Carlo simulations by Southern and Young[34] of the spin stiffness seemed to provide partial support for this picture. In subsequent work, Southern and Xu[2] calculated the rigidity of the isotropic system against the formation of free vortices at low temperatures. The vorticity stiffness was found to be finite at low T and disappeared abruptly near $T = 0.31J$. This behaviour is consistent with a possible Kosterlitz-Thouless defect unbinding transition. It appears that the stiffness and vorticity behave quite differently in the isotropic model. The stiffness is zero on long length scales indicating that the two-spin correlations decay exponentially at all finite T. However, the vorticity indicates that an unbinding of topological defects occurs at a finite T_c.

In order to further clarify the role of defects in this system, Stephan and Southern [3] studied the classical Heisenberg model with an easy axis exchange anisotropy. This model has a nontrivial degeneracy due to frustration. At zero temperature the spins lie in a plane which contains the easy z-axis. In addition to the S_1 degeneracy related to the rotation of this plane about the z-axis, there is also a non-trivial S_1 degeneracy of the ground state related to rotations of the spins within the plane. The planar spin configuration distorts as it is rotated about an axis normal to the plane but the energy remains constant. The Monte Carlo results displayed strong evidence for the occurence of two distinct Kosterlitz-Thouless types of defect-mediated phase transitions in this model. The rigidity of the system against both spin wave deformations and the formation of free vortices at low temperatures for several values of the easy axis anisotropy was calculated. In each case a universal value of the stiffness or vorticity modulus, $\rho_c/T_c = v_c/T_c = 2/\pi$, was found. In addition, the spin correlation length exponent had the universal value $\eta = 1/4$. These are the same values that are predicted by the Kosterlitz-Thouless theory for defect unbinding transitions in two dimensions. It was found that the spin stiffnesses and the corresponding vor-

ticity moduli behaved identically for the easy axis case. In contrast, at the isotropic Heisenberg limit, the spin stiffness vanishes at large length scales whereas the vorticity moduli are non-zero at low T and vanish abruptly at a finite temperature.

Previous work on the XY model [35] also indicated that the vorticity and stiffness behave identically in the case where the transition is of the Kosterlitz-Thouless type. The frustrated XY model displays two closely spaced transitions with the upper transition involving chiral degrees of freedom and the lower one involving vortices. Recent work by Capriotti et. al. [36] has also found similar behaviour in the easy plane exchange anisotropy case. The structure of the phase diagram suggests that the Heisenberg point is a multicritical point where possibly four phase transition lines meet.[4] The behaviour of these transition lines as the Heisenberg point is approached from both sides strongly suggests that there is a finite temperature phase transition in the Heisenberg model . Since the spin stiffness is zero at large length scales for all finite temperatures in this limit, the spin correlations decay exponentially. Thus the transition would be quite different from the KT transition where spin correlations acquire a power law decay with a temperature dependent exponent. The transition at the Heisenberg point would be purely topological in character. Further theoretical investigations of this possibility are desirable as well as of the more general question about the role that topological defects play in the chiral and spin ordering of three dimensional frustrated systems.

1.3 Overview of thesis

At the present time there is a great deal of debate about the critical properties of three dimensional systems with noncollinear order.[12, 16] These systems[38] can be of the stacked triangular type where short range antiferromagnetic couplings lead to frustration or of the rare earth type where long ranged oscillating interactions lead to spiral orderings. In both cases, the order is also accompanied by the appearance

of a chiral degree of freedom. These systems have been studied both experimentally as well as theoretically. Experiments are consistent with a second order transition belonging to a new chiral universality class. Some Monte Carlo calculations support this view but others favour a first order transition. Field theoretical methods also seem to be in disagreement. Low order perturbative schemes[13] predict a first order transition in three dimensions for both the XY and Heisenberg models. However, recent calculations to higher order[53] find a stable chiral fixed point with exponents close to those found experimentally and in the Monte Carlo simulations.

In the present work a study of frustrated magnets is carried out using Monte Carlo simulation methods to investigate the role of topological defects in frustrated magnetic models and related systems. Attention is focused on the spin stiffness whose scaling behaviour will yield the correlation exponent ν directly whereas other thermodynamic response functions yield ratios of exponents to ν.

The organization of the thesis is as follows. A brief review of some of the important ideas of statistical mechanics and phase transitions are given in Chapter 2. The roles of symmetry and defects on the critical properties of simple models are described. Response functions, such as stiffness and vorticity, which measure the rigidity of a system to defect structures are also introduced. Chapter 3 describes the numerical methods used in our studies. The methods of analysis using finite size scaling techniques are also described. Frustrated models and the effects of both geometry and dimension are described in Chapter 4. The role that symmetries play in determining the nature of excitations is also discussed. The results of both experimental and various theoretical investigations are described and summarized. In Chapter 5, the results of a study of the crossover from $d = 2$ to $d = 3$ are presented. The role played by topological excitations are investigated as the number of layers of a stacked triangular geometry is increased. Chapter 6 describes the results of a study of a the $3d$ stacked triangular geometry. The spin stiffness is calculated using two different Monte Carlo techniques. Chapter 7 presents results for an XY model with an additional constraint

which allows us to tune the system continuously from a first order to second order transition. A summary and possible future directions are given in Chapter 8.

Chapter 2

PHASE TRANSITIONS, DEFECTS AND RIGIDITY

In this chapter we give a general overview of some of the elementary concepts of statistical mechanics, critical phenomena and the role played by defects.

2.1 Review of statistical mechanics

Statistical mechanics establishes a connection between a macroscopic description of the thermodynamic properties of a system, usually expressed in terms of thermodynamic potentials, and the microscopic properties which are described by a Hamiltonian. There are various approaches to establishing this connection which involve different distributions at fixed energy, temperature or chemical potential. A convenient distribution is the canonical, or Boltzmann, distribution which is characterized by a fixed value of the temperature T. The Boltzmann distribution law states that the probability of the occurence of individual microscopic states with energy E in contact with a heat reservoir at a given temperature T is proportional to $e^{-\beta E}$, where $\beta = 1/k_B T$, and k_B is the Boltzmann constant. A microscopic state of a system consisting of a large number of particles ($10^{23} \sim 10^{24}$) can be described as point in an abstract space called a phase space. For a magnetic system this description involves all degrees of freedom of all magnetic moments (spins) making up a system. The state (point in phase space) i with energy E_i has a probability

$$P_i = \frac{e^{-\beta E_i}}{\sum_i e^{-\beta E_i}} \tag{2.1}$$

where P_i is normalized such that $\sum_i P_i = 1$. The denominator above is called the partition function of the system and is expressed as

$$Z(T) = \sum_i e^{-\beta E_i} \tag{2.2}$$

where the sum runs over all possible microstates of the system (all possible points in phase space). Calculating $Z(T)$ is the central problem of statistical mechanics.

The thermodynamic potential corresponding to the canonical ensemble is the Helmholtz free energy

$$F = E - TS \tag{2.3}$$

where E is the internal energy and S is the entropy. F is related to the partition function as follows

$$F = -k_B T \ln Z. \tag{2.4}$$

This connection of the partition function Z and the thermodynamic potential F allows all macroscopic thermodynamic quantities to be expressed as derivatives of Z. Various responses of the system to external influences such as changes in temperature or magnetic field can be calculated from Z. The internal energy and the specific heat C_V are expressed in terms of the partition function as follows

$$\begin{aligned} E &= -\frac{\partial}{\partial \beta}(\ln Z) \\ C_V &= -k_B \beta^2 \frac{\partial E}{\partial \beta} \mid_V = k_B \beta^2 \frac{\partial^2}{\partial \beta^2}(\ln Z) \mid_V . \end{aligned} \tag{2.5}$$

The magnetization M_h in the direction of an applied field h and the magnetic susceptibility χ are given by

$$\begin{aligned} M_h &= \frac{1}{\beta}\frac{\partial}{\partial h}(\ln Z) \mid_T \\ \chi &= \frac{\partial M_h}{\partial h} \mid_T = \frac{1}{\beta}\frac{\partial^2}{\partial h^2}(\ln Z) \mid_T . \end{aligned} \tag{2.6}$$

In addition to these well known response functions, we will also consider the response of the system due to a deformation of the order parameter which is characterized

by a twist angle Θ. This is the spin stiffness ρ and it can be obtained as a second derivative of the free energy with respect to the twist angle Θ in the limit when Θ tends to zero.

$$\rho = \frac{\partial^2 F}{\partial \Theta^2} \mid_{\Theta=0} = -\frac{1}{\beta Z}\left[\frac{\partial^2 Z}{\partial \Theta^2} - \frac{1}{Z}\left(\frac{\partial Z}{\partial \Theta}\right)^2\right] \mid_{\Theta=0} \tag{2.7}$$

This response function and another closely related response function called the vorticity will be discussed in more detail later in this chapter.

2.2 Spontaneous symmetry breaking

A model system possesses a symmetry if the Hamiltonian describing that system is invariant under a set of transformations that form a symmetry group. This symmetry group can be discrete or continuous. Discrete symmetry groups have a countable number of elements. The spin 1/2 Ising model is an example of a system with a discrete symmetry described the by two element group Z_2. The continuous groups have an uncountable continuum of elements. An example of such a group is the orthogonal group of rotations $O(n)$, where $n = 2$ is the symmetry group of the XY spin model and $n = 3$ is the group of the Heisenberg model Hamiltonian. These models possess a global symmetry, i.e., the systems are invariant under a uniform rotation applied globally to the entire system.

The majority of real physical systems with many-body interactions tend to have a lowest energy state that does not have the same symmetry properties of space or, in the case of Hamiltonian systems, of the Hamiltonian describing their interactions [18]. There are a vast variety of ordered and disordered systems in nature. Disordered states are entropy-dominated and usually have the same symmetry properties as a Hamiltonian itself, i.e., their symmetry is described by the same symmetry group. Ordered states do not have the full symmetry of the Hamiltonian but they may be invariant under a subgroup of the symmetry group of the Hamiltonian or have none of the Hamiltonian's symmetry. The tendency of systems to change from a state

of full symmetry to state of a lower symmetry is called **spontaneous symmetry breaking** and it is ubiquitous in nature. The most important consequences of a broken symmetry are summarized below [39].

- Occurrence of a **phase transition**. The free energy exhibits non-analytic behaviour at some temperature called the critical temperatute T_c.

- Appearance of a **rigidity**. Any attempt to change the way a system has broken its symmetry results in a resistance since the system prefers to stay in the low energy broken-symmetry state.

- A perfectly ordered zero temperature state is weakened by **excitations** of the order parameter at finite temperatures. In magnetic systems these exitations are called spin waves.

- The breaking of symmetry can happen differently in two adjacent parts of a macroscopic sample. This results in appearance of **defects** at the interface between these regions. A simple example is domain wall structures in magnetic media.

2.3 Phase transitions

Phase transitions accompanied by a spontaneous symmetry breaking are central issues in modern statistical as well as in condensed matter physics. A system in which the macroscopic properties change abruptly with a continuous change of the thermodynamic parameters, such as temperature or external field, undergoes a phase transition. A change of one phase of matter to another can be discontinuous with the coexistence of both phases at the critical point or continuous with a unique phase at the critical point. These are called phase transitions of first and second order respectively. At

a first order transition, first derivatives of the free energy with respect to thermodynamic parameters are discontinuous whereas, at a continuous phase transition, the first derivatives of the free energy vary smoothly through the critical region and the second derivatives generally show diverging behaviour.

Spontaneous symmetry breaking refers to the loss of the symmetry of the disordered state when the system undergoes a change of phase. It implies a sudden change from a symmetric disordered state to a long-ranged ordered state in which some symmetry-breaking order parameter acquires a non-zero value. The order parameter is an appropriate thermodynamic quantity to distinguish the two phases: it has a non-zero value in an ordered phase and is zero in the disordered phase. In the phase transition process, the order parameter balances the external influences on the physical system with the internal tendency of system to attain a minimum energy state. The ordering that takes place in apparently different types of systems such as ferromagnets, antiferromagnets, liquid crystals and superconductors may be described by order parameters of a similar character and symmetry. The order parameter can be as simple as a scalar, an axial vector, a vector or even more intricate such as a tensor.

The order parameter is defined at any point of the physical space and is really a field. The system can break its symmetry in many different equivalent ways. As an illustration, consider a Heisenberg ferromagnet with order parameter field $\vec{M}(\vec{r})$, where $\vec{M}$ is the magnetization and $\vec{r}$ is the position vector in the physical space. Undergoing a phase transition the system breaks the rotational symmetry $O(3)$ of the disordered phase by choosing one of the many directions for the magnetization $\vec{M}$. At zero temperature all of these choices lie on the *surface* of a sphere. A system with long-range order can be described by a symmetry group that transforms one state from the manifold of ground states to another equivalent state. This is the symmetry of the order parameter and it can be discrete or continuous.

2.3.1 Continuous phase transitions : critical exponents, scaling and universality

A continuous phase transition is characterized by a singularity in the free energy with a divergence of its second derivatives. The order parameter changes from zero to a non-zero value at the critical point in a continuous way which is characterized by a nonanalytic power law behaviour and is described by a critical exponent. Usually, in the vicinity of a critical point, the correlation length and other thermodynamic quantities such as the specific heat and the magnetic susceptibility exhibit a power law dependence on a parameter which measures the distance from the critical point. In zero applied magnetic field, the distance from the critical point in magnetic systems can be described by a reduced temperature t defined as

$$t = \frac{T - T_c}{T_c} \tag{2.8}$$

where T_c denotes the critical temperature. The definition of various critical point exponents[64] in the vicinity of the critical point is summarized as follows:

Susceptibility	$\chi \sim t^{-\gamma}$	$t > 0$
	$\chi \sim (-t)^{-\gamma'}$	$t < 0$
Specific heat	$C_V \sim t^{-\alpha}$	$t > 0$
	$C_V \sim (-t)^{-\alpha'}$	$t < 0$
Order parameter	$m \sim (-t)^{\beta}$	$t < 0$
Correlation length	$\xi \sim t^{-\nu}$	$t > 0$
	$\xi \sim (-t)^{-\nu'}$	$t < 0$
Correlation function	$G(q) \sim q^{-2+\eta}$	$t = 0$

The homogeneity or scaling properties of the correlation function and related thermodynamic quantities close to the critical point yield relations among the critical exponents and not all of the exponents are independent. These dependencies are called scaling relations and some of them[64] follow:

$$\begin{aligned} \alpha + 2\beta + \gamma &= 2 \\ \gamma &= (2-\eta)\nu \\ \beta &= \frac{1}{2}(d-2+\eta)\nu \\ d\nu &= \gamma + 2\beta \end{aligned} \tag{2.9}$$

The last two scaling relations explicitly involve the spatial dimension d and are called hyperscaling relations.

The universality hypothesis states that many apparently different types of phase transitions occuring in nature may be characterized by the same set of critical exponents. The critical exponent values depend only on the dimensionality of the physical system, the symmetry describing the order parameter and whether the interactions are short or long ranged. The systems that are characterized by the same spatial dimension, symmetry of the order parameter and the range of interaction are said to form a universality class.

2.3.2 Absence of phase transition in finite systems or in infinite systems of low dimensionality

Spontaneous symmetry breaking occurs only if we consider an infinite number of degrees of freedom of a physical system. The free energy density and related thermodynamic variables exhibit singular behaviour at the phase transition only in an infinite system, i.e., in the thermodynamic limit. This is true for order parameters with both discrete and continuous symmetry. In each case, the probability of a change from one symmetry broken state to another in the manifold of energetically equivalent states

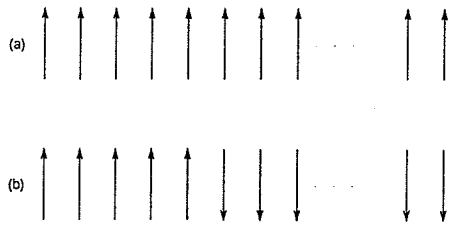

Figure 2.1: The one dimensional Ising model (a) one of the two possible minimum energy configurations and (b) with a single defect added (domain wall).

vanishes only in the thermodynamic limit and the equivalent ordered states become 'ergodically' separated. Although the thermodynamic limit is a necessary condition for the existence of a phase transition, the spatial dimension of the physical system and the symmetry of the order parameter play crucial roles as well.

Consider, for example, a $d = 1$ Ising model with ferromagnetic interactions. We expect an ordered state at zero temperature with all spins aligned in the one of the two possible directions (up or down). The interacting system is described by

$$H = -J \sum_i S_i^z S_{i+1}^z \tag{2.10}$$

where $J > 0$ is the strength of the exchange interaction. In equilibrium, free energy $F = E - TS$ is a minimum and any perturbation away from equilibrium involves a change in free energy. Some deviations from equilibrium require additional energy input and some may occur spontaneously. The lowest energy state of the one dimensional Ising chain is shown in figure 2.1a. Now consider the free energy cost to add a single defect such as the one pictured in figure 2.1b to the system. Introducing a defect to the system increases its energy by $\Delta E = 2J$ since we have changed one favorable interaction into an unfavorable one. However this defect can be intro-

duced at any location in the chain and this choice results in an entropy gain equal to $\Delta S = k_B \ln N$ where N is number of spins in the chain. The resulting change in free energy $\Delta F = \Delta E - T\Delta S = 2J - k_B T \ln N$ is negative at any finite temperature. This means that defects can be formed spontaneously at any finite temperature and the ordered ground state is unstable to their formation. Hence the one dimensional Ising system only orders at $T = 0$ since the free energy cost of introducing a defect is only positive at $T = 0$.

The same argument of balancing the entropy and the energy can be applied to ferromagnetically interacting Ising spins on a two dimensional lattice.[63] The defect

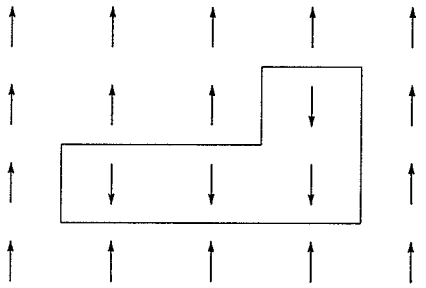

Figure 2.2: Two dimensional Ising model. Defect is a compact cluster of spins pointing in the opposite direction with respect to the majority of spins and has a perimeter of length L.

structure of the ground state is shown in figure 2.2 where the solid line is the perimeter of the defect cluster. The energy cost to create the defect is proportional to the perimeter length and the entropy is related to the number of such clusters. Both the energy and the entropy scale in the same way with the perimeter of the defect boundary length L and the free energy change can be written as $\Delta F = [2J - k_B T \ln(z-1)]L$, where z is the coordination number and is related to number of ways the defect with perimeter L can be realized. This simple argument indicates that the free energy

changes below a finite temperature $T = T_c = 2J/k_B \ln(z-1)$ are positive and that the ordered state is stable against the formation of defects at low temperatures but becomes unstable at T_c. The exact solution of the two-dimensional Ising model was found by Onsager[62] and indeed shows that this model has a nontrivial phase transition. Thus the discrete Ising spin model model with Z_2 order parameter symmetry exhibits a finite temperature phase transition in two dimensions but not in one dimension. The dimension $d = 1$ is called the lower critical dimension for this model.

In the remainder of this thesis we shall only consider order parameters which correspond to a continuous symmetry as they are relevant to the models that we will investigate. It is generally accepted that an ordered phase with continuous symmetry cannot occur in one and two dimensions. Peierls[?, ?] was the first to point out that long wavelength lattice vibrations destroy long-range periodic order in both $d = 1$ and $d = 2$ crystals. The argument was later refined and extended by Mermin and Wagner[5] and Hohenberg[6]. We can illustrate this argument in magnetic systems by examining the stability of long-range order in systems with continuous degrees of freedom in different spatial dimensions. The simplest such system is the XY spin model which has a two component vector order parameter described by the $O(2)$ symmetry group. The order parameter of this model can be written in terms of real components $\vec{S}(\vec{r}) = S(\cos\theta(\vec{r}), \sin\theta(\vec{r}))$ or in the complex form $Se^{i\theta(\vec{r})}$ where $\theta(\vec{r})$ is the angle which indicates the direction of the spin at position $\vec{r}$. In the ferromagnetic case, the ground state will have the same value of the angle everywhere. Excitations away from this uniform state can be written in terms of gradients of the phase angle as follows

$$\Delta F = \int d^d r \frac{\rho}{2} \mid \nabla\theta(\vec{r}) \mid^2 \tag{2.11}$$

where the angle $\theta(\vec{r})$ is assumed to be slowly varying in space.The quantity ρ plays the role of an elastic constant and is called the spin-wave stiffness, or helicity modulus. Using this long wavelength form of the free energy, information about long-range order can be obtained by calculating the spin-spin correlation function

$$\begin{aligned} G(\vec{r},0) = \langle \vec{S}(\vec{r}).\vec{S}(0)\rangle &= S^2\langle cos(\theta(\vec{r})-\theta(0))\rangle \\ &= S^2 Re\langle e^{i(\theta(\vec{r})-\theta(0))}\rangle \\ &= S^2 e^{-g(\vec{r})}. \end{aligned} \tag{2.12}$$

The free energy (2.11) has only harmonic terms in $\nabla\theta(\vec{r})$ and the thermodynamic average in (2.12) can be found by transforming into Fourier space and using the method of Gaussian integrals (for a detailed derivation see [23]). This approach leads to the following expression for the integral $g(\vec{r})$ in spatial dimension d

$$g(\vec{r}) = T\int \frac{d\vec{k}}{(2\pi)^d}\frac{1-e^{i\vec{k}\cdot\vec{r}}}{\rho k^2} \tag{2.13}$$

which, in the asymptotic limit of $\mid \vec{r} \mid \rightarrow \infty$, behaves in the following way

$$g(r) \simeq \begin{cases} \frac{T}{\rho(d-2)}\left(\frac{\pi}{a}\right)^{d-2} & (d>2) \\ \frac{T}{2\pi\rho}\ln(r/a) & (d=2) \\ \frac{T}{2\rho}r & (d=1) \end{cases} \tag{2.14}$$

Here a is the lattice spacing denoting a short distance cut-off in the integral $g(\vec{r})$. Hence the correlation function in $d = 1$ decays exponentially and only short range order is possible at all non-zero temperatures. The decay of the correlation function in two dimensions is algebraic and tends to zero at large distances implying a lack of conventional long-range order. However, an algebraic order referred to as 'quasi-long-range order' is possible in two dimensional systems. In higher dimensions ($d > 2$) the correlation function approaches a non-zero constant value and long-range order is present at low temperatures. Long wavelength fluctuations are responsible for the destruction of long-range order at any finite temperature in dimension $d \leq 2$ and this result is often referred to as the Mermin-Wagner-Hohenberg theorem.[5, 6] Hence the dimension $d = 2$ is the lower critical dimension for systems with a continuous symmetry.

2.3.3 Elementary excitations

Uniform changes of the ground state under the symmetry group of the order parameter do not cost any energy. However, it was pointed out by Goldstone[65] that whenever a continuous symmetry is broken, long wavelength modulations of the ground state should lead to low frequency excitations commonly referred to as Goldstone modes [39]. In magnetically ordered systems such modulations are called spin waves. In general, the breaking of a continuous symmetry is accompanied by the appearance of the Goldstone modes, i.e. low energy, long wavelength excitations. These modes have a soft dispersion relation, and $\omega(k) \rightarrow 0$ when $k \rightarrow 0$. They are the thermodynamically active degrees of freedom that describe thermal energy excitations and thermodynamic fluctuations in equilibrium.

2.4 Topological defects

The considerations of the spatial correlations in the previous section suggest the absence of long-range order in a two dimensional system with a $n \geq 2$ component parameter. The result implies a vanishing of the magnetization at all finite temperatures. However, the spatial correlations exhibit power-law decay which admits the possibility of *quasi-long-range order* at low temperatures. The high temperature behaviour can be found from high temperature series expansion estimates of the spin-spin correlation function. In this limit, the spin-spin correlation function decays exponentially as

$$G(\vec{r},0) = \langle \vec{S}(\vec{r})\vec{S}(0)\rangle \sim e^{-r/\xi(T)} \tag{2.15}$$

with a characteristic length scale $\xi(T)$ which is called the correlation length. The distinction between the nature of the decay at low and high temperatures allows for the possibility of a finite temperature phase transition. This phase transition has a topological character.

Topological defects play an important role in determining the properties of real

materials such as superfluid helium, various nematic liquid crystals and superconductors to mention a few. Phase transitions involving a continuous symmetry breaking provide a mechanism for the generation of topological defects in many natural processes. In this section we focus on the topological attributes of the physical space in relation to the phase transition.

2.4.1 Ordered media and characterization of topological defects

An ordered medium can be regarded as an order parameter field $\vec{f}(\vec{r})$ where the vector function $\vec{f}$ assigns an value of the order parameter to each point of a particular region of space. In an uniform medium the order parameter function $\vec{f}$ is constant throughout the medium and describes the state of the system with lowest energy. Nonuniform media, where the order parameter field $\vec{f}$ varies continuously throughout the medium except at the isolated core regions which have a lower dimension than the medium itself, constitute topological defects. Stable topological defects are characterized by a singular core region where the medium order is destroyed. It is not possible to transform such nonuniform configurations to the uniform state by any continuous deformation of the order parameter.

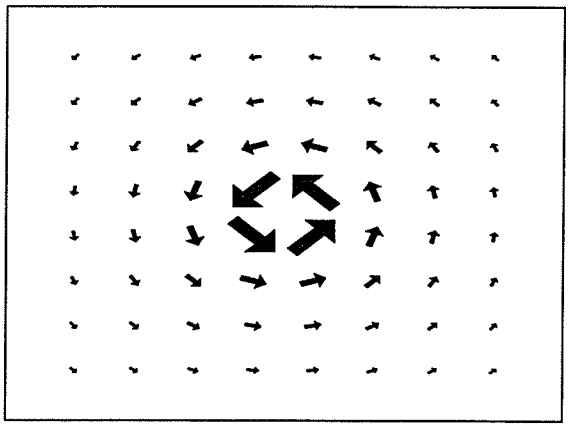

Figure 2.3: An isolated vortex with winding number $m = 1$.

Figure 2.3 illustrates a medium of planar spins in a two dimensional physical space with a topological defect called a vortex. The orientation of each spin in figure (2.3) can be described by a field angle $\Phi(r,\theta)$ at the position given by the polar coordinates r and θ where the origin is at the center of the vortex. Measuring the total change in the value of $\Phi(\theta,r)$ while traversing a closed contour that encirles the origin yields changes which are integer multiples of 2π. Thus we have

$$\oint d\vec{l}\cdot\vec{\nabla}\Phi = 2\pi m \qquad \nabla\Phi = \frac{m}{r}\hat{\theta} \tag{2.16}$$

for any loop enclosing a vortex center. Making the radius of this loop infinitely small, $\nabla\Phi \sim 1/r$ diverges indicating a singularity at the center of vortex, also called the vortex core. The integer m is called the strength of the vortex or the winding number, and in order to have a singularity m has to be non-zero. There is no continuous deformation of spins in the figure 2.3 that can bring spins into the equilibrium ground state configuration which has all spins parallel and the vortex is said to be topologically stable. The topological stability of the order parameter defect depends on the symmetry of the order parameter and the so called codimension $d' = d - d_d$, where d is the spatial dimension and d_d is the dimension of the defect core [27]. The $O(n)$ models have stable defects if the dimension n of the order parameter is equal to the codimension d'. Thus, the core of the stable defect $n = 2 = d'$ in the example of planar spins on a $d = 2$ lattice is a point with $d_d = 0$. The same model on a $d = 3$ lattice has a stable defect with defect core of dimension $d_d = 1$, i.e. a line.

Media with a defect present have a higher energy than the ground state configuration, but they are stable since it costs an infinite amount of energy to reach the ground state.

2.4.2 Order parameter space and homotopy

In order to characterize topological defects in general it is convenient to introduce the concepts of order parameter space and homotopy groups. The possible values that an

order parameter can have constitute a space known as order parameter space V or a manifold of internal states. This is an abstract space: for example, a complex scalar or $2d$ unit vector order parameter is the circumference of a unit circle. A $3d$ unit vector order parameter corresponds to the surface of a unit sphere and a general $d = n$ unit vector is the surface (S_{n-1}) of the n dimensional sphere. This space has important topological properties such as its connectivity which is used for the characterization of topological defects.

The order parameter field can be visualized as a mapping from a real space to order parameter space V. A closed loop (or any closed surface) in the physical space around a defect core is associated to a certain closed path in the order parameter space. In the vortex example of $2d$ spins in a plane in the previous section, specification of the spin directions on the loop Γ encircling a vortex core in the physical space defines a mapping from the loop Γ to the one dimensional unit sphere S_1 (circle). The path in the order parameter space V, or more precisely, a set of paths that can be continuously deformed from one to another within a manifold of internal states characterizes the topology of defects encircled by the loop Γ. Any loop in the physical space of the system in the equilibrium ground state maps into a single point in the order parameter space. Thus any path in the order parameter space V that can be continuously deformed into a single point characterizes unstable topological defects. Otherwise, if it cannot be transformed into a point the defect is topologically stable.

Mappings that can be continuously deformed into each other are defined to be homotopic. The possible maps of a subspace Γ surrounding a defect to an order parameter space V can be classified into classes of equivalent maps which can be continuously transformed from one to another within the order parameter space. Defects are in the same homotopy class if the mappings of all the paths enclosing them can be continuously deformed into each other. The ensemble of these classes is called the k^{th} homotopy group of the order parameter space V and is denoted by $\pi_k(V)$.

2.4.3 Kosterlitz Thouless phase transition

The consideration of spatial correlations in section 2.3.2 suggests the possibility of quasi long range order in the XY model in two dimensions and the occurrence of a phase transition from this state to a high temperature state with short range order. The vortices discussed in section 2.4.1 are excitations that can take the system from its low temperature critical phase to the high temperature disordered phase. At low T single vortices are topologically stable and cost an infinite amount of energy to form. However, vortices can appear as tightly bound pairs that unbind at the critical temperature. This is referred to as a Kosterlitz -Thouless phase transition due to the unbinding of vortices.

To see how this mechanism can give rise to the phase transition, consider an isolated vortex as shown in the figure 2.3. The energy of an isolated vortex is

$$E = \frac{1}{2}\rho \int d^2r(\vec{\nabla}\Phi)^2 = \pi\rho m^2 \int_a^L \frac{dr}{r} = \pi m^2 \rho \ln(L/a). \tag{2.17}$$

The energy of single vortex in thermodynamic limit ($L \to \infty$) is infinite suggesting that there cannot be a finite density of these objects due to thermal fluctuations. However, vortices cannot be completely neglected as can be seen by calculating a free energy change to add such a vortex. The entropy of a single vortex depends on the number of ways that the vortex can be introduced into the system, or on the area of the lattice, and can be written as

$$S = k_B \ln(L/a)^2 \tag{2.18}$$

Thus the change in free energy as result of introducing a single vortex into this system is

$$\Delta F = (\pi\rho m^2 - 2k_B T)\ln(L/a). \tag{2.19}$$

At low temperatures the free energy cost is positive with larger winding numbers costing the most and no isolated vortices are present. However, the lowest temperature

above which the entropy wins corresponds to $m = \pm 1$ and is given by

$$k_B T = \frac{\pi}{2}\rho. \tag{2.20}$$

Above this temperature, the free energy cost is negative and such defects can appear spontaneously. However, at low temperatures, there is a small but finite density of bound vortex pairs. The energy of a vortex pair with opposite winding numbers m_1 and m_2, separated by distance r_{12} is finite

$$E_{pair} = \frac{1}{2}\rho \int d^2 r (\vec{\nabla}\Phi_1 + \vec{\nabla}\Phi_2)^2 \tag{2.21}$$

$$\sim m_1 m_2 \ln \left| \frac{r_{12}}{a} \right|. \tag{2.22}$$

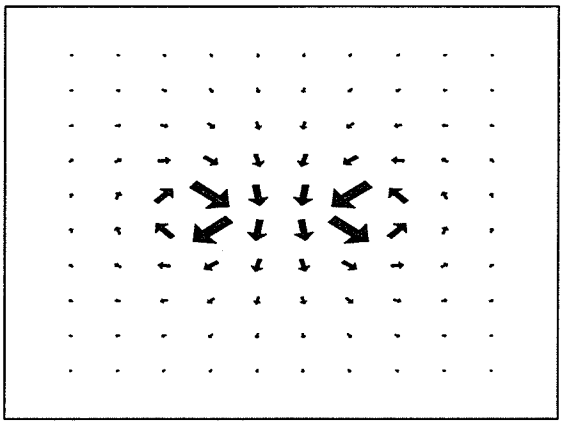

Figure 2.4: A pair of vortices with equal and opposite winding numbers ± 1.

Vortices with opposite winding number such as those shown in figure 2.4 attract and the creation of such a pair costs a finite amount of energy. Above the transition temperature, each vortex becomes essentially free and this disassociation leads to large phase fluctuations which destroy the algebraic order and reduce it to a short-range order with exponential decaying correlations.

2.5 Generalized Rigidity

Breaking the symmetry in the same way throughout the system yields the minimum energy state and the order parameter field is uniform. Modulating the order parameter costs energy, and hence the breaking of the symmetry results in a system which has rigidity. This concept can be generalized to all instances of broken symmetry and is called generalized rigidity [18]. In solid systems, small elastic deformations are present and there is an elastic energy associated with the deformation. In the spin systems, deformations correspond to gradients of the spin direction, and the deformation energy is proportional to $(\vec{\nabla}S)^2$ and can be written as

$$E = E_0 + \int d^d r \rho (\vec{\nabla} S)^2 \tag{2.23}$$

where ρ is the rigidity constant. In magnetic systems the parameter characterizing the rigidity of the system is called the spin wave stiffness.

2.5.1 Stiffness

The spin wave stiffness is the fundamental parameter that determines the low-energy excitations of magnetic systems. It can be understood as a rigidity of the order parameter and emerges as a consequence of spontaneous symmetry breaking in systems with continuous symmetry. It can be defined in terms of the free energy change under an imposed twist of an equilibrium configuration of spins located at lattice sites. The imposed twist corresponds to the creation of a fluctuation away from the equilibrium state [28]. In the disordered phase, such a fluctuation costs no energy. The creation of spin waves in the ordered state results in an increased free energy. There is a nonzero spin wave stiffness as a result of the system's attempt to restore long range order. Hence the spin wave stiffness is zero in the disordered phase and non-zero in the ordered phase. Consequently, it can serve as an alternative to an order parameter to determine the existence of long range order. This provides an unbiased measure-

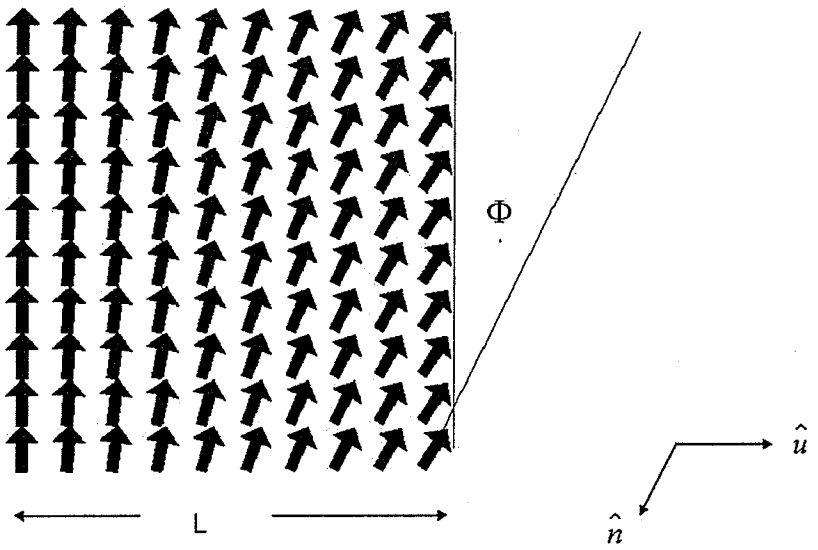

Figure 2.5: Schematic view of the spin stiffness for a ferromagnet.

ment which does not require knowledge of the broken symmetry and hence the order parameter. A schematic picture of the stiffness is shown in figure 2.5

The spin wave stiffness can be calculated as a response function to an imposed twist or gradient on the spin degrees of freedom using (2.7) yielding the following expression

$$\rho_{\hat{n}} = -\frac{1}{L^d}\sum_{i<j} J_{ij}(\hat{e}_{ij}\cdot\hat{u})^2\left\langle(\vec{S}_i\cdot\hat{n})(\vec{S}_j\cdot\hat{n}) - \vec{S}_i\cdot\vec{S}_j\right\rangle$$
$$-\frac{1}{L^dT}\left\langle\left[\sum_{i<j} J_{ij}(\hat{e}_{ij}\cdot\hat{u})\hat{n}\cdot(\vec{S}_i\times\vec{S}_j)\right]^2\right\rangle. \qquad (2.24)$$

In this expression $\hat{e}_{ij}$ is a unit vector connecting nearest neighbour spin sites, $\hat{u}$ is a unit vector describing the direction of the imposed gradient and $\hat{n}$ is the axis in spin space about which the spins are rotated. The detailed derivation of this expression is given in appendix A.

The effect of thermally activated vortex pairs is described by the temperature dependence spin wave stiffness. A finite density of vortex-antivortex pairs reduces

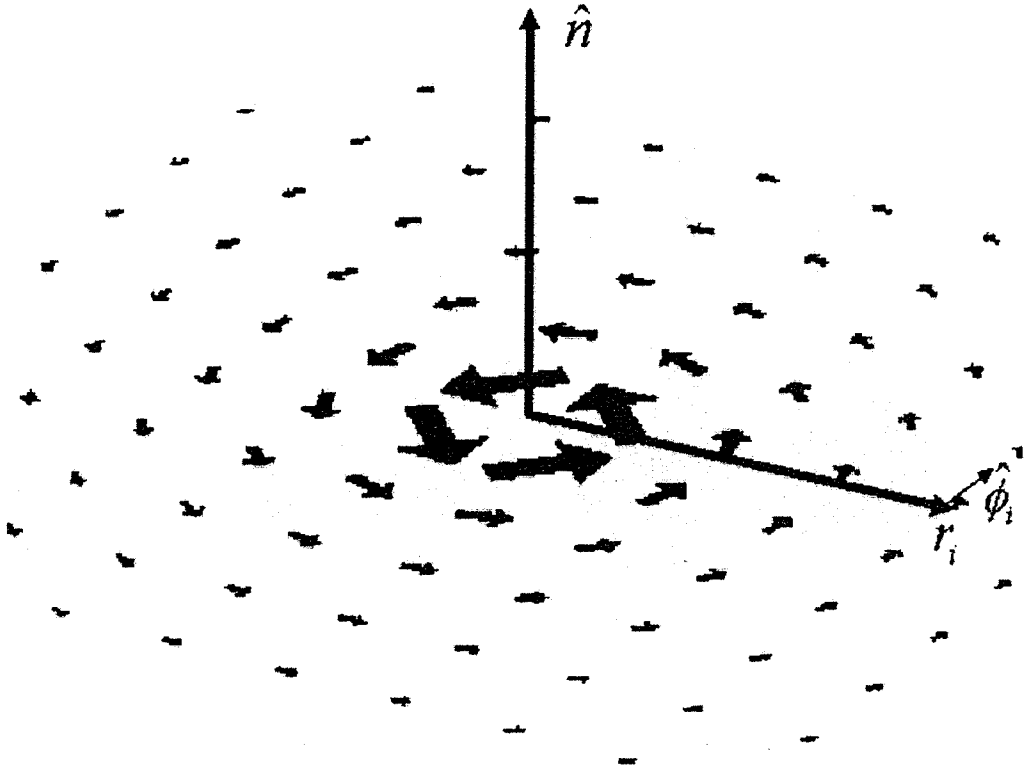

Figure 2.6: Schematic view of vorticity

the spin wave stiffness and also the order parameter amplitude. Vortices are mobile degrees of freedom that distribute themselves such that the free energy of system is minimized.

2.5.2 Vorticity

The spin stiffness is essentially a measure of the response of the spin system to an imposed gradient on the spin degrees of freedom. We can also consider the situation in which a curl is imposed and ask what is the response of the system in this case. Figure 2.6 shows a schematic picture of an imposed curl. The vorticity is measure of the response of the spin system to an imposed twist about an given axis $\hat{n}$ in spin space along a closed path that encloses a vortex core. The vorticity can be calculated as the

second derivative of the free energy with respect to the strength of the vortex denoted by the winding number m, when $m = 0$. A detailed description of the derivation is given in appendix B. and leads to the following expression for the vorticity

$$V_{\hat{n}} = -\frac{1}{L^{d-2}}\frac{\sqrt{3}}{4\pi}\sum_{i<j} J_{ij}(\frac{\hat{e}_{ij}\cdot\hat{\phi}_i}{r_i})^2 \left\langle (\vec{S}_i\cdot\hat{n})(\vec{S}_j\cdot\hat{n}) - \vec{S}_i\cdot\vec{S}_j \right\rangle$$
$$- \frac{1}{L^{d-2}}\frac{\sqrt{3}}{4\pi}\left\langle \left[\sum_{i<j} J_{ij}(\frac{\hat{e}_{ij}\cdot\hat{\phi}_i}{r_i})\hat{n}\cdot(\vec{S}_i\times\vec{S}_j)\right]^2 \right\rangle \qquad (2.25)$$

where r_i is the distance of site i from the vortex core and $\hat{\phi}_i$ is tangent to the circular path in the lattice passing through site i and enclosing a the vortex core.

The vorticity $V_{\hat{n}}$ contains a contribution due to the vortex core as well as a part which is proportional to $\ln(L/a)$ and can be written as

$$V_{\hat{n}} = C_{\hat{n}} + v_{\hat{n}}\ln(L/a) \qquad (2.26)$$

where $v_{\hat{n}}$ is called the vorticity modulus.

These two response functions, stiffness and vorticity, will be used extensively in this thesis to study the nature of topological defects on phase transitions in frustrated systems.

Chapter 3

NUMERICAL METHODS

3.1 Introduction

Most problems in condensed matter and statistical physics, as in nature itself, are nonlinear and cannot be treated by standard perturbation methods. Analytical tools are best suited to the analysis of linear problems. Many natural phenomena are nonlinear and must be studied using computer simulation methods. Various numerical methods, such as Monte Carlo simulations can be employed in the investigation of these phenomena. The advantage of such approaches is that they do not necessarily rely on simplifying assumptions or approximations, and the design of various algorithms is closely related to experience, as in the case of real experimental setups. The goal of numerical simulations is to provide a better understanding of the physical properties and processes relying on perfect control over the processes and possibility of examining every aspect of the system configurations in detail. The control over various aspects of the problem is important, especially in the case of the rather complicated phenomena exhibited by real materials. In numerical simulations each factor that contributes to the physical properties of the material can be studied separately with the final aim of understanding the underlying mechanism responsible for the observed phenomena.

In order to calculate the thermal averages of an interacting many particle system using equilibrium statistical mechanics, the Monte Carlo method is used to simulate the appropriate statistical distribution such as the canonical or microcanonical distribution [98, 97]. In general, the number of representative states of a finite system are

generated in a stochastic manner which depends on a sequence of random numbers generated during the simulation. Different sequences of random numbers yield results that agree within some statistical error. Calculated thermodynamic averages are extrapolated to relevant values in thermodynamic limit (systems of infinite size). Based on the ergodic hypothesis requirement, namely, the requirement that all possible microstates are equally probable, we also assume that the averages of thermodynamic quantities over time can be replaced by statistical ensemble averages. In the next section we give an overview of the most important concepts related to Monte Carlo simulations.

3.2 Overview of Monte Carlo Simulations

The essential feature of the Monte Carlo method is the concept of Markovian chains [97]. In order to understand this concept, consider a finite set $\{S_i\}$ of all possible states that can be realized at different times t_i, where i labels consecutive discrete time intervals. Denote by X_t a state of the system at time t. We can form a sequence of states $\{X_{t_i}\}$ such that they satisfy a conditional probability, namely $X_{t_n} = S_n$ given that at the preceding time the system was in state $X_{t_{n-1}} = S_{n-1}$ and at the time step before that in state $X_{t_{n-2}} = S_{n-2}$, and so on. The conditional probability can be written as

$$P(X_{t_n} = S_n | X_{t_{n-1}} = S_{n-1}, X_{t_{n-2}} = S_{n-2}, ..., X_{t_1} = S_1). \tag{3.1}$$

When the conditional probability depends only on the immediate predecessor and not on any other preceding states, the sequence of states $\{X_{t_i}\}$ is called a Markovian chain. In such a chain no memory of the previous states except that of the immediate predecessor state exists, meaning that the conditional probability

$$P = P(X_{t_n} = S_j | X_{t_{n-1}} = S_i) \tag{3.2}$$

can be understood as a transition probability W_{ij} to move from state i to state j, i.e.

$$W_{ij} = P(X_{t_n} = S_j | X_{t_{n-1}} = S_i). \tag{3.3}$$

The transition probability has to satisfy the requirement of positive definiteness as well as a normalization requirement expressed by

$$W_{ij} \geq 0, \qquad \sum_i W_{ij} = 1. \tag{3.4}$$

The probability $P(S_j, t)$ of the system to be in state S_j at time t depends only on the preceding state of the system and can be written as

$$P(S_j, t) = W_{ij} P(S_i, t). \tag{3.5}$$

In other words, if the system is in a given microstate i, the next state in the Markovian sequence is selected with a transition probability W_{ij} that does not depend on the previous history of the system. Continually applying this process on newly generated microstates, after some transient time, all states will reach a unique steady-state probability distribution

$$P(j) = P(S_j) = \sum_i W_{ij} P(S_i). \tag{3.6}$$

The most common choice for the steady-state distribution is the Boltzmann canonical distribution

$$P(j) = \frac{e^{-\beta E_j}}{Z} \tag{3.7}$$

where Z is the partition function and β is the inverse temperature.

The evolution in time of this probability is expressed through the so called master equation

$$\frac{dP(S_j, t)}{dt} = \sum_i \left(W_{ij} P(S_i, t) - W_{ji} P(S_j, t) \right). \tag{3.8}$$

When the system reaches an steady-state, meaning it is in equilibrium, its macroscopic properties are time independent and the probability of the system $P_{eq}(S_j, t)$ to be in

state S_j at an instant t is constant and equal to the steady-state probability i.e.

$$\frac{dP(S_j,t)}{dt} = 0. \tag{3.9}$$

Using expressions (3.8) and (3.9), we can write this condition as follows

$$W_{ij}P_{eq}(S_i,t) = W_{ji}P_{eq}(S_j,t). \tag{3.10}$$

This is the principle of detailed balance, which is a sufficient condition for arriving at the correct probability distribution. Any algorithm used for the simulation of the equilibrium properties has to satisfy the principle of detailed balance and the transition probability W_{ij} has to be chosen appropriately. This is called importance sampling since the available points in phase space are sampled with different probability weights so that the principle of detailed balance (3.10) holds.

In the general case, a Monte Carlo simulation consists of the following steps:

- Choose an initial microstate - configuration of magnetic moments.
- Select a move - anticipated change of the configuration.
- Accept or reject the move using a criterion based on detailed balance.
- Repeat the last two steps above until enough data is collected.

The initial microstate is arbitrary and an initial number of Monte Carlo steps is discarded to allow the system to approach an equilibrium state before samples of data are taken. In addition to eliminating these transients, we want to generate a sequence of uncorrelated microstates. In order to avoid possible correlations a certain number of Monte Carlo steps are performed between the microstates that are considered for sampling the configurations.

Since the simulations are performed on finite systems, it is important to chose appropriate boundary conditions in order to eliminate boundary and edge effects of the

finite sample [99]. The most common type of boundary conditions used in the simulation of lattice Hamiltonians are periodic boundary conditions. In a d dimensional sample of finite length L in each direction, the use of periodic boundary conditions means that the system is periodically extended in each coordinate. We assume that any local quantity, particularly a local order parameter $\Phi(x, y, z)$ satisfies

$$\Phi(x, y, z) = \Phi(x + L, y, z) = \Phi(x, y + L, z) = \Phi(x, y, z + L) \tag{3.11}$$

In Chapter 5 we shall also study $2d$ systems which have a finite number of layers H in the third direction. In this case we only use periodic boundary conditions in two directions and use free boundary conditions at the top and bottom surface layers. Free boundary conditions means that the system is not periodically repeated in the third direction. The local order parameter $\Phi(x, y, z)$ in the direction normal to the layers satisfies

$$\Phi(x, y, z \pm H) = 0 \tag{3.12}$$

Information about the system in a Monte Carlo simulation can be obtained by calculating any of the physical quantities (e.g. energy, order parameter, susceptibility) A_i for each of M generated microstates. The mean value of $\langle A \rangle$ can be then be calculated as

$$\langle A \rangle = \lim_{M \to \infty} \frac{1}{M} \sum_i A_i \tag{3.13}$$

where each state i is generated according to the appropriate probability distribution.

When the system is held at a constant value of an intensive variable such as the temperature T or magnetic field h, the conjugate extensive variable such as energy or magnetization will fluctuate with time and we expect to observe these fluctuations during a Monte Carlo simulation. The fluctuations in energy are related to the specific heat C_V as follows

$$C_V = \left(\frac{\partial \langle E \rangle}{\partial T} \right)_V = \frac{\langle E^2 \rangle - \langle E \rangle^2}{T^2} \tag{3.14}$$

Similar fluctuations exist in other quantities. For example the isothermal susceptibility χ is related to fluctuations of the magnetization M by

$$\chi = \left(\frac{\partial \langle M \rangle}{\partial h}\right)_T = \frac{\langle M^2 \rangle - \langle M \rangle^2}{T}. \tag{3.15}$$

In the cases where the order of the phase transition is in question, not only the lowest order moments are of interest but also their full probability distributions. For a system in a pure phase, the probability distribution of the quantity A is given by a simple Gaussian distribution

$$P(A) = \left(2\pi\sigma^2\right)^{-1/2} \exp\left[(A - \langle A \rangle)^2 / 2\sigma^2\right]. \tag{3.16}$$

where

$$\sigma(A)^2 = \langle A^2 \rangle - \langle A \rangle^2 \tag{3.17}$$

In the case of first order transitions, the probability distribution can be a superposition of Gaussians centered at different values of $\langle A \rangle$ and a measurement of the higher moments $\langle A^n \rangle$ can be used to study these cases.

3.2.1 Statistical and other errors

Statistical errors are an inherent feature of any algorithm that uses only a finite number of sample configurations to compute various statistical averages [98, 97]. The average value of a quantity $\bar{A}$ for a finite number of samples M is

$$\bar{A} = \frac{1}{M} \sum_{i=1}^{M} A_i. \tag{3.18}$$

In the limit $M \to \infty$, $\bar{A}$ we will have a Gaussian distribution independent of the distribution used to generate the random configurations in the Monte Carlo simulation. In statistics this is known as the central limit theorem. If the quantity A is distributed according to a Gaussian distribution (3.16) with a mean value $\langle A \rangle$ and distribution width σ then the value $\bar{A}$ is a finite sample estimate of the quantity $\langle A \rangle$

with a statistical error ϵ given by

$$\epsilon = \sigma(A)/\sqrt{M} \tag{3.19}$$

In order to estimate σ from a finite number of samples M, we can calculate the mean square deviation

$$\delta\bar{A}^2 = \frac{1}{M}\sum_{i=1}^{M}(\delta A_i)^2 = \bar{A}^2 - (\bar{A})^2 \tag{3.20}$$

where $\delta A_i = A_i - \bar{A}$. The expectation value $\langle\delta\bar{A}^2\rangle$ in (3.20) is related to σ as

$$\langle\delta\bar{A}^2\rangle = \sigma^2(1 - 1/M). \tag{3.21}$$

Thus by calculating the variance δA_i, the statistical error ϵ of the average $\bar{A}$ of M uncorrelated samples can be written as

$$\epsilon = \sqrt{\sum_{i=1}^{M}(\delta A_i)^2/[M(M-1)]}. \tag{3.22}$$

In addition to statistical errors there are also errors associated with the way any computer operates. In general, computers deal with a limited word length and round off errors may affect the calculations significantly. Systematic errors in the program are also possible and an effort should be made to detect and eliminate such errors.

In the following sections we describe two algorithms used in our simulations: a standard Heat Bath algorithm [100] and also the Broad Histogram Method [48, 49, 50, 51].

3.3 Heat bath Monte Carlo Method

The heat bath Monte Carlo method generates a sequence of configurations which simulate a canonical ensemble of states in thermal equilibrium at a constant temperature T. Given a configuration of the spins in a system, the direction of each spin is updated assuming that the spin is in contact with a heat bath that puts it into local equilibrium with the surrounding spins.

The systems that we shall study are described by a Hamiltonian of the form

$$H = -\sum_{<ij>} J_{ij}\vec{S}_i \cdot \vec{S}_j \tag{3.23}$$

where $\vec{S}_i$ is a classical vector with n components located at the site i of a lattice and J_{ij} is the strength of the exchange interaction between nearest neighbour pairs of spins. The orientation of the spin S_i is determined by the net effect of the neighbouring spin orientations, the strength of the interaction J_{ij} and the temperature T. The neigbouring spins exert a local effective magnetic field at site i given by

$$\vec{H}_{ieff} = \sum_j J_{ij}\vec{S}_j \tag{3.24}$$

This field direction provides a local coordinate frame for the spin $\vec{S}_i$. In the case of Heisenberg spins ($n = 3$), the spin direction with respect to the local field $\vec{H}_{ieff}$ can be described using the azimuthal and polar angles ϕ_i and θ_i respectively. The

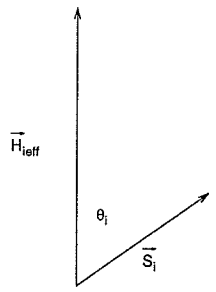

Figure 3.1: At each site i there is an instantaneous local field $\vec{H}_{ieff} = \sum_j J_{ij}\vec{S}_j$. The azimuthal angle ϕ_i singles out a plane containing both $\vec{H}_{ieff}$ and $\vec{S}_i$. The orientation of $\vec{S}_i$ with respect to $\vec{H}_{ieff}$ in this plane is described by the polar angle θ_i.

equilibrium probability of the spin direction at site i is given by the Boltzmann factor

$$P(\theta_i, \phi_i) = \frac{e^{\beta\vec{S}_i \cdot \vec{H}_{ieff}}}{C} \tag{3.25}$$

where C is a normalization factor. Note that

$$\vec{S}_i \cdot \vec{H}_{ieff} = |\vec{S}_i||\vec{H}_{ieff}| \cos(\theta_i) = H_{ieff} \cos(\theta_i) \tag{3.26}$$

In the case of XY spins ($n = 2$) the azimuthal angle can be neglected since the spins and the field are confined to a plane. The normalization factor C depends on the number of spin components n. For $n = 3$, it is given by the integral

$$\begin{aligned} C &= \int_0^{2\pi} \int_0^{\pi} e^{(\beta) H_{ieff} \cos(\theta_i)} \sin(\theta_i) d\theta_i d\phi_i \\ &= 4\pi \frac{\sinh(\beta H_{ieff})}{\beta H_{ieff}}. \end{aligned} \tag{3.27}$$

Hence the normalized probability distribution for a Heisenberg spin can be written as

$$P(\theta_i, \phi_i) = \frac{\beta H_{ieff} e^{\beta H_{ieff} \cos(\theta_i)}}{4\pi \sinh(\beta H_{ieff})} \tag{3.28}$$

We can separate this into the product of independent distributions for $\cos(\theta_i)$ and ϕ_i as follows

$$P(\phi_i) = \int_{-1}^{1} P(\cos(\theta_i), \phi_i) d\cos(\theta_i) = \frac{1}{2\pi} \tag{3.29}$$

$$\begin{aligned} P(\cos(\theta_i)) &= \int_0^{2\pi} P(\cos(\theta_i), \phi_i) d\phi_i \\ &= \frac{1}{2} \frac{\beta H_{ieff} e^{\beta H_{ieff} \cos(\theta_i)}}{\sinh(\beta H_{ieff})} \end{aligned} \tag{3.30}$$

A random number generator can now be used to generate values of the independent variables $\cos(\theta_i)$ and ϕ_i which are distributed according to the probability functions $P(\cos(\theta_i))$ and $P(\phi_i)$. The integrated probability distributions are in the range [0,1] and can be set equal to a random number which is uniformly distributed on this same interval. In general, for a variable x which has a probability density $P(x)$, the cumulative probability distribution

$$P_c(X) = \int_{-\infty}^{X} P(x) dx \tag{3.31}$$

represents the probability of choosing a value of the variable x to be less then or equal to X. We set $P_c(X) = r$ where r is uniformly distributed on the unit interval and solve for X in terms of r. Hence for the $\cos(\theta_i)$ and ϕ_i we can write

$$\begin{aligned} P_c(\cos(\Theta)) &= \int_{-1}^{\cos(\Theta)} P(\cos(\theta_i))d\cos(\theta_i) = r1 \\ P_c(\Phi) &= \int_0^{\Phi} P(\phi_i)d\phi_i = r2 \end{aligned} \tag{3.32}$$

where $r1, r2$ are independent random numbers uniformly distributed on $[0, 1]$. Equations (3.32) can be inverted to yield

$$\begin{aligned} \cos(\Theta) &= 1 + \frac{1}{\beta H_{ieff}} \ln\left((1 - r1)e^{-2\beta H_{ieff}} + r1\right) \\ \Phi &= 2\pi r2 \end{aligned} \tag{3.33}$$

The random numbers $r1, r2$ are generated and the new direction of the spin relative to the local field direction is chosen using the above method. Since the local field direction is known, this new spin direction can then be transformed from the local frame defined by $\vec{H}_{ieff}$ to the global coordinate system.

This heat bath method for the case of Heisenberg spins generates spin updates which are in agreement with the Boltzmann canonical probability distribution and consequently the principle of detailed balance is always satisfied. At each each Monte Carlo step, there is a spin update and hence no moves are rejected. This is a very efficient way to sample the accessible microstates [100].

For the XY model it is not possible to follow this same procedure since the inversion process cannot be carried out analytically. Hence in the case of $n = 2$ models we must use a Metropolis algorithm.

3.4 Metropolis Method for XY models

In the Metropolis algorithm [101] the sampling configurations are generated according to the Boltzmann probability distribution (3.7) directly from a previous configuration

such that the principle of detailed balance (3.10) is satisfied. Generating a Markovian chain such that a new microstate follows from the previous one means that the relative probability of the two states is the ratio of their Boltzmann factors and thus depends on the energy difference $\Delta E = E_n - E_m$ of the two states m and n. Hence the transition probability that satisfies (3.10) can be written as [101]

$$\begin{aligned} W_{m\to n} &= e^{-\Delta E/k_B T}, & \Delta E > 0 \\ &= 1 & \Delta E < 0 \end{aligned} \tag{3.34}$$

The steps to follow in order to generate the Makovian sequence using a Metropolis algorithm are as follows:

1. Chose a starting microstate
2. Chose a lattice site i randomly or sequentially
3. Determine the local field at this site
4. Choose a new random direction for the spin
5. Calculate the energy change ΔE which results if the spin at site i is actually oriented in the new direction
6. Generate a random number r uniformly distributed between 0 and 1
7. If $r \leq e^{-\Delta E/k_B T}$ accept the change in spin direction at site i
8. Go back to the second step and repeat the process

At very low temperatures, the accepted changes in the spin direction will be small and hence we must restrict the choice of random new directions so that a reasonable acceptance rate is obtained.

3.5 Broad Histogram Method

The methods described above are carried out at a fixed value of the temperature and a separate Monte Carlo run must be performed for each temperature of interest. Another approach which can be used for evaluating thermodynamic quantities is based on the microcanonical ensemble. The broad Histogram Method (BHM) estimates a density of states $g(E)$ at fixed energy E by considering the number of ways to change a current microstate of a system belonging to a particular energy level into one of the possible states from a different energy level and vice versa [48, 49]. In this approach the system is completely isolated from its environment and its energy E is kept constant as opposed to the Heat bath algorithm where the system is put in contact with a heat bath at fixed T.

The temperature dependence of any thermodynamic quantity Q in thermodynamic equilibrium can be calculated if the intrinsic properties of the system such as the density of states $g(E)$ and the microcanonical averages $\langle Q(E)\rangle_E$ are known using the following

$$\langle Q(E)\rangle_T = \frac{\sum_E \langle Q(E)\rangle_E \, g(E) e^{-E/T}}{\sum_E g(E) e^{-E/T}}. \tag{3.35}$$

where the microcanonical average of Q at fixed E can be calculated as

$$\langle Q(E)\rangle = \frac{\sum_s Q_s}{g(E)} \tag{3.36}$$

The sum runs over all possible microstates s belonging to the particular energy level E and each state s contributes with equal weight. Q_s is value of the quantity Q in a particular microstate s and $g(E)$ counts the number of all possible microstates having energy E. Knowledge of the density of states $g(E)$ and the microcanonical averages $\langle Q(E)\rangle_E$ for all energies allows us to calculate the thermodynamic averages at constant temperature $\langle Q(E)\rangle_T$ using (3.35).

In order to understand the basic ideas of the BHM method in more detail, consider the case of a magnetic system described by the lattice Hamiltonian (3.23). The

magnetic properties of each ion (atom) situated at each lattice point are represented by its magnetic moment or spin. Any configuration of all the spins at all lattice sites represents a point in the phase space of all microstates. At a fixed value of the energy E, these points lie on a hypersurface in phase space. The energy density of states $g(E)$ is thus related to the area of this hypersurface.

A determination of $g(E)$ is possible by considering a protocol of allowed movements in phase space such that changing from one configuration to another is allowed if and only if the reverse change is also allowed. This is the requirement that the protocol of changes be micro-reversible. Such a protocol can involve the change of direction of a single spin or the change in the directions of a cluster of spins. If the system is in a current configuration X with energy E, there may or may not be a way to change the current configuration into a new spin configuration X' with energy E' according to the adopted protocol. Micro-reversibility means that the change from configuration X to X' is allowed or forbidden only if the change from configuration X' to X is allowed or forbidden according to adopted protocol as symbolically presented in following expression

$$X \to X' \qquad \Longleftrightarrow \qquad X' \to X$$

allowed (forbidden) allowed (forbidden)

The configuration changes are only virtual in that they are not actually performed in the simulation but are used only to estimate the density of states $g(E)$.

Let us denote the number of changes of a configuration X by $N_{up}(X)$ if the changes describe movements that increase energy from E to $E+\Delta E_{fix}$ and by $N_{dn}(X)$ if they are a collection of movements decreasing the energy from E to $E-\Delta E_{fix}$. Here ΔE_{fix} is the energy difference between E and E' and it has a fixed value for any two such levels. The microcanonical averages of the possible movements $\langle N_{up}(E)\rangle$ and $\langle N_{dn}(E)\rangle$ from the energy level E to the energy level $E' = E \pm \Delta E_{fix}$ can be calculated using some micro-reversible protocol. Using the definition of microcanonical averages

(3.36), the fundamental equation of the BHM method [51] is

$$g(E)\,\langle N_{up}(E)\rangle = g(E+\Delta E_{fix})\,\langle N_{dn}(E+\Delta E_{fix})\rangle \tag{3.37}$$

This relation simply states that the number of possible movements from the energy level E to the energy level E', summed over all states with energy E, is equal to the number of all possible movements from E' to E, summed over all states with energy E'. This relation is exact for any statistical model and energy spectrum [51]. Equation (3.37) can be also written in the following form

$$\ln g(E+\Delta E_{fix}) - \ln g(E) = \ln\left(\frac{\langle N_{up}(E)\rangle}{\langle N_{dn}(E+\Delta E_{fix})\rangle}\right) \tag{3.38}$$

By dividing equation (3.38) by ΔE_{fix} , we can estimate the inverse microcanonical temperature $\beta(E)$ =$1/T(E)$ as follows

$$\beta(E) \equiv \frac{d\ln g(E)}{dE} \simeq \frac{\ln g(E+\Delta E_{fix}) - \ln g(E)}{\Delta E_{fix}} \tag{3.39}$$

$$\simeq \frac{1}{\Delta E_{fix}} \ln\left(\frac{\langle N_{up}(E)\rangle}{\langle N_{dn}(E+\Delta E_{fix})\rangle}\right) \tag{3.40}$$

The density of states $g(E)$, or rather $\ln g(E)$, can be found by numerically integrating $\beta(E)$ starting at any initial values $(E_0, \ln g(E_0))$. The choice of $\ln g(E_0)$ is arbitrary and does not effect the estimates of the thermodynamic averages $\langle Q(E)\rangle_T$ since the method determines $g(E)$ up to multiplicative constant $g(E)/g(E_0)$ which cancels out in equation (3.35).

The Hamiltonian (3.23) describes a continuous spin model and the energy spectrum is also continuous. In order to apply the ideas of BHM to a system with a continuous energy spectrum, it is necessary to divide the energy axis into bins of finite width $\Delta E = E_{max} - E_{min}$ where E_{min} and E_{max} are energies at the beginning and at the end of the bin. The continuous energy spectrum is replaced by a discretized spectrum with an energy E_n associated with each bin n. E_n is the energy at the midpoint of the bin $E_n = E_{min} + \frac{\Delta E}{2}$. Clearly, the discrete energy spectrum becomes

a better approximation to the continuous spectrum as a larger number of bins are used. The microcanonical averages $\langle N_{up}(E)\rangle$ and $\langle N_{dn}(E)\rangle$ involved in the fundamental BHM equation can be found either analytically or by Monte Carlo simulation depending on the particular model.

Muñoz and Herrmann [49, 50, 61] proposed the following protocol of random virtual movements in phase space for systems with continuous spin degrees of freedom. For each allowed movement in phase space, the probability to perform the move is equal to the probability to reverse it

$$P\left(X \to X'\right) = P\left(X' \to X\right) \tag{3.41}$$

The energy level in this case can be understood not as an hypersurface of constant energy but rather as a shell of width ΔE. In the case of the XY model, for example, the configuration X has a particular spin in some direction denoted by θ_{old}. A new value of the angle θ_{new} can be chosen at random from the range $[-\pi, \pi]$. The probability density function of finding a particular new value in the range θ to $\theta + d\theta$ is $f(\theta_{new}) = 1/2\pi$. For each random choice of θ_{new}, there is a corresponding change in energy given by $\Delta E = E_{new} - E_{old}$. Once the protocol of random moves is defined by giving the probability density function for the system variable θ_{new}, it is straightforward to find the probability density function $f_{\Delta E}(\Delta E)$ for obtaining an energy change between ΔE and $\Delta E + d\Delta E$. Once the protocol of virtual moves is defined, the density of states can be found using the following replacements for the quantities N_{up} and N_{dn}

$$\begin{aligned} N_{up}(E) &= f_{\Delta E}\left(\Delta E_{fix}\right) \\ N_{dn}(E) &= f_{\Delta E}\left(-\Delta E_{fix}\right). \end{aligned} \tag{3.42}$$

For the simulation of the Heisenberg model described by (3.23) we adopt the following protocol of virtual movements. We choose one spin at random. Its orientation with respect to the local field due to its nearest neighbours is defined by two angles,

ϕ_i and θ_i, as discussed in the section on the heat bath method. We use the angles θ_{iold} and ϕ_{iold} to denote the current spin orientation at the selected site i and we choose a new spin orientation $(\theta_{inew}, \phi_{inew})$ as a random point on the surface of a unit sphere from the distribution

$$f_{\theta,\phi}(\theta,\phi) = \frac{1}{4\pi}\sin(\theta) \tag{3.43}$$

where θ and ϕ lie in the intervals (0,π) and (0,2π) respectively. The angles θ_{new} and ϕ_{new} are random variables with a probability density function $f_{\theta_{inew},\phi_{inew}}(\theta_{inew}, \phi_{inew})$. In order to estimate the quantities N_{up} and N_{dn} consider the changes in energy ΔE between the old and new configurations corresponding to these angles. Since only one spin is moved, the change in energy depends only on the spin at site i and on the local field due to nearest neighbour spins. One can define a bond energy ε_i as follows

$$\varepsilon_i = \sum_j J_{ij}\vec{S}_i \cdot \vec{S}_j = \vec{S}_i \cdot \vec{H}_i = H_i\cos(\theta_i) \tag{3.44}$$

The change in energy ΔE depends only on the bond energies and is given by $\Delta E = \varepsilon_{inew}$ - ε_{iold}. Since ε_{inew} is only a function of the random variable θ_{inew}, it is possible to find the probability density function $f_{\varepsilon_i,\phi_i}(\varepsilon_i, \phi_i)$ from [102]

$$f_{\varepsilon_i,\phi_i}(\varepsilon_i,\phi_i) = \frac{f_{\theta_i,\phi_i}(\theta_i,\phi_i)}{\mid \mathbf{J}(\theta_i,\phi_i) \mid} \tag{3.45}$$

where $\mathbf{J}(\theta_i, \phi_i)$ is the Jacobian of the transformation $\theta_i = \cos^{-1}(\varepsilon_i/H_i)$ and $\phi_i = \phi_i$. The index *new* has been omitted for clarity of the expressions. The Jacobian can be evaluated to give

$$\mathbf{J}(\theta_i,\phi_i) = \begin{vmatrix} \frac{\partial\varepsilon_i}{\partial\phi_i} & \frac{\partial\phi_i}{\partial\phi_i} \\ \frac{\partial\varepsilon_i}{\partial\theta_i} & \frac{\partial\phi_i}{\partial\theta_i} \end{vmatrix} = \begin{vmatrix} 0 & 1 \\ -H_i\sin(\theta_i) & 0 \end{vmatrix} = H_i\sin(\theta_i) \tag{3.46}$$

Combining this expression with (3.45), the probability density for the random variables ε_i and ϕ_i is

$$f_{\varepsilon_i,\phi_i}(\varepsilon_i,\phi_i) = \frac{1}{4\pi H_i}. \tag{3.47}$$

The ϕ_i dependence can be integrated out and $f_{\varepsilon_i}(\varepsilon_i)$ for $|\varepsilon_i| < H_i$ follows immediately

$$f_{\varepsilon_i}(\varepsilon_i) = \int_0^{2\pi} f_{\varepsilon_i,\phi_i}(\varepsilon_i, \phi_i) d\phi_i = \frac{1}{2H_i}. \tag{3.48}$$

Since $\varepsilon_i = \varepsilon_{inew} = \varepsilon_{iold} + \Delta E$, the probability density distribution of ΔE corresponding to the change of the spin at site i is given by

$$f^i_{\Delta E}(\Delta E) = \begin{cases} \frac{1}{2H_i} & |\Delta E + \varepsilon_{iold}| < H_i \\ 0 & \text{otherwise} \end{cases} \tag{3.49}$$

Any of the spins can be chosen with equal probability and thus the probability of obtaining an energy change ΔE in the range between ΔE and $\Delta E + d\Delta E$ is equal to sum of $f^i_{\Delta E}(\Delta E)$ over all spins divided by total number of spins N

$$f_{\Delta E}(\Delta E) = \frac{1}{N} \sum_i f^i_{\Delta E}(\Delta E). \tag{3.50}$$

We now introduce N^i_{up} and N^i_{dn} using the definitions

$$N^i_{up} \equiv f^i_{\Delta E}(\Delta E_{fix}) \; ; \quad N^i_{dn} \equiv f^i_{\Delta E}(-\Delta E_{fix}) \tag{3.51}$$

and thus N_{up} and N_{dn} for a given configuration are obtained as averages over all spins

$$N_{up} = \frac{1}{N} \sum_i N^i_{up} \; ; \quad N_{dn} = \frac{1}{N} \sum_i N^i_{dn}. \tag{3.52}$$

In order to estimate the microcanonical averages we divide the energy range of interest into bins of size $\Delta E_{fix} = E_{max} - E_{min}$, where E_{max} and E_{min} are the upper and lower energy limits of a bin. The value of ΔE_{fix} is chosen to be the same value of ΔE_{fix} in the expression for the inverse microcanonical temperature $\beta(E)$ (3.40).

Starting from a configuration with its energy inside a particular bin n, a spin is chosen randomly and a new spin direction is chosen such that the energy of the new configuration stays within the bin n. This can be realized by choosing a spin direction $\vec{S}_i(\theta, \phi)$ according to the probability distribution

$$f_{\theta,\phi}(\theta, \phi) \propto \sin(\theta) \tag{3.53}$$

with θ in the range $(\theta_{min}, \theta_{max})$ and ϕ uniformly distributed in the range $(0, 2\pi)$. Here θ_{min} and θ_{max} are the lower and upper bounds for the angle θ that the spin is allowed to have relative to the local field such that the energy of the new configuration stays within the energy bin. Their values are given by

$$\theta_{min} = \cos^{-1}(-\varepsilon_{imin}/H_i) \; ; \qquad \theta_{max} = \cos^{-1}(-\varepsilon_{imax}/H_i). \tag{3.54}$$

An entire lattice sweep is performed by repeating this procedure for all spins of the system. A new starting configuration is chosen after a fixed number of sweeps in order to avoid possible correlations among consecutive configurations. This sampling procedure ensures a uniform visitation rate within a single bin, sampling all states with the same probability and satisfies the principle of detailed balance.

3.6 Finite size scaling

The modern theory of phase transitions and critical phenomena is based on the scaling properties of the free energy. A continuous phase transition is characterized by a singular behaviour of the free energy and related quantities when the system has an infinite number of particles, i.e. in the thermodynamic limit. However, in numerical simulations, one deals with systems of finite size. In these cases, mathematical singularities are modified and become regular functions. Over some region close to the critical point the singularities of the infinite system become rounded and shifted in the finite system. The amount of rounding and shifting depends on the size of the system. With increasing system size this region shrinks and in the thermodynamic limit it becomes a critical point. When interpreting Monte Carlo simulation results in the study of phase transitions, the most important task is to extrapolate the data obtained for finite systems to the thermodynamic limit. Such extrapolations are possible by using Finite Size Scaling theory (FSS) [103, 104, 108].

The theory of finite size scaling has been of great value in the quest for a better understanding of critical phenomena and phase transitions in condensed matter

physics as well as in other fields. It was introduced in the early seventies by Fisher [103, 104], Kadanoff [105] and others as a phenomenological theory. Later on, equilibrium critical phenomena and finite size scaling were explained analytically by the framework of a new theoretical approach called the 'Renormalization Group'.

In the many-body interacting system fluctuations of the microscopic degrees of freedom close to a critical point become more correlated and the distance over which microscopic order parameter fluctuations are significantly correlated is called a correlation length. The finite size scaling approach assumes that near the critical point the only significant characteristic length in the system is correlation length. The finite size effects depend upon the ratio of the linear dimension of the system to the correlation length L/ξ. Using this approach, we can obtain a very good description of the critical properties of a system by studying systems of varying finite size using Monte Carlo simulations. Finite size scaling can be used to describe both continuous and first order phase transitions.

3.6.1 Finite Size Scaling at Second Order Transitions

At a second order transition, the free energy density $f(T,h)$ for an infinite system has a singular part that can be written in the form

$$\beta f(T,h) \sim t^{2-\alpha} Y(h/t^{\Delta}) \tag{3.55}$$

where t is the reduced temperature introduced in section (2.3). The so called gap exponent Δ is related to α and γ by $\Delta = \frac{1}{2}(2-\alpha+\gamma)$ and the scaling function Y is a universal function of a single argument. The correlation length diverges at the critical point in the thermodynamic limit and the divergence is usually described by the power law form $\xi \sim |t|^{-\nu}$ where and ν is the correlation length critical exponent. Hence the above scaling form can be rewritten as

$$\beta f(T,h) \sim \xi^{(\alpha-2)/\nu} Y(h\xi^{\Delta/\nu}) \tag{3.56}$$

In a finite size system, the correlation length is limited by the system size L and the corresponding free energy density $f_L(T,h)$ is assumed to also depend on the ratio L/ξ with the scaling form

$$\beta f_L(T,h) \sim L^{(\alpha-2)/\nu} Y(L/\xi, hL^{\Delta/\nu}) \tag{3.57}$$

In the limit where $\xi = L$ and both diverge, this finite size scaling form reduces to (3.55). The arguments of the scaling function can also be written in the form $Y(tL^{1/\nu}, hL^{\Delta/\nu})$.

For finite size, the thermodynamic functions such as specific heat and susceptibility do not diverge but reach maximum values which increase with L. The positions of the maxima also shift with the value of L. Replacing the correlation length in the expression $\xi \sim |t|^{-\nu}$ by L predicts that the shift in temperature of the maxima is given by

$$T - T_c \sim L^{-\nu} \tag{3.58}$$

Binder[?] has also proposed the following scaling form for the order parameter probability distribution function $P_L(m)$ in zero field

$$P_L(m) = C(L)\tilde{P}(mL^{\beta/\nu}, L/\xi) \tag{3.59}$$

where $C(L)$ is a normalization factor.

Using the thermodynamic definitions of the various quantities introduced in section 2.1, their scaling relations are easily obtained from (3.57) by taking derivatives with respect to t and h

$$M = L^{-\beta/\nu} f_M(tL^{1/\nu}) \tag{3.60}$$

$$\chi = L^{-\gamma/\nu} f_\chi(tL^{1/\nu}) \tag{3.61}$$

$$C_V = L^{-\alpha/\nu} f_{C_V}(tL^{1/\nu}) \tag{3.62}$$

$$\rho = L^{2-d} f_\rho(tL^{1/\nu}) \tag{3.63}$$

where the magnetic field h has been set to zero and each quantity has its own universal scaling function with a single argument. At the critical point the scaling functions become constant and the prefactors describe the size dependence of the various quantities

$$M \propto L^{-\beta/\nu} \tag{3.64}$$

$$\chi \propto L^{-\gamma/\nu} \tag{3.65}$$

$$C_V \propto L^{-\alpha/\nu} \tag{3.66}$$

$$\rho \propto L^{2-d} \tag{3.67}$$

A convenient quantity for locating the critical temperature is the normalized fourth-order cumulant of the distribution (3.59)

$$U_L = 1 - < m^4 >_L /(3 < m^2 >_L^2). \tag{3.68}$$

At high T the distribution is a single gaussian and the ratio of the fourth to the second moment squared is a constant which depends on the number of components of the order parameter whereas, at $T << T_c$, the moments of the order parameter become equal and $U_L \sim 2/3$. At T_c itself U_L approaches a fixed value U^* since (3.59) and (3.68) yield the scaling form

$$U_L = \tilde{U}(L/\xi) \tag{3.69}$$

In the limit where $L \to \infty$, the arguments of the scaling functions become large and vary as a power of the argument which exactly cancels the L dependence of the prefactor in each case. For example, the scaling function for the stiffness behaves as

$$\rho \sim L^{2-d}(tL^{1/\nu})^{(d-2)\nu} \sim t^{(d-2)\nu}$$

These relations can be used to find ratios of the critical exponents, or in the case of the spin stiffness, the exponent ν directly. Once this is done, the scaling functions can be determined by collapsing the data for several different sizes onto to a universal curve.

3.6.2 Finite Scaling at First Order Transitions

In addition to studying continuous transitions which are characterized by a diverging correlation length, FSS theory can be also used for distinguishing between first and second order phase transitions [98, 97]. At a first order transition, the correlations grow but the correlation length does not diverge. Hence the size dependence of physical quantities is somewhat different from that discussed above.

At a first order transition the energy or the order parameter is discontinuous in an infinite system. In a finite system the discontinuities are rounded off and become smooth functions. The higher derivatives such as the specific heat or the susceptibility display rather broad maxima over a range in temperature $T-T_c \sim L^{-d}$. The positions of these maxima shift as the system size increases and plots of the positions of the maxima as a function of size L can be used to determine the bulk T_c. The maxima increase in height for small sizes as the correlations increase but eventually saturate since there is no divergence.

Histograms of the energy $P(E)$ are a useful way of identifying first order transitions where a double peak should be present at T_c. The peaks sharpen as the system size increases and a deep minimum between the two peaks develops.[95]

Chapter 4

FRUSTRATED ANTIFERROMAGNETS

The critical behaviour of antiferromagnets on the stacked triangular lattice (STA) geometry remains a controversial topic even after some twenty years of studies. Reviews of both the experimental and theoretical results can be found in the articles by Gaulin[24], Collins and Petrenko[38], Kawamura[10], Pelissetto and Vicari[76] and Delamotte et al[12]. In this chapter we introduce the models and describe how frustration changes the symmetry of the order parameter leading to some interesting consequences.

4.1 n-vector model

The starting point for most investigations of magnetic systems is a model of spins located at the sites of a lattice whose interactions are described by a Hamiltonian containing various terms.[23] Magnetism arises due to the exchange interaction of electron spins and is purely quantum mechanical in origin.[17] The exchange interaction involves both the Coulomb electrostatic energy and the Pauli exclusion principle and is a difference in energy between the states of a two electron system that depends solely on the exchange of coordinates of the two identical electrons. Electrons are of course quantum spin 1/2 particles but the net spin of the atoms localized at the lattice sites can have larger values. If the spin magnitude of the atom at a lattice site is sufficiently large, the interactions are commonly described in terms of a set of classical vectors as follows

$$H = -\sum_{i<j} J_{ij}\vec{S}_i \cdot \vec{S}_j. \tag{4.1}$$

where $\vec{S}_i$ is classical vector of unit length with n components describing the average spin polarization at site i and J_{ij} is strength of the exchange interaction between spins situated on sites i and j. The sum in (4.1) is over all nearest neighbour pairs. The simple Hamiltonian (4.1) only depends on the *relative* orientation of the neighbouring spin vectors and any additional effects such as spin-orbit or dipolar interactions that introduce anisotropy have to be introduced separately into the Hamiltonian. The sign of the coupling J_{ij} indicates which minimum energy state a pair of interacting spins prefers. The spins $\vec{S}_i$ and $\vec{S}_j$ favour a parallel (ferromagnetic) spin arrangement if J_{ij} is positive and an antiparallel (antiferromagnetic) arrangement if J_{ij} is negative. The classical model has the same symmetry and the same low energy excitations as the quantum mechanical analogue. Of course, the thermodynamic properties of classical and quantum systems differ at low temperatures where quantum statistics play an important role. However, at temperatures which are a significant fraction of the exchange interaction, the differences are not important. The model in (4.1) is called the n-vector model where n is the number of components of the classical vectors and it is invariant under uniform rotations of the spin system

4.2 Geometrical Frustration

The type of magnetic order favoured by a classical antiferromagnetic interaction between nearest neighbour spins suggests that an antiparallel arrangement of the magnetic moments in the lowest energy state[17] should occur. However, this type of local order cannot propagate throughout the lattice when the elementary building unit of the crystal structure is a triangle or a tetrahedron.

Examples of such crystal structures include the two dimensional triangular and kagome lattices and the three dimensional hexagonal and pyroclore lattices [22]. The

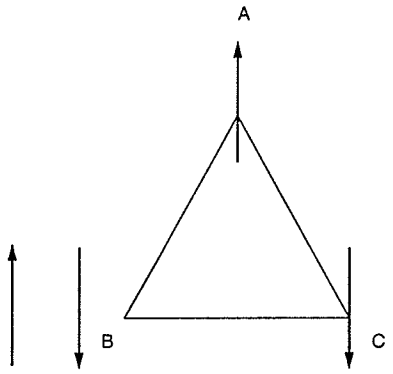

Figure 4.1: Possible ground state spin configuration of three antiferromagnetically coupled Ising spins on a triangle. Magnetic moments on sites A and C are aligned antiparallel and form state of minimum energy, but magnetic moment at site B cannot align itself antiparallel to both moments A and C simultaneously and is frustrated. As a consequence the ground state has a non-trivial degeneracy.

impossibility of assigning the lowest energy antiparallel spin configuration simultaneously to each pair of spins throughout such lattices yields interesting consequences for the equilibrium spin arrangements [10]. Consider, for example, three Ising spins ($n = 1$) located at triangular sites and interacting antiferromagnetically. Figure 4.1 illustrates the intrinsic inability of such a spin triplet to simultaneously satisfy all antiferromagnetic nearest neighbour interactions on a triangle leading to a macroscopic **frustration**[67]. In this example the frustration results in a nontrivial degeneracy of the ground state[66]. Among the 2^3 possible spin configurations of the three spins, 6 correspond to the minimum energy configuration which has two spins oriented up or down and the third in the opposite direction.

The minimum energy for such physical systems is constrained not only by external parameters such as temperature or pressure but also by the geometry of the corresponding lattice. Consequently these systems are **geometrically frustrated.**

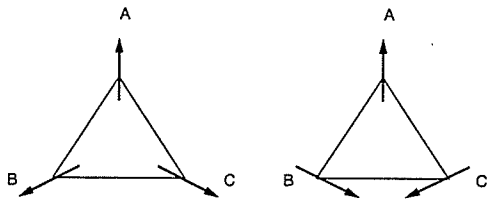

Figure 4.2: The ground state spin configuration of three antiferromagnetically coupled spins with continuous degrees of freedom on a triangle. Spins on different sublattice sites are canted and form an non-collinear ordered state.

These frustrated systems, in general, have an enlarged degeneracy of the ground state compared to non-frustrated cases.

The level of frustration also depends on the number of degrees of freedom associated with the magnetic moment. The ground state of an antiferromagnetic Ising spin model on the triangular lattice is infinitely degenerate or fully frustrated[66]. The ordering in this model is suppressed by frustration effects and the system does not exhibit a phase transition at any finite temperature. The additional degrees of freedom in the XY and Heisenberg spin models reduce the level of frustration and lift the non-trivial degeneracy. Consequently, continuous spin systems exhibit long-range magnetic order at zero temperature. However, the ground state spin configuration of these continuous spin models is non-collinear.

Figure 4.2 shows two such spin configurations on a single triangle where the spins point at an angle of 120° to one another. Comparing these two coplanar configurations, it is evident that the spin arrangements on the left and right triangles are mirror images of one another when reflected through a vertical plane. This property

can be described in terms of a chirality, or handedness. The two configurations in figure 4.2 are have opposite opposite chirality. Kawamura[11] introduced the following definition of chirality

$$\vec{K}_p = \frac{2}{3\sqrt{3}} \sum_{<ij>} \left(\vec{S}_i \times \vec{S}_j \right) \tag{4.2}$$

where the sum is over all different spin pairs on the triangular plaquette p taken in cyclic order. For Heisenberg spins, the chirality $\vec{K}_p$ is an axial vector which is normal to the spin plane formed by the three spins in the 120^0 ground state. The two possible chiralities correspond to the two possible normal directions. For XY spins , the chirality is a pseudoscalar with two possible values ± 1. The role of chirality in various continuous spin systems is considered further in the following section.

4.3 Symmetry of the ordered state and the local order parameter

Both the triangular and hexagonal (stacked triangular) lattice have triangles as the elementary units. Figure (4.3) shows a portion of a two dimensional triangular layer. The lattice is partitioned into disconnected triangular plaquettes. For simplicity the

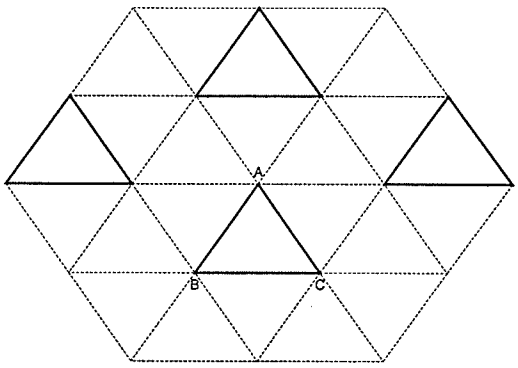

Figure 4.3: Part of a triangular lattice indicating the partition into disconnected triangular plaquettes shown by the solid lines. In the ordered state of continuous spin systems the pattern labeled A, B, C has the identical spin structure as that shown in figure 4.2 and it repeats itself periodically throughout the lattice.

following discussion refers to the two dimensional triangular lattice and will be extended to include the specifics of the three dimensional hexagonal lattice model later. In the ground state of continuous spin systems, the plaquettes have one of the equivalent spin arrangements from a manifold of minimum energy structures such as those shown in figure 4.2. The plaquettes can be considered as a basis of a new superlattice. The minimum energy structure assigned to each plaquette propagates through the triangular layer of the entire lattice resulting in a $\sqrt{3} \times \sqrt{3}$ periodicity and a chirality. This non-collinear ordering breaks the rotational symmetry of the model Hamiltonian (4.1).

The chiral degrees of freedom, or equivalently, the non-collinear order in these frustrated systems leads to important differences when compared to the unfrustrated cases. For example, the $n = 3$ Heisenberg ferromagnet has a broken symmetry where the spins align to form a collinear ground state with all spins parallel to some direction in spin space. This resulting ground state is invariant under global spin rotation about the magnetization direction. In the frustrated case, there is no such invariance. The ground state cannot be described in terms of a single vector. The 120^0 spin structure spans a two dimensional space in the $n = 3$ spin space. To describe a local order parameter of the Heisenberg model, Dombre and Read [21] fixed a reference frame on each plaquette, such that the spin vectors at the triangular vertices have the following directions

$$\vec{S}_A = (0, 1, 0)\,; \vec{S}_B = \left(-\sqrt{3}/2, -1/2, 0\right); \vec{S}_C = \left(\sqrt{3}/2, -1/2, 0\right). \tag{4.3}$$

This structure is identical to the ordered state on the left-hand side of figure (4.2) where a right-handed reference frame is used with the y axis along the spin direction at site A. Other degenerate ground states can be obtained from this reference state by a global orthonormal transformation

$$\vec{S}_i' = R\vec{S}_i \tag{4.4}$$

where R is a 3×3 rotation matrix which satisfies $R^TR = RR^T = 1$ and belongs to the $SO(3)$ rotation group. Hence the order parameter space of the frustrated Heisenberg spin model is isomorphic to the three dimensional rotational group $SO(3)$.

In the case of the frustrated XY model, the spins only have $n = 2$ components and the chirality has an Ising Z_2 symmetry[26]. The $SO(2)$ rotational symmetry of the spins in the xy plane and the Z_2 symmetry of the chirality means that the order parameter space is isomorphic to $Z_2 \times SO(2) = O(2)$ where the group $O(2)$ includes spin reflections as well as rotations.

The symmetries of these models can be discussed in terms of topological spaces[27]. Order parameter space is a topological space isomorphic to the set of ordered states of the system. It can be defined by dividing the entire symmetry group of the Hamiltonian by the subgroup which describes the broken symmetry state. The symmetry group of the Hamiltonian (4.1) is $O(n)$ which describes its invariance under uniform spin rotations and inversion. In the case of non-frustrated systems where a collinear ground state emerges, the invariant subgroup is $O(n-1)$ which corresponds to rotations about the collinear direction. Hence the order parameter space is isomorphic to the $(n-1)$-dimensional hypersphere $S_{n-1} = O(n)/O(n-1)$. In the frustrated models where the order parameter is non-collinear, the invariant subgroup is $O(n-2)$ instead of $O(n-1)$. This means that the order parameter space is $O(n)/O(n-2)$ in general. Since $O(0) = 1$ and $O(1) = Z_2$, this means that in the $n = 2$ and $n = 3$ cases we have the following order parameter spaces: for $n = 2$ it reduces to $O(2)$ whereas, for $n = 3$, it is $O(3)/Z_2 = SO(3)$ in agreement with the earlier discussion.

These differences in symmetry between the nonfrustrated and frustrated models suggest that the critical behaviour can be quite different and that the frustrated systems may belong to a new universality class[10].

4.3.1 Topological defects in frustrated antiferromagnets

The order parameter space of the frustrated Heisenberg model is isomorphic to the rotational group $SO(3)$ and can be regarded as the surface of a four dimensional hypersphere with identified antipodal points. Application of homotopy theory to the parameter space $SO(3)$ yields the following homotopy groups[1]

$$\pi_0(SO(3)) = 0, \quad \pi_1(SO(3)) = Z_2, \quad \pi_2(SO(3)) = 0 \tag{4.5}$$

implying the existence of a topologically stable point defect (vortex) corresponding to the two element group Z_2. This vortex is different from the Z-vortex predicted for XY systems. The existence of a stable topological defect for the frustrated Heisenberg case suggests the possibility of a purely topological phase transition for the two dimensional lattice [1, 7, 3, 4].

In the case of the stacked triangular geometry in three dimensions, the point defects described above will appear as line defects. The role that they play in the ordering process is one of the questions that we wish to investigate in this thesis.

4.4 Experimental studies of frustrated magnetic materials

There are several experimental realizations of the stacked triangular geometry in which the exchange interactions are antiferromagnetic. Examples include the ABX_3 -type compounds where A is an element such as Cs or Rb, B is a magnetic ion such as Mn, Cu, Ni or Co, and X is a halogen such as Cl, Br or I. Another group that has been investigated is the vanadium dihalides which include VCl_2 and VBr_2 as examples. For most of these materials, the Hamiltonian is not completely isotropic and the additional anisotropic terms can confine the spins to be in the plane normal to the c axis or parallel to it. The Hamiltonian for the stacked triangular materials takes the form[38]

$$H = -J' \sum_{i<j}^{chains} \vec{S}_i \cdot \vec{S}_j - J \sum_{k<l}^{planes} \vec{S}_k \cdot \vec{S}_l - D \sum_i (S_i^z)^2 - \sum_i \vec{H} \cdot \vec{S}_i \tag{4.6}$$

where first sum is along chains of spins situated in different triangular planes with a coupling constant J', the second sum is over neighbouring spins within the triangular planes with coupling J, the third term represents a single ion anisotropy with anisotropy constant D and fourth term is the Zeeman energy of the spins in the presence of an external field $\vec{H}$. In some cases the exchange along the chains is dominant and the materials exhibit a quasi-1d behaviour whereas, in other cases, the exchange interactions within each plane are dominant and the materials form quasi-2d systems. If the anisotropy constant $D > 0$, this favours an alignment of the spin moments perpendicular to the triangular planes whereas $D < 0$ favours the confinement of the spins in the planes. In both cases the Heisenberg symmetry is broken. The latter case $D < 0$ changes the symmetry of the ordered phase to XY. In addition to the single-ion anisotropy D, these materials may also have exchange anisotropy with the isotropic exchange term replaced by

$$H = -J \sum_{k<l} (S_k^x S_l^x + S_k^y S_l^y + A S_k^z S_l^z) \tag{4.7}$$

where the parameter A is the exchange anisotropy. Values of $A > 1$ favour an easy axis whereas $A < 1$ favours the xy plane.

Magnetic neutron scattering and specific heat measurements on these systems have revealed the occurence of finite temperature phase transitions which appear to be continuous. Some materials have large values of the anisotropy D which favours either Ising ($n = 1$) or XY ($n = 2$) symmetries. Other materials have relatively small values of D compared to the exchange terms and should therefore behave more like the Heisenberg model ($n = 3$).

Table 4.1 gives a summary of some of the experimentally measured values of the critical exponents for systems which are expected to have an XY model symmetry. The values of the exponents in table 4.1 are clearly different from those expected for the $d = 3$ XY ferromagnet with $O(2)$ symmetry. Delamotte et al[12] have recently suggested that the experimental values are not at all consistent with a continuous

Material	Ref.	α	β	γ	ν
$CsMnBr_3$	[78]		0.22(2)		
	[79]		0.25(1)		
	[80]		0.24(2)		
	[81]		0.21(2)	1.01(8)	0.54(3)
	[82]			1.10(5)	0.57(3)
	[83]	0.39(9)			
	[84]	0.40(5)			
$RbMnBr_3$	[86]		0.28(2)		
	[85]	0.22-0.42			
$CsCuCl_3$	[87, 88]		0.25(2)		
O(2)	[77]	-0.0146(8)	0.3485(2)	1.3177(5)	0.67155(27)

Table 4.1: Experimental values for the critical exponents for STA XY antiferromagnets. The last line is the field theory results for the $O(2)$ Heisenberg universality class

transition. They have used the scaling law $\eta = 2\beta/\nu - 1$ to estimate the anomalous dimension η which characterizes the decay of the correlation function at T_c and find it to be negative. They argue that η should be positive for a true second order phase transition and conclude that the entire class of materials exhibit weak first order transitions.

Table 4.2 gives a summary of some of the experimentally determined critical exponents for materials that behave as Heisenberg antiferromagnets (or nearly Heisenberg). The values of the exponents in table 4.2 vary somewhat from material to material. This can be due to the presence of various types of anisotropies which may change the universality class. However, the values of the exponents do not belong

Material	Ref.	α	β	γ	ν
VCl_2	[68]		0.20(2)	1.05(3)	0.62(5)
VBr_2	[69]	0.30(5)			
$CsNiCl_3$	[70, 73]	0.25(8)			
	[71]	0.23(4)			
	[72]		0.28(3)		
$RbNiCl_3$	[75]		0.28(1)		
$CsMnI_3$	[70]	0.28(6)			
O(3)	[74]	-0.1336(15)	0.3689(3)	1.3960(9)	0.7112(5)

Table 4.2: Experimental values for the critical exponents for STA Heisenberg (or nearly Heisenberg) antiferromagnets. The last line is the field theory results for the $O(3)$ Heisenberg universality class

to any of the well known Wilson-Fisher universality classes and are clearly different from those of the $d = 3$ $O(3)$ ferromagnetic Heisenberg model. The experimental values strongly suggest that these frustrated materials belong to a new universality class if the transitions are indeed continuous. Delamotte et al[12] have again argued that these exponents cannot describe a true second order phase transition. Although there are fewer measurements for the Heisenberg-like materials, they conclude that the anomalous dimension η is again negative and that all of the STA materials undergo weakly first order transitions in $d = 3$ with effective exponents.

4.5 Chiral universality class

The first theoretical prediction of a new universality class for frustrated antiferromagnets on the stacked triangular geometry was made by Kawamura[25, 43, 44] based on an analysis of the symmetry of the ground state for both XY and Heisenberg spin

Model	Ref.	α	β	γ	ν
XY	[11, 43]	0.34(6)	0.253(10)	1.13(5)	0.54(2)
	[89]	0.46(10)	0.24(2)	1.03(4)	0.50(1)
	[90]	0.43(10)			0.48(2)
Heisenberg	[11, 25]	0.240(80)	0.300(20)	1.170(70)	0.590(20)
	[91]	0.242(24)	0.285(11)	1.185(3)	0.586(8)
	[92]	0.245(27)	0.285(11)	1.176(26)	0.585(9)
	[15]	0.230(30)	0.280(15)		0.590(10)
	[33]				0.589(7)

Table 4.3: Numerical values for the critical exponents for STA XY and Heisenberg antiferromagnets.

models. The rather unusual symmetry of the order parameter lead Kawamura to conjecture that these system exhibit a novel kind of phase transition due to the presence of chiral degrees of freedom and possibly belong to the new universality class named *the chiral universality class.* Monte Carlo simulations supported this idea since the measured critical exponents for both XY ($n = 2$) and Heisenberg ($n = 3$) models were quite different from those of the standard $O(n)$ model. A variety of Monte Carlo methods have been used by other authors and the majority of these calculations predict a continuous phase transition in $d = 3$ with novel exponents. Table 4.3 gives a list of the critical exponents which have been calculated using Monte Carlo methods for both the XY and Heisenberg cases.

4.6 The field theoretical approach to frustrated spin systems

Experimental measurements and Monte Carlo simulations provide detailed information about phase transitions in specific materials and in the simplified models used

to describe them. Another approach that has been quite successful for understanding the physics of critical phenomena is the field theoretical renormalization group (RG). This has been especially true for systems described by $O(n)$ symmetry in dimension d which are described by the so-called Wilson-Fisher universality classes. The critical properties vary smoothly with dimension between $d = 2$ and $d = 4$ and become mean field-like for $d > 4$.

There are three basic field theory approaches to describing the physics behind critical phenomena. These are: i) the Landau-Ginzburg-Wilson (LGW) method which expands the free energy in powers of the order parameter as well as the dimension $d = 4 - \epsilon$, ii) the non-linear sigma model (NLσ) which expands the free energy about the low temperature ordered state and is essentially a low T expansion about the dimension $d = 2 + \epsilon$, and iii) the effective average action method which is a nonperturbative method based on the idea of block spins and integrates out short wave length fluctuations progressively to obtain the long distance behaviour.

All of these methods have been used to study frustrated systems with the aim to understand the nature of the transition in the physical dimension $d = 3$. Generally, the frustrated models have a larger degree of symmetry breaking compared to ferromagnetic models. Lower symmetry means that the effective Hamiltonian describing these the frustrated systems have more coupling constants and hence the RG flow takes place in a multi-dimensional space. There can be several attracting fixed points with quite different behaviour and exponents. Thus the concept of universality is nontrivial since the critical behaviour depends on the domains of attraction of the various fixed points. The success of these methods for ferromagnetic models is primarily due to the fact that the symmetry is higher and the number of coupling constants is reduced to essentially a single constant. The RG flow is very simple and does not change in the range of dimensions from $d = 2$ to $d = 4$. However, it is not obvious that such a simple picture will emerge in the case of the lower symmetry frustrated models.

The results of each of these approaches are somewhat contradictory. In the sections that follow we will briefly outline each method and its predictions for the frustrated triangular antiferromagnets.

4.6.1 Continuum limit description of frustrated systems

The field theories use the continuum limit of the lattice model Hamiltonian in order to study its long distance behaviour. In the simpler example of ferromagnetic systems, the continuum limit is achieved by letting the spins fluctuate around their common expectation value. Considering small long wavelength fluctuations only, the scalar product $\vec{S}_i \cdot \vec{S}_j$ can be approximated by a quadratic term in $(\nabla S(x))^2$ yielding the continuum limit Hamiltonian

$$H \sim constant + \int d^D (\partial \vec{S})^2 \tag{4.8}$$

with the constraint that $\vec{S}^2 = 1$. Frustrated magnets differ in many ways from these conventional non-frustrated magnets. The magnetic frustration affects the minimum energy spin structure resulting in a non-collinear or canted spin structure in the ordered state of models with continuous spin symmetry. As opposed to non-frustrated spin system where both the fluctuating fields at short distances (on the scale of the lattice spacing) and the long wavelength fluctuations are described in terms of the same quantity, i.e. the spin vector, the fluctuating fields of frustrated magnets on short and long length scales differ. The relevant low energy fluctuating field is the order parameter, which is rotation matrix R belonging to $SO(3)$ in the case of Heisenberg spins, while on the scale of lattice spacing the fluctuating field is the spin vector.

Identifying the proper order parameter is important in order to derive the effective action $\mathcal{S}$ of frustrated systems. It is convenient to identify a superlattice such as the one described in section 4.3 and consider the basic building block as a plaquette of three spins. On each elementary plaquette of the superlattice, an orthonormal basis

$\mathbf{e}_a(x)$ can be defined such that

$$\mathbf{e}_a(x) \cdot \mathbf{e}_b(x) = \delta_{ab}; \qquad a, b = 1, 2, 3 \tag{4.9}$$

where x is the superlattice index. Then each spin $\mathbf{S}^\alpha$ belonging to the plaquette can be expressed as linear combination of these three vectors as follows

$$\mathbf{S}^\alpha(x) = \sum_a C_a^\alpha(x)\mathbf{e}_a(x). \tag{4.10}$$

It is important to note that all spins $\mathbf{S}^\alpha$ in the ground state are not independent, and the linear combinations of the $\mathbf{S}^\alpha$ that yield a zero expectation value in ground state can be excluded as part of order parameter. These linear combinations correspond to the spin motions within an elementary plaquette. They have short range correlations and thus are irrelevant to the long range critical behaviour. They can be ignored by imposing the constraint that locally (within each plaquette) the spins are in their ground state configuration $S_A + S_B + S_C = 0$. Hence the order parameter is the orthonormal basis $\{\mathbf{e}_a(x)\}$ defined on each plaquette. The effective action $\mathcal{S}$ can be obtained through the gradient expansion of the $\mathbf{e}_a$ in the same way as it is done for a spin vector order parameter in (4.8). The continuum limit action for the frustrated Heisenberg antiferromagnet can be written as

$$S \sim \int d^D x \sum_{a=1}^{3} p_a(\partial \mathbf{e}_a(x))^2. \tag{4.11}$$

where the fields $\mathbf{e}_a$ are constrained to be orthogonal as in (4.9) and the p_a are the coupling constants. Note that three of them are needed for this $SO(3)$ frustrated system.

4.6.2 The Nonlinear Sigma ($NL\sigma$) model approach

The $NL\sigma$ model expands about a low temperature broken symmetry phase of the system. It is a perturbative approach in both temperature and dimension. Since the lower critical dimension for continuous spin models is $d = 2$, it is a low temperature

expansion around two dimensions. The first quantum $NL\sigma$ model relevant to the frustrated Heisenberg model was derived by Dombre and Read [21]. Azaria et al [7] studied the $(NL\sigma)$ model in the classical limit using the expansion technique in $d = 2 + \epsilon$. They found that system has an enlarged symmetry. The symmetry breaking scheme $(O(3) \times O(2))/O(2)$ is enlarged to $(O(3) \times O(2))/O(3)$ or equivalently $O(4)/O(3)$. At the scale of the lattice the coupling constants in (4.11) are $p_3 = 0$ and $p_1 = p_2$ but under the rescaling transformation they approach a higher symmetry fixed point with $p_1 = p_2 = p_3$. Hence the $NL\sigma$ model relevant to frustrated magnets corresponds to the same symmetry breaking scheme as for the non-frustrated 4-component vector model. This approach suggests that the critical properties between 2 and 4 dimensions should be governed by the standard $O(4)/O(3)$ universality class. These findings are in strong disagreement with both experimental and numerical results. It is important to note as well that properties of this approach depend only on the local properties of the coset, usually denoted as G/H where G and H are symmetry groups of the high and low temperature phase, excluding its global structure and the topological properties of these spaces.

4.6.3 Landau-Ginzburg-Wilson (LGW) model approach

In the *LGW* model approach, the constraint (4.9) is replaced by an appropriate potential. In the RG analysis, expansions are carried out around dimension 4, $\epsilon = 4 - d$ or in terms of a $1/n$ expansion where n is number of spin components. With the potential included, the Hamiltonian can be written in terms of spin variables of unconstrained length. The action $\mathcal{S}$ when the field $\mathbf{e_3}$ is integrated out due to the constraint $\mathbf{e_3} = \mathbf{e_1} \wedge \mathbf{e_2}$ can be written as

$$S \sim \int d^D x((\partial \mathbf{e}_1)^2 + (\partial \mathbf{e}_2)^2) + V(\mathbf{e}_1, \mathbf{e}_2). \tag{4.12}$$

The potential $V(\mathbf{e}_1, \mathbf{e}_2)$ is chosen such that it disfavors field configurations that do not satisfy (4.9). This approach does not yield a stable fixed point for the case of three

dimensional spin systems with $n = 2, 3$. The naive extrapolation of the expansions at the lower critical dimension ($d = 2$) and the upper critical dimension ($d = 4$) to the $d = 3$ are contradictory in the case of frustrated Heisenberg magnets. The existence of a nontrival fixed point in $NL\sigma$ $d = 2 + \epsilon$ expansion and the absence of such point in LGW $d = 4 - \epsilon$ expansion cannot be reconciled.

The perturbative field theories obtained using a low temperature expansion about $d = 2$, a weak coupling expansion around $d = 4$ or a large n-expansion all fail to describe the physics of the physical $n = 2, 3$ frustrated models in $d = 3$. The stability and existence of various fixed points depends on the value of the number of spin components n as well as the dimension d. There is no smooth interpolation of the results between $d = 2$ and $d = 4$.

There have also been studies based on the LGW model in fixed dimension $d = 3$ to higher order perturbation theory in the coupling constants. Calabrese et al[94] have used six-loop RG expansions to study the RG flows for arbitrary values of n and they find three distinct types of behaviour. For values of $n > n_{c1} = 6.4(4)$ they find that the transition is continuous and described by a stable chiral fixed point that is related to earlier work using the $d = 4 - \epsilon$ and $1/n$ expansions. On the other hand for $n_{c1} > n > n_{c2} = 5.7(3)$, they do not find any evidence of a stable fixed point and conclude that the transition is first order for values of n in this range. In the range $n < n_{c2}$, there is a chiral fixed point which is quite distinct from that found in the range $n > n_{c1}$. The RG trajectories approach the fixed point in a spiral-like manner and the transition is continuous. This range corresponds to the physical values $n = 2, 3$ and the authors speculate that the peculiar approach to the fixed point could lead to a rather complicated crossover phenomena with exponents that vary in a nonmonotonic way. They conclude that this may explain the variation of the measured exponents from material to material as well as the apparent negative values for the exponent η.

4.6.4 Non-perturbative approach

The non-perturbative approach is also based on the Wilson renormalization group idea and is called the effective average action method[12]. This method is non-perturbative in both temperature and the coupling constants. It is able to recover the perturbative results at the upper ($d = 4$) and lower ($d = 2$) critical dimensions as well as some non-perturbative features involving topological excitations. The method identifies a breakdown of the NLσ model approach as a function of d. The $O(4)$ fixed point found by Azaria et al[7] collapses with another unstable fixed point at $d_c \sim 2.87$. Hence the transition in $d = 3$ is found to be of first order, with very large correlation length ξ. The large correlation length and the proximity of d_c to $d = 3$ suggest that a pseudoscaling behavior occurs due to a very slow flow of the RG trajectories. and that an "almost second-order phase transition" should be observed.

It is clear that the perturbative approach used in the NLσ model does not include topologically nontrivial states. However, it is not at all clear how these effects are taken into account in the non-perturbative approach. The separation of the effects of vortices and spin waves on the critical properties of frustrated magnets remains a challenging problem.

Chapter 5

FINITE NUMBER OF TRIANGULAR LAYERS

5.1 Introduction

The behaviour of the Heisenberg antiferromagnet on triangular geometries is quite unusual. One might have guessed that the physics of the Heisenberg model in $2d$ would be quite uninteresting since it has been shown that there is no long range order at finite temperature in systems with a continuous symmetry(Peierls[?], Mermin and Wagner 1966 [5] , Hohenberg 1967 [6]). In $d = 2$, however, there is a finite temperature vortex unbinding transition which is purely topological in character[1, 2, 3, 4]. Both above and below this temperature the spin-spin correlation function decays exponentially with distance. This behaviour is quite different from that which occurs in the Kosterlitz-Thouless transition[29, 30] which occurs in two-dimensional XY models including $2d$ XY magnets, $2d$ superconductors and superfluids. In these cases the correlations are exponential at high T and decay with a power law at all temperatures below the transition. There is no long range order but there is a finite spin wave stiffness in the low temperature phase. The specific heat exhibits a maximum at a temperature above the transition but no apparent singular behaviour when the power law decay sets in. In the Heisenberg antiferromagnet, both the sublattice magnetizations *and* the spin wave stiffness are zero at *all* finite temperatures. On the other hand the vorticity modulus is nonzero at low T and drops to zero at the transition. Hence the phase transition is similar to the Kosterlitz-Thouless transition in that vortices are involved but it is different in that the correlations decay exponentially at all finite temperatures.

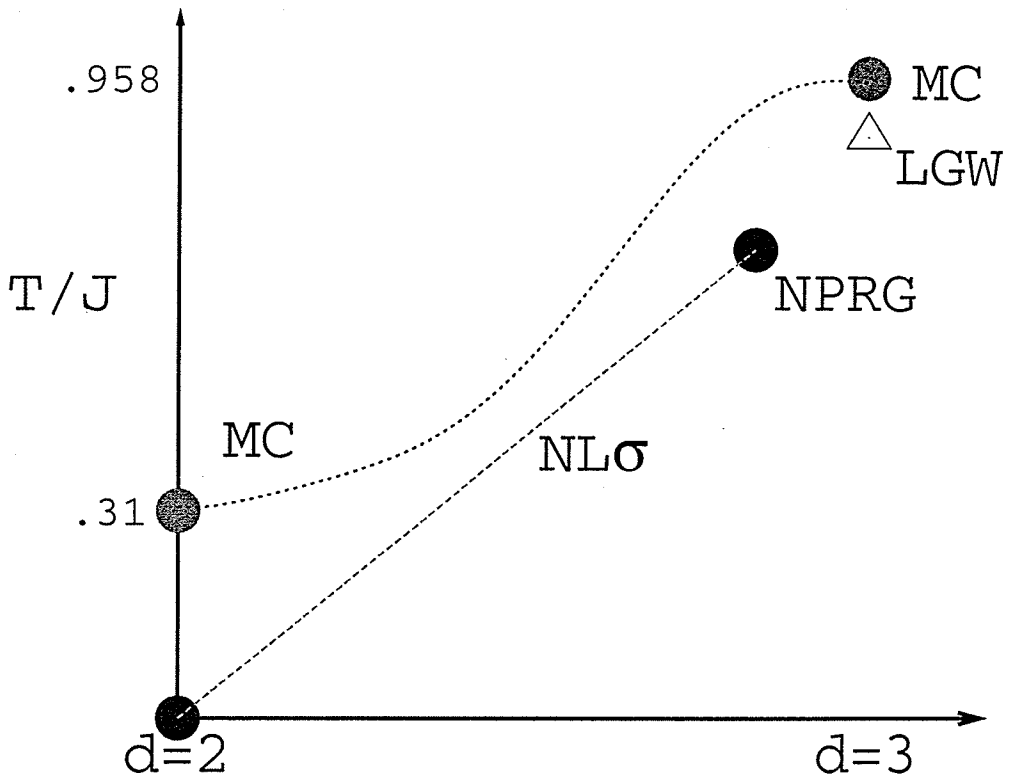

Figure 5.1: Schematic phase diagram of the isotropic Heisenberg antiferromagnet between dimensions $d = 2$ and $d = 3$.

Field theoretic studies of this model in terms of the nonlinear sigma model ($NL\sigma$) predict that there is only a transition at $T_c = 0$ in two dimensions. This latter approach is basically a low T perturbation expansion about the ground state and does not include topological defects. In $d = 3$ both theory and experiment indicate that there is a conventional phase transition with the appearance of an order parameter below the critical temperature. However there is a great deal of debate about the nature of this transition. Monte Carlo studies indicate a continuous transition which belongs to a new chiral universality class whereas early RG studies indicated

a first order transition. The experimental studies of these three dimensional stacked triangular systems find that they exhibit a continuous phase transition with a set of critical exponents that do not belong to any of known universality classes . Numerical studies of the model on the hexagonal lattice also indicate that the system exhibits a continuous phase transition that cannot be described by the Heisenberg universality class [11, 33]. On the other hand, non-perturbative RG (NPRG) studies indicate a phase transition which is very weakly first order with effective exponents [13, 12]. A very recent numerical study of RG flow in the LGW Hamiltonian by Itakura [16] also suggests a possible weak first order transition for the Heisenberg spin model but with much stronger evidence for a first order transition in the case of XY spins.

Figure 5.1 shows a schematic phase diagram in the T vs d plane. In this diagram the results of the various approaches that have been used to study the phase transition between two and three dimensions are summarized. The numerical Monte Carlo simulation results are labeled MC and, as discussed in the previous chapter, they suggest the existence of a phase transition at finite temperature in both the two dimensional triangular lattice and the three dimensional stacked triangular lattice. The phase transition in two dimensions is purely topological in character, whereas in three dimensions, it is a conventional second order transition belonging to a new chiral universality class. The prediction of a stable chiral fixed point in the Landau-Ginzburg-Wilson renormalization group approach in fixed dimension $d = 3$ is labeled by LGW. The notation NLσ denotes the low temperature expansion results of the $d = 2 + \epsilon$ perturbative approach which connects the predicted zero temperature transition in $d = 2$ with the limiting value at $d_c < 3$ predicted by the non-perturbative RG approach (NPRG) . The dashed curve connecting the Monte Carlo results in $d = 2$ with those in $d = 3$ is the subject of investigation in this chapter. In particular we are interested in how the topological transition in $d = 2$ evolves as the number of triangular layers is increased.

Two important questions that can be asked are:

- How does the $d = 2$ behaviour cross over to the $d = 3$ behaviour?
- What is the nature of the transition in $d = 3$?

In this chapter we explore the first of these questions. The second question will be explored later in chapters 6 and 7. In order to explore the crossover of the $d = 2$ behaviour to $d = 3$, we will study the nature of the ordering process of a layered triangular system having dimensions $L \times L \times H$ with the number of stacked triangular layers ranging from $H = 2$ to $H = 24$ and the linear size of each layer L ranging from 18 to 120 by means of Monte Carlo simulations. In what follows, we shall see that the layered system exhibits a crossover from two to three dimensional behaviour as the number of layers increases. We observe that the two dimensional behaviour in the system persists for an arbitrary number of layers provided that H $\ll$ L and one is sufficiently close to the critical temperature. When H becomes large and proportional to L the system exhibits a conventional three-dimensional transition with an order parameter which vanishes continuously at the transition.

5.2 Model and Methods

We consider an isotropic Heisenberg model of classical spins interacting via nearest neighbour exchange on a layered triangular lattice described by the following Hamiltonian

$$H = -\sum_{i<j} J_{ij} \vec{S}_i \cdot \vec{S}_j \tag{5.1}$$

where $\vec{S}_i$ is a classical three component vector of unit length and J_{ij} is the strength of the exchange interaction between spins situated at sites i and j. Within each triangular layer the spins interact antiferromagnetically $J_{ij} < 0$. Between adjacent layers the interaction can be taken to be positive or negative with no essential difference since there is no frustration associated with these interactions and hence there is a symmetry with respect to the sign. We shall choose it to be ferromagnetic $J_{ij} > 0$

so that we do not have to work with a larger number of sublattices. In the following we set $|J_{ij}| = J = 1$ for all interactions and both energy and temperature will be measured in units of J.

The layered geometry has dimensions $L \times L \times H$ where each triangular plane has L^2 sites and the system has a finite thickness H such that $H \ll L$. We perform our numerical simulations using the heat bath Monte Carlo method described in chapter 3. We calculate a number of thermodynamic quantities including the sublattice magnetization, the specific heat, the spin stiffness as well as the response of the system to an isolated vortex. From this vorticity response we extract a vorticity modulus. The ground state of the system is described by a wavevector $\mathbf{Q} = (4\pi/3, 0, 0)$ which corresponds to three sublattices of spins oriented at 120^0 to one another in a plane and located at the vertices on each elementary triangle. The spin plane can be oriented in any direction in space since the spin and lattice spaces are independent. Periodic boundary conditions are applied in the plane of each triangular layer where, in order to preserve the 3-sublattice structure, it is important to choose L to be a multiple of 3. The finite layer thickness, H, can have any integer value since we have chosen the inter-planar interactions to be ferromagnetic. The top and bottom surface layers are subject to free boundary conditions.

The spin stiffness [7], or helicity modulus, is a measure of the increase in free energy associated with a twisting of the order parameter in spin space by imposing a gradient of the twist angle about some axis $\hat{n}$ in spin space along some direction $\hat{u}$ in the lattice. The spin stiffness can be written as a second derivative of the free energy with respect to the strength of the gradient and can be calculated as an equilibrium response function. The spin stiffness corresponding to twists about an arbitrary axis $\hat{n}$ in spin space has been derived in appendix A and has the form

$$\rho_{\hat{n}} = -\frac{1}{HL^2} \sum_{i<j} J_{ij} (\hat{e}_{ij} \cdot \hat{u})^2 \left\langle (\vec{S}_i \cdot \hat{n})(\vec{S}_j \cdot \hat{n}) - \vec{S}_i \cdot \vec{S}_j \right\rangle$$

$$-\frac{1}{HL^2T}\left\langle\left[\sum_{i<j}J_{ij}(\hat{e}_{ij}\cdot\hat{u})\hat{n}\cdot(\vec{S}_i\times\vec{S}_j)\right]^2\right\rangle \tag{5.2}$$

where $\hat{e_{ij}}$ is unit vector directed along the nearest neighbour bond from site i to j, $\hat{u}$ is a gradient direction in lattice and $\hat{n}$ denotes the axis in spin space about which a twist is imposed. The volume factor L^d is replaced by HL^2 in the present geometry. Diagonal elements of the spin wave stiffness tensor can be calculated by choosing an orthogonal triad for the directions of three principal axis in spin space. The symmetry of the ground state suggests that two of the principal axes correspond to two perpendicular directions $\hat{\perp}_1$ and $\hat{\perp}_2$ in the spin plane and that the third is perpendicular to this plane [1]. This third axis is conveniently chosen to point along the average chirality direction $\hat{K}$. Here chirality is defined on each disconnected triangle of the triangular planes containing sites that belong to three different sublattices A, B and C at the vertices as follows

$$\vec{K}_\triangle = \vec{S}_A\times\vec{S}_B + \vec{S}_B\times\vec{S}_C + \vec{S}_C\times\vec{S}_A. \tag{5.3}$$

The other quantity of interest when topological properties of the system are to be considered is the vorticity [2]. The vorticity is a measure of the response of the spin system to an imposed twist about an given axis $\hat{n}$ in spin space along a closed path that encloses a vortex core. The vorticity can be calculated as the second derivative of the free energy with respect to the strength of the vortex, or winding number m, when $m = 0$. As described in chapter 2 and appendix B, the vorticity about an arbitrary direction $\hat{n}$ in spin space is

$$\begin{aligned} V_{\hat{n}} = &-\frac{1}{H}\frac{\sqrt{3}}{4\pi}\sum_{i<j}J_{ij}\left(\frac{\hat{e}_{ij}\cdot\hat{\phi}_i}{r_i}\right)^2\left\langle(\vec{S}_i\cdot\hat{n})(\vec{S}_j\cdot\hat{n})-\vec{S}_i\cdot\vec{S}_j\right\rangle \\ &-\frac{1}{H}\frac{\sqrt{3}}{4\pi}\left\langle\left[\sum_{i<j}J_{ij}\left(\frac{\hat{e}_{ij}\cdot\hat{\phi}_i}{r_i}\right)\hat{n}\cdot(\vec{S}_i\times\vec{S}_j)\right]^2\right\rangle \end{aligned} \tag{5.4}$$

where r_i is the distance of site i from the vortex core and $\hat{\phi}_i$ is tangent to the circular path in the lattice passing through site i and enclosing the vortex core, $\hat{e_{ij}}$ and $\hat{n}$ have

[1] In the ground state all spins lie in a plane which is perpendicular to the chirality vector.

the same meaning as in expression (5.2). The vorticity $V_{\hat{n}}$ contains a contribution due to the vortex core as well as part which is proportional to $\ln(L/a)$. This can be written as

$$V_{\hat{n}} = C_{\hat{n}} + v_{\hat{n}} \ln(L/a). \tag{5.5}$$

where $C_{\hat{n}}$ is a temperature dependent constant describing the core and $v_{\hat{n}}$ is called the vorticity modulus. It plays a similar role to the spin stiffness and vanishes at a phase transition. It can be extracted from the raw vorticity data by comparing the results obtained for different sizes L of the system. We use following comparison of the pair of sizes L_1 and L_2 to extract the vorticity modulus

$$v_{\hat{n}}(L_1, L_2) = \frac{V_{\hat{n}}(L_1) - V_{\hat{n}}(L_2)}{\ln(L_1) - \ln(L_2))} \tag{5.6}$$

The final value of the vorticity modulus $v_{\hat{n}}$ is obtained as an average over all pairs of linear sizes.

We also calculate an order parameter given as

$$M = \frac{1}{N}\sqrt{3\sum_{i=1}^{3} M_i^2} \tag{5.7}$$

where M_i is total sublattice magnetizations of sublattice i.

5.3 Results

It has been proven by Mermin and Wagner [40, 5] and Hohenberg[6] that conventional long range order in two dimensional systems with continuous spin degrees of freedom is destroyed by spin wave excitations. This means that in two dimensional systems an order parameter such as the magnetization is zero in the thermodynamic limit at any finite temperature. Systems of finite size L should exhibit strong finite size effects at all T. In figure 5.2 the temperature dependence of the magnetization for a two layer system ($H = 2$) is shown. The results clearly indicate that magnetization of the layered triangular lattice does indeed tend to decrease with increased size L down to

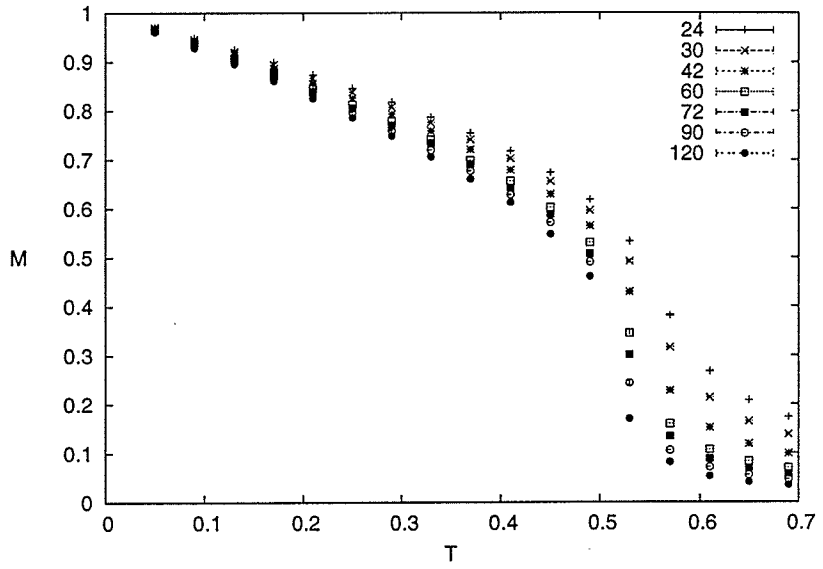

Figure 5.2: Staggered magnetization of a $L \times L \times 2$ lattice shows a strong size dependence on L at any finite temperature T.

the lowest temperatures studied in the simulation. This behaviour is consistent with the absence of a finite temperature phase transition. The finite size effects are largest near $T \sim .52$ which coincides with the temperature of the specific heat maximum.

The specific heat for a number of different linear sizes L in the case of a $H = 2$ and $H = 8$ layer system are shown in figures 5.3 and 5.4 respectively. The peaks saturate with increased system size L indicating a non-divergent specific heat. The specific heat peaks sharpen and move toward higher temperatures as the thickness H increases. The temperature T_c indicated in the figures lies below the peak temperature and indicates where a topological phase transition occurs. Similar behaviour occurs at the Kosterlitz-Thouless phase transition, where a nonuniversal specific heat peak is associated with the entropy liberated by unbinding of vortex pairs [23]. The nature of the transition at T_c will be described in more detail below.

The sublattice magnetization and specific heat results shown in figures 5.2,5.3

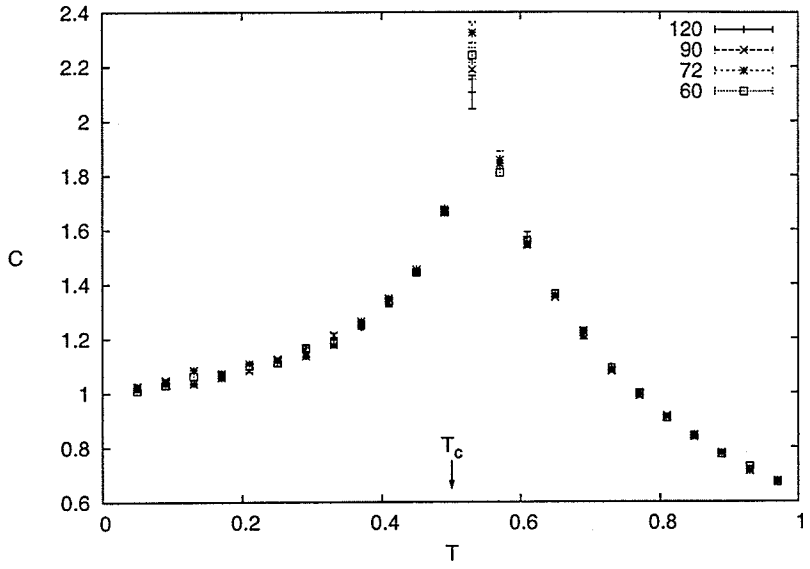

Figure 5.3: Specific heat of a $L \times L \times 2$ layered system. The peak saturates with increased system size L.

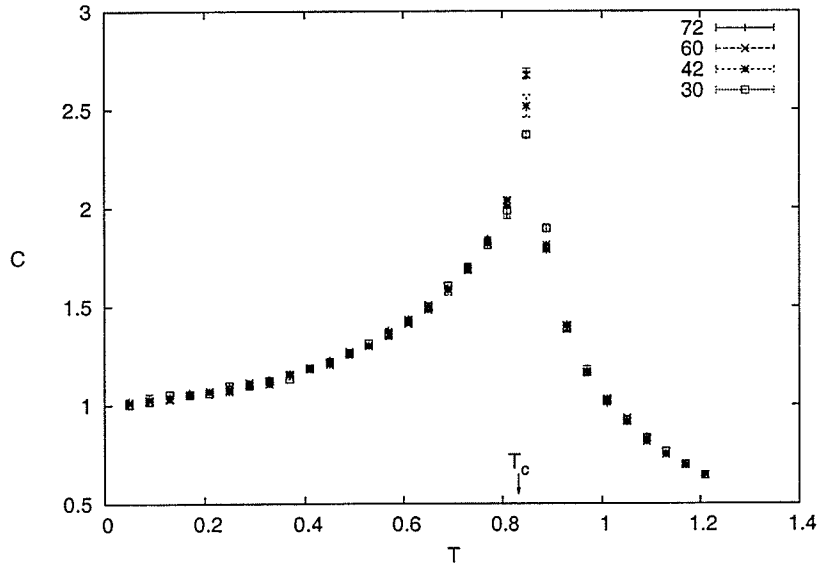

Figure 5.4: Specific heat of a $L \times L \times 8$ layered system. The peak is sharper than for the 2-layer system but it still saturates with increasing layer size L.

and 5.4 show no indication of a finite temperature phase transition. We have also studied the spin stiffness and the temperature dependence of the three principal spin wave stiffness coefficients are shown in figure 5.5. The vertical axis is the stiffness $\rho_{\hat{n}}$ calculated using equation (5.2) and the horizontal axis is the temperature T in units of $J = 1$. Both $\rho_{\hat{1}_1}$ and $\rho_{\hat{1}_2}$ correspond to twists about axes in the plane of the spin ordering whereas $\rho_{\hat{K}}$ measures the stiffness about the average chirality direction which is normal to the spin plane. At very low temperatures the stiffnesses approach the values $\rho_{\hat{K}} = 2\rho_{\hat{1}_1} = 2\rho_{\hat{1}_2} = 3/4$. [2] The stiffnesses show a strong size dependence at all temperatures, decreasing with an increase in the planar dimension L. As discussed previously in chapter 2, the $d = 2$ Kosterlitz-Thouless transition is characterized by a universal value of the ratio $\rho/T = 2/\pi$. In the present layered geometry, this expression would be modified to $\rho/T = 2/(\pi H)$. The dotted line in the figure is the corresponding line for two layers and has slope $1/\pi$. It intersects the stiffness data at a temperature near the specific heat maximum. However, the large finite size effects at all T are consistent with the absence of spin stiffness at all finite temperatures and would seem to indicate that there is no phase transition.

Azaria *et al.* [7] have made detailed predictions for the dependence of these stiffnesses on the linear size of the system for single layers based on the continuum limit of this model. Their results for a nonlinear sigma model (NLσ) using renormalization group (RG) techniques showed that the spin wave stiffness of the triangular antiferromagnet is a nontrivial function of $\ln(L)$ at low temperatures where L is the linear dimension of triangular lattice. At any finite temperature T, the stiffnesses are zero on length scales large compared with the correlation length. However, on length scales $1 \ll L \ll \xi$, the stiffnesses are nonvanishing at low T. The asymptotic scaling expressions for the spin wave stiffness tensor derived by Azaria *et al.* [7] in our notation

[2] The normalization of the stiffnesses differs from that used by Southern and Young[34] by a factor $\sqrt{3}/2$ which is the area per site in the triangular layers.

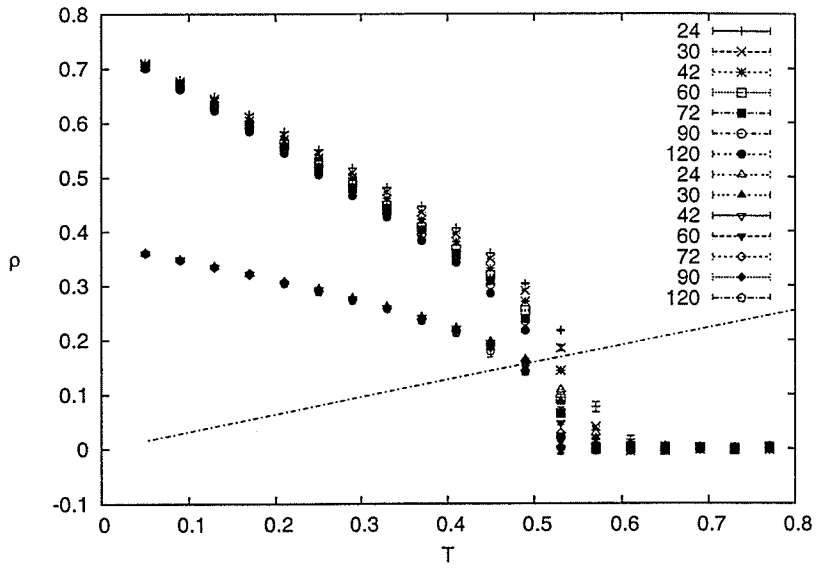

Figure 5.5: Spin stiffness data ρ for a $L \times L \times 2$ lattice. The upper points are for $\rho_{\hat{K}}$ and the lower sets of points are for $\rho_{\hat{\perp}_1}$ and $\rho_{\hat{\perp}_2}$. The dotted line has slope $\frac{2}{\pi H}$ and is a prediction obtained from the KT theory.

are as follows

$$\begin{aligned} \frac{d\rho_{\hat{\perp}}}{d\ln L} &= -\frac{\sqrt{3}t}{2}\left(1-\frac{1}{2}\lambda\right) - \frac{3}{4}\left(\frac{t^2}{\rho_\perp}\right)\left(\frac{5}{8}\lambda^2 - \frac{3}{2}\lambda + 1\right) \\ \frac{d\rho_{\hat{K}}}{d\ln L} &= -\frac{\sqrt{3}t}{2}\left(\frac{1}{2}\lambda^2\right) - \frac{3}{4}\left(\frac{t^2}{\rho_\perp}\right)\left(\frac{1}{8}\lambda^3\right) \end{aligned} \tag{5.8}$$

Here $t = T/2\pi$, $\rho_{\hat{\perp}} = \rho_{\hat{\perp}_1} = \rho_{\hat{\perp}_2}$ and $\lambda = \frac{\rho_{\hat{K}}}{\rho_{\hat{\perp}}}$.

At the microscopic lattice scale $\rho_{\hat{K}} = 2\rho_{\hat{\perp}} = 3/4$ but these values are renormalized under length scaling. In order to make a comparison of our calculated stiffnesses with the predictions of the RG equations, we first calculate the stiffnesses for linear size $L = 18$ so that the condition $H \ll L$ is satisfied. Using the values at this length scale, we numerically integrate the expressions (5.8) with these initial values to predict the behaviour at larger length scales. We then compare the predicted curves with the values obtained directly using Monte Carlo methods at the relatively low temperatures $T = 0.1$ and $T = 0.2$ for different layer thicknesses. Our system

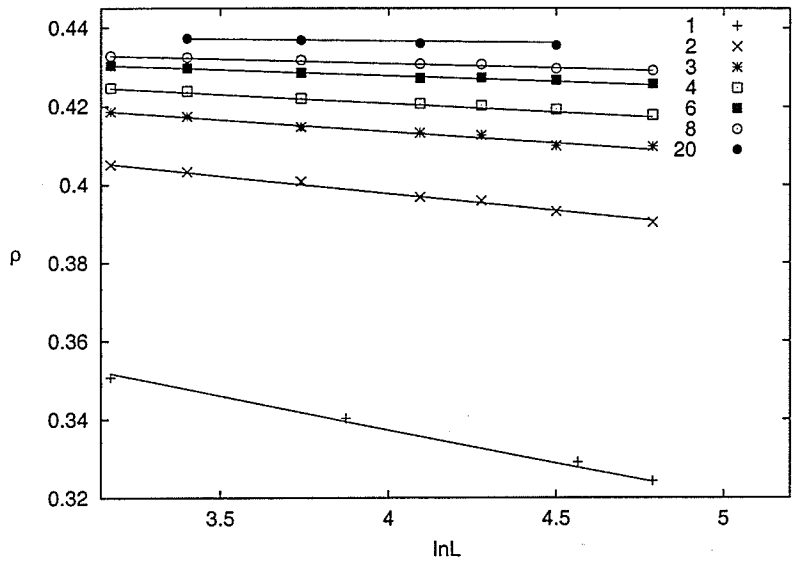

Figure 5.6: Average spin stiffness plotted as a function of $\ln L$ for different layer thicknesses H at $T = 0.2$.The solid lines are the low temperature RG predictions obtained by integrating expressions (5.8) from $L = 18$.

sizes vary from $L = 18$ to $L = 120$, satisfying the condition $H \ll$L. The dependence of the average of the three principal stiffnesses, $\bar{\rho} = \frac{1}{3}\sum_{n=1}^{3}\rho_n$, on $\ln L$ is shown in figure 5.6 for various values of H with $T = 0.2$. In this figure the solid lines are the low temperature $T = 0.2$ RG predictions using equation (5.8) and the points are the Monte Carlo results. The data points agree very well with the predictions of the NLσ model at this low temperature. The stiffnesses decrease proportional to $\ln L$ and the results indicate that there is no stiffness at large length scales. Hence it would appear that the finite layer systems behave in the same way as the single layer system with no indication of a finite temperature phase transition in the stiffnesses. However, as the the number of layers increases the slopes of the lines in figure 5.6 decrease indicating that the stiffnesses should approach a finite value at large length scales as the system becomes fully three dimensional. Figure 5.7 indicates how the slope $\frac{d\bar{\rho}}{d\ln L}$ behaves with increasing number of layers at the two temperatures $T = 0.1$ and

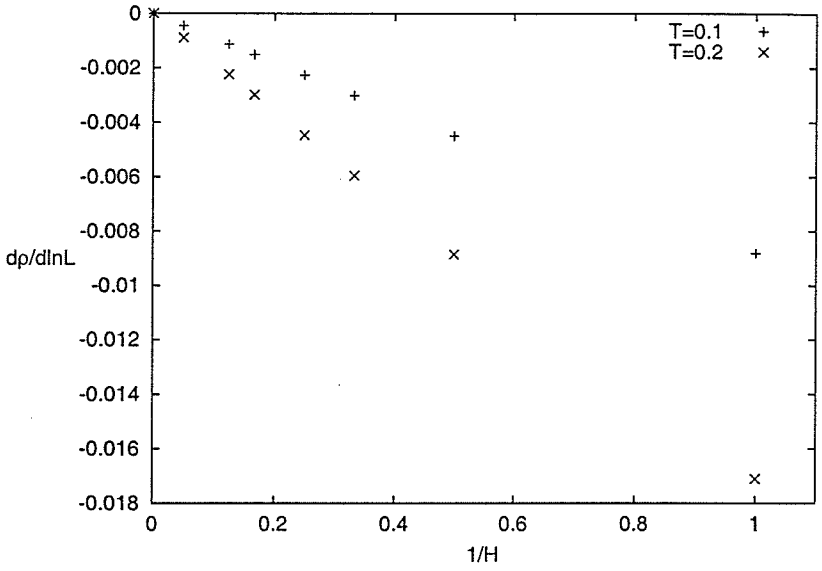

Figure 5.7: $\frac{d\bar{\rho}}{d\ln L}$ dependence on inverse number of layers at $T = 0.1$ and $T = 0.2$.

$T = 0.2$. The slope of $\frac{d\bar{\rho}}{d\ln L}$ becomes less negative tending to zero slope in a linear fashion with respect to $\frac{1}{H}$. This behaviour indicates that the strong size dependence of the stiffnesses observed in figure 5.5 decreases as the layer thickness increases. In the limit of an infinite number of layers, the stiffnesses will approach non-zero values at low temperatures suggesting that a finite temperature phase transition at a higher temperature occurs in this limit.

The excellent agreement of the Monte Carlo results and the RG predictions above indicate that topological excitations are not important in this system at low T. However, at higher temperatures they may play an important role. These topological degrees of freedom are not included in the RG analysis. In order to study the vortex degrees of freedom directly, we have also calculated the response of the system to the presence of a single virtual vortex. We calculate this vorticity response according to the expression (5.4) for a fixed number of layers H and for various linear sizes L. In figure 5.8 the temperature dependence of the vorticity data for $H = 2$ and

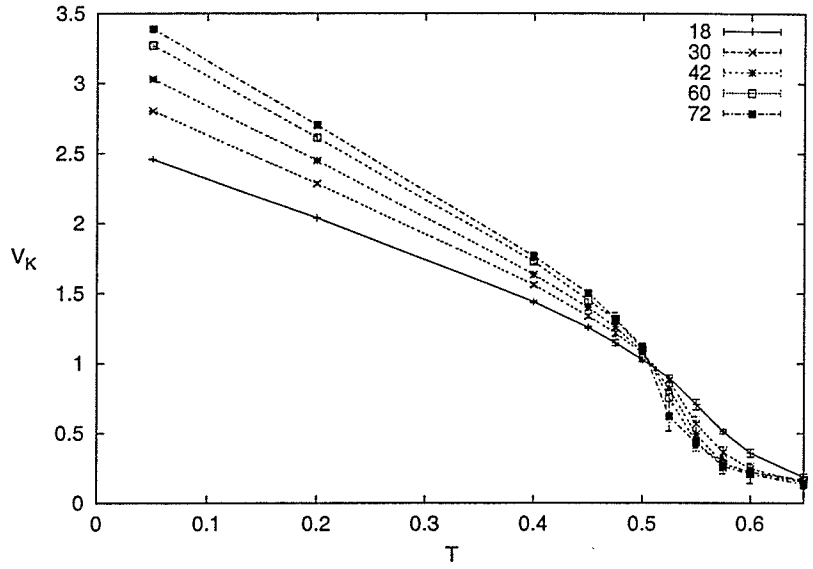

Figure 5.8: Vorticity data for $H = 2$ and different linear sizes $L = 18, 30, 42, 60, 72$ as function of temperature.

various linear sizes L is shown. The curves for different sizes L all cross at a common temperature point near $T = 0.51$. This behaviour suggests that there is a free energy cost to creating isolated vortices in the system below this temperature but that they should spontaneously appear above it.

At any value of T we can study the size dependence of the vorticity using equation (5.5) to extract the coefficient of the $\ln L$ term which we call a vorticity modulus. Figure 5.9 shows the $\ln L$ dependence of the average vorticity $V = 1/3 \sum_{n=1}^{3} V_{\hat{n}}$ for the temperatures corresponding to the points in figure 5.8. The lines are fits to the form (5.5) with the slopes corresponding to the average vorticity modulus for $H = 2$. The almost perfect linear dependence of V on $\ln L$ suggests a size independent core term $C_{\hat{n}}$ and we can extract the vorticity moduli by comparing pairs of sizes L_1, L_2 using the expression (5.6).

Figure 5.10 shows the temperature dependence of the average vorticity modulus

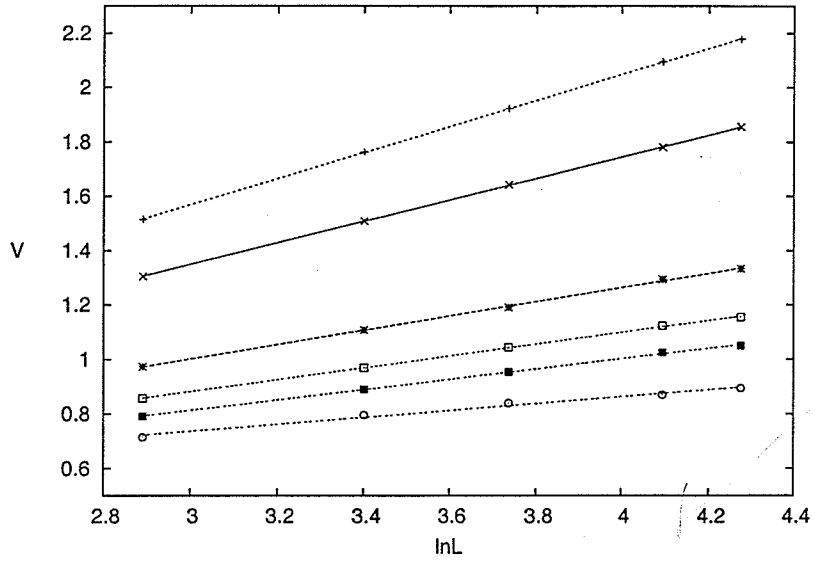

Figure 5.9: Average vorticity for $H = 2$ and temperatures T as function of $\ln L$. The temperature values are 0.05, 0.2, 0.4, 0.45, 0.475 and 0.5 corresponding to the lines from top to bottom in the figure.

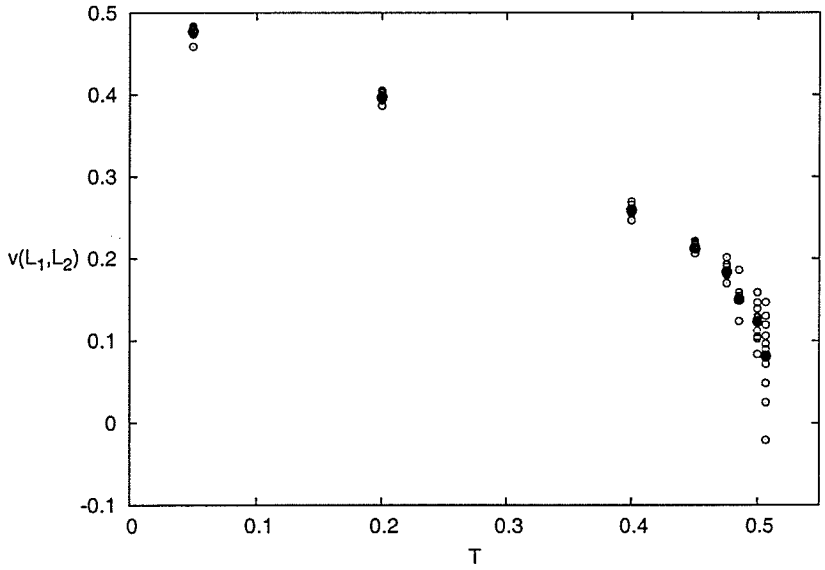

Figure 5.10: Temperature dependence of the vorticity moduli calculated using (5.6) by comparing sizes $L = 18, 30, 42, 60$ and 72. Black dots represent the averages of the different pairs.

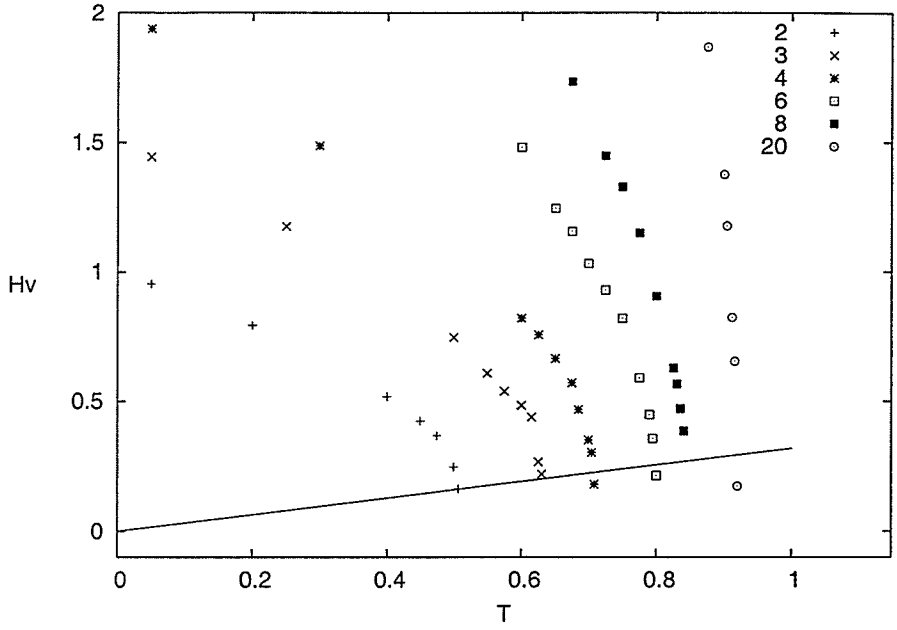

Figure 5.11: Temperature dependence of H times the average vorticity moduli for systems of different thicknesses $H = 2, 3, 4, 6, 8$ and 20. The solid line represents the ratio $Hv/T = \frac{1}{\pi}$.

as a function of temperature extracted from the curves in figure 5.9. The vorticity modulus decreases as the temperature increases and drops abruptly at the same temperature where the raw vorticity data cross in figure 5.8.

The vorticity moduli have been determined for systems having a different number of layers H. In each case, the vorticity moduli abruptly drop to zero at the same temperature where the raw vorticity curves cross. Figure 5.11 shows the average vorticity moduli $v = \frac{1}{3}\sum_{n=1}^{3} v_n$ multiplied by the layer thickness H as a function of temperature for several layer thicknesses. The solid line represents the ratio $Hv/T = \frac{1}{\pi}$ which intersects the corresponding layer vorticity modulus at the temperature where the raw vorticity curves cross. This suggests that the average vorticity modulus exhibits a universal jump , $v/T_c = 1/(\pi H)$, at the transition which decreases as the number of layers H increases.

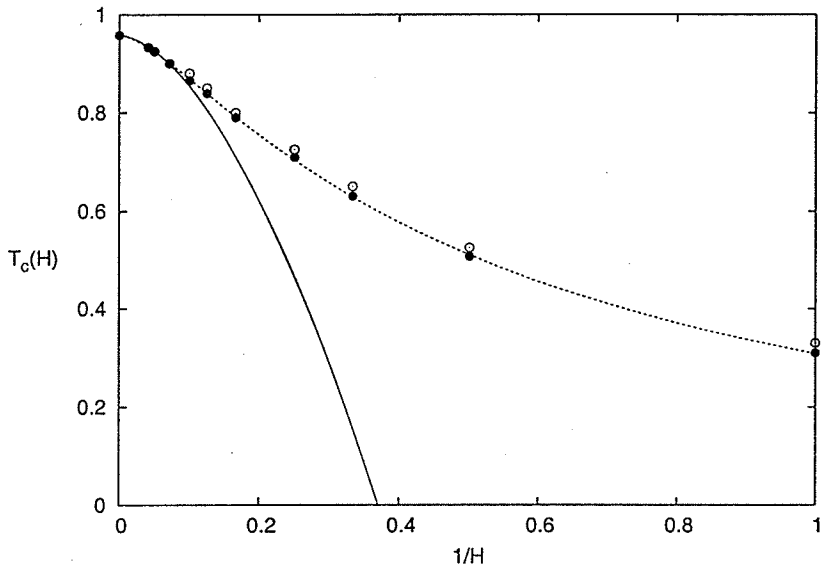

Figure 5.12: $T_c(H)$ dependence on $1/H$ is indicated by the solid circles and the temperatures of the specific heat maxima are indicated by open circles. The dotted line represents a fit to the prediction of FSS theory given in (5.10) and solid line is a fit to the FSS prediction given by (5.9).

Figure 5.12 shows a plot of T_c as well as the temperature of the specific heat maximum versus the inverse number of layers . As $\frac{1}{H} \rightarrow 0$ the system becomes three dimensional with the critical temperature[33] equal to $T_c(3d) = 0.958$. The specific heat maxima lie above the temperatures where the vorticity modulii drop to zero but the two temperatures merge together as $1/H \rightarrow 0$. Finite size scaling (FSS) theory predicts the following dependence of the critical temperature on layer thickness when $T_c(H)$ is close to $T_c(3d)$

$$T_c(H) = T_c(3d)\left(1 - \frac{const}{H^{\frac{1}{\nu}}}\right). \tag{5.9}$$

The correlation length exponent ν in the above expression is the value for the three dimensional case[33] and equals ν= 0.59. Attempted fits of the data in figure 5.12 (solid line) using this form are are only possible for large values of $H > 8$ and there are strong deviations for smaller values of H as shown in same figure.

However, the data points can be fit very well by the slightly modified form

$$T_c(H) = T_c(3d)\left(1 - \frac{C_1}{(H + H_1)^{\frac{1}{\nu}}}\right) \tag{5.10}$$

where both C_1 and H_1 are constants. This modified form reduces to (5.9) in the limit $H >> H_1$. Using the values $C_1 = 7.28$ and $H_1 = 3.06$, this curve is also plotted in figure 5.12 as the dashed line. This modified form provides an excellent fit over the entire range of layer thicknesses.

The quantity $H + H_1$ behaves as an effective layer width which may be related to the boundary conditions at the upper and lower surfaces. Figures 5.13 and 5.14 show the average vorticity modulus $v(z)$ for each individual layer for the cases of $H = 6$ and $H = 14$ respectively. The dotted horizontal curve in each figure is the corresponding average over all layers. The deviations of $v(z)$ from the average are larger for thin films than for thicker films. The free boundary conditions at the top and bottom layers cause $v(z)$ to rise sharply from the outer layers towards the middle layers where it has a maximum value. The values of $v(z)$ near the center of the films

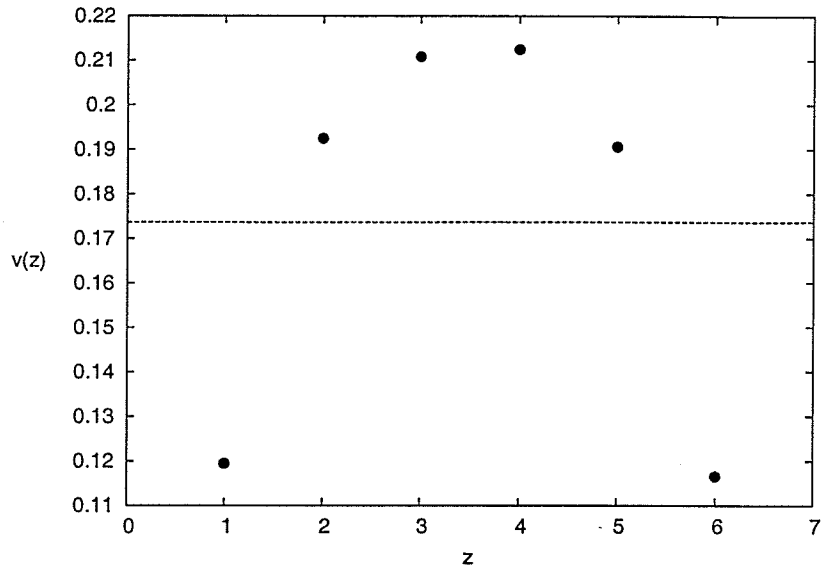

Figure 5.13: Average vorticity $v(z)$ for $H = 6$ for each individual layer at $T = 0.7$. The dotted line is the average over all layers.

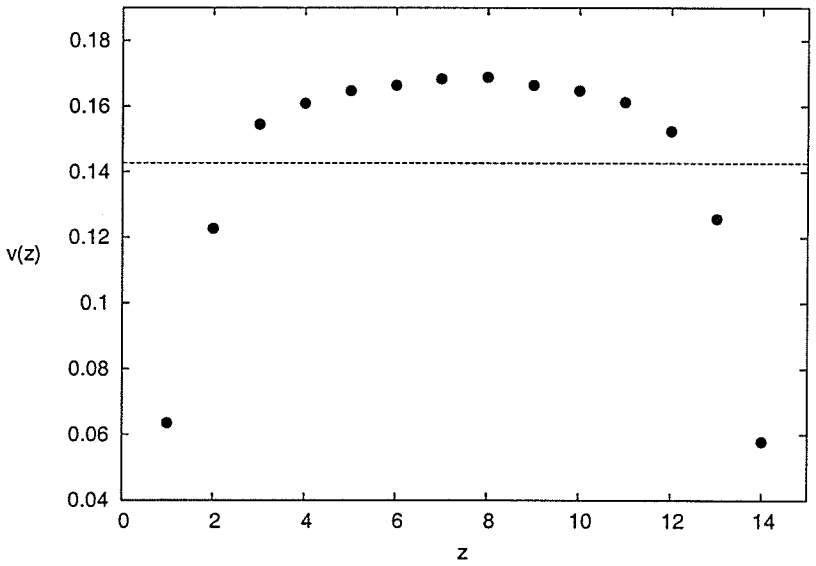

Figure 5.14: Average vorticity $v(z)$ for $H = 14$ for each individual layer at $T = 0.8$. The dotted line is the average over all layers.

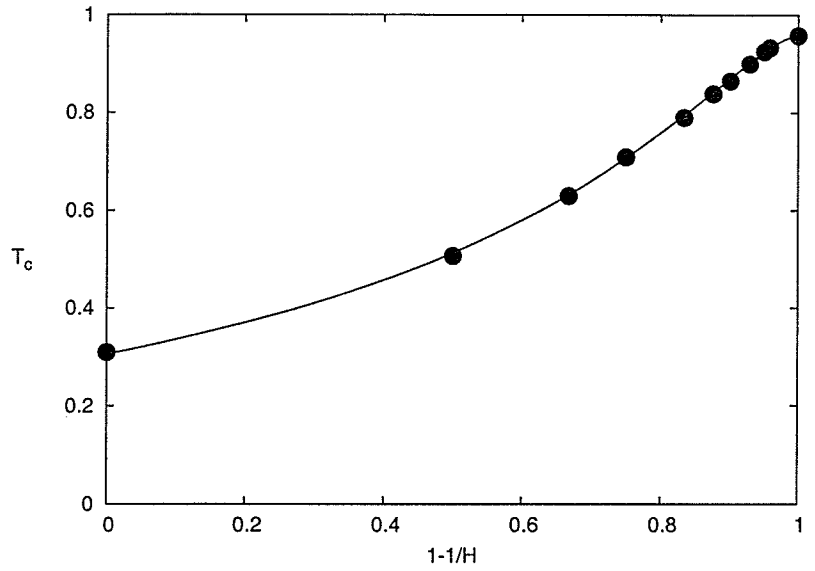

Figure 5.15: $T_c(H)$ dependence on $1 - 1/H$. The dotted line represents a fit to the data using equation (5.10).

are actually larger than the average values over the film. For small values of H the contribution of surface layers is significant and in the vicinity of the critical point the thickness H is not the only relevant length scale. It is being modified by the additional constant H_1 which is related to how quickly $v(z)$ changes near the surface due to the free boundary conditions.

Figure 5.15 shows another plot of $T_c(H)$ versus $1 - 1/H$ which can be compared with figure 5.1. The horizontal axis $1 - 1/H$ essentially describes the variation of dimension between $d = 2$ and $d = 3$.

Finite scaling theory predicts that the vorticity moduli v should scale with respect to the layer thickness H as follows

$$Hv = f(H^{1/\nu}|t|) \tag{5.11}$$

where t is the reduced temperature $(T_c(3d) - T_c(H))/T_c(3d)$ and $\nu = 0.59$ is value of critical exponent of the three dimensional system. The sizes $H > 8$ scale according

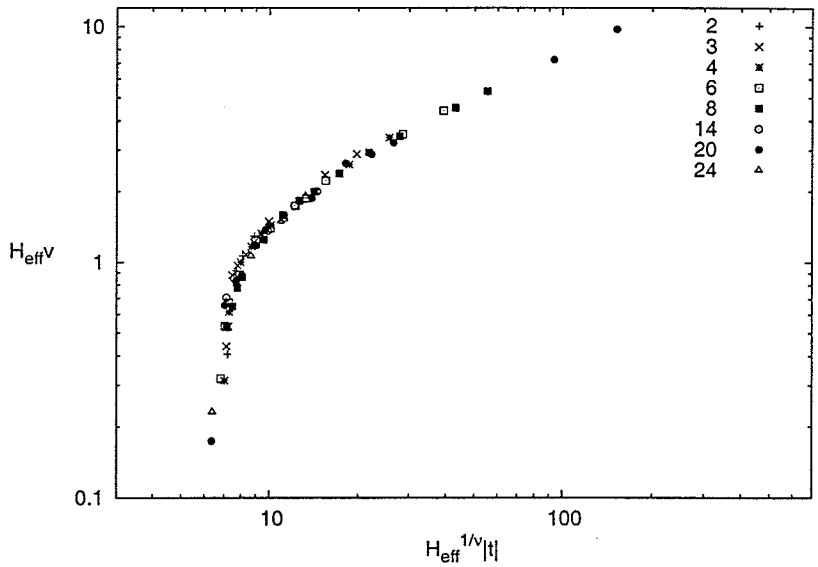

Figure 5.16: The scaling of the average vorticity moduli v. $H = 14, 20, 24$ scale according to (5.11) while $H = 2, 3, 4, 6, 8$ scale according to (5.12). The data for all sizes collapse onto a universal scaling function.

to 5.11. However for smaller values of $H << 8$ the scaling form (5.11) is modified to include the effective width $H_{eff} = H + H_1$ as follows

$$(H + H_1)v = f((H + H_1)^{1/\nu}|t|). \tag{5.12}$$

The scaling function for both scaling forms (5.11) and (5.12) is the same in the large H limit. Figure 5.16 shows a plot of $H_{eff}v$ in terms of the variable $H_{eff}^{1/\nu}|t|$. The vorticity moduli curves for different thicknesses collapse onto a universal curve. For thicknesses $H > 8$ the scaling form (5.11) is used whereas for $H < 8$ the scaling form (5.12) is used.

The results above are similar to those found in studies of ^{4}He superfluid fims[110, 8, 9]. In these systems the order parameter is a complex number $\psi(\vec{r})$ which has the same symmetry as the ferromagnetic XY model. The polar angle of the spins represents the phase of the complex order parameter. The superfluid transition in

$d = 2$ can be described in terms of the Kosterlitz-Thouless transition where vortices destroy the ordered phase. Ambegaokar et al[110]argued that the KT theory can be extended to films of finite thickness and that the transition should continue to have the $2d$ character provided the thickness is not too large. Schultka and Manousakis[8] have studied the same problem numerically and found that the results could indeed be described by the KT theory using finite scaling theory. However, a detailed fit for a small number of layers required the introduction of an effective width for the films.[9] The reason for the effective width being larger than the film thickness was attributed to the boundary conditions on the surfaces which forced the superfluid density to zero.

Our results for the frustrated Heisenberg model are quite similar but there are some important differences. In the XY model, the transition is accompanied by a jump in the stiffness with a power law decay of the correlations below this temperature. This behaviour perists for films of arbitrary thickness until the $3d$ bulk limit is reached where the transition becomes the usual λ transition. In our case, the $d = 2$ behaviour observed[1, 2, 3, 4] for a single layer also persists as the number of layers increases. The stiffness is zero at all finite T indicating that the spin correlations decay exponentially at all temperatures. However, the vorticity modulus exhibits a universal jump at a finite temperature indicating that a topological phase transition occurs involving vortices. The size of the jump varies as $1/H$ and hence approaches zero in the limit of $d = 3$. In addition, the stiffness also approaches a nonzero value at temperatures below the critical temperature in this same limit. This indicates that the $2d$ behaviour approaches the $3d$ behaviour in a continuous way and that topological excitations play an important role between the two limits.

The results obtained here may have some application to superfluid ^{3}He films. For superfluidity in ^{4}He the broken symmetry is a gauge symmetry corresponding to the phase of the wavefunction. In the case of ^{3}He atoms, the superfluid phase is much more complex since a triplet pairing of the fermions occurs. The topological properties

of the superfluid phases are much richer than those associated with a single complex order parameter[111]. In the superfluid ^{3}He phases, the broken symmetry associated with the orbital pairing is also $SO(3)$. The first homotopy group π_1 allows for a Z_2 topological defect similar to the vortices in the Heisenberg STA. However, for very thin films the orbital moment is perpendicular to the surface and reduces the symmetry to the usual gauge symmetry found in ^{4}He films. In the case of thicker films, the effect of the boundaries may be weaker and the variation of the condensation temperature with film thickness may be similar that found here for the Heisenberg model.

Chapter 6

SPIN STIFFNESS OF STACKED TRIANGULAR ANTIFERROMAGNETS

6.1 Introduction

As the previous chapters have indicated, the magnetic ordering of geometrically frustrated antiferromagnets differs substantially from the conventional magnetic ordering in nonfrustrated magnets[10, 42]. Indeed, the nature of the phase transition in the case of stacked triangular antiferromagnets remains controversial[24, 38, 11, 45, 46, 47, 13, 52, 53, 54]. The geometry of the stacked triangular lattice has triangles as the elementary units and this arrangement inhibits an anti-parallel alignment of the spins in each triangular layer. Consequently, the system is said to be geometrically frustrated. This frustration leads to a compromise where the spins on each triangle adopt a non-collinear spin ordering at low temperatures. The spins form a planar configuration in which nearest neighbours are oriented at an angle of 120 degrees with respect to one another. The ground state can be described by a matrix like order parameter giving the orientation of each spin on the elementary triangles and forms an SO(3) parameter space[21]. This unusual symmetry of the order parameter and the appearance of 'chiral' degrees of freedom which correspond to the ground state having two possible realizations, left and right handed, lead Kawamura[25] to conjecture the existence of a new chiral universality class . The chiral degrees of freedom are believed to be responsible for the novel critical behaviour but they are not decoupled from the spin degrees of freedom and the two quantities order simultaneously. While recent field-theoretic renormalization group studies of this system using an expansion up to

six loops in fixed dimension $d = 3$ indicate the existence of a stable fixed point that corresponds to the proposed chiral universality class[52, 53], similar analyses using a three loop perturbation technique as well as an epsilon expansion approach to the same order, did not find a stable fixed point and hence exclude the possibility of a continuous phase transition for this frustrated system[46, 47]. Non perturbative RG approaches find that the phase transition is possibly a very weak first order transition with effective critical exponents[13]. Calabrese et. al.[56] have recently shown using five and six loop renormalization group approximations in fixed dimension that the critical behaviour of both two and three dimensional chiral models is governed by a stable fixed point which attracts RG trajectories in a spiral-like manner. This behaviour could lead to oscillations in the effective exponents close to the stable fixed point. The results of the previous chapter also indicate that topological excitations may play an important role even in $d = 3$.

In this chapter we use both a standard heat bath Monte Carlo method as well as a recently developed broad histogram method[48] to study the classical isotropic antiferromagnet on this geometry. In particular, we study the spin stiffness which provides a direct measure of the correlation length exponent ν. The spin stiffness is a convenient quantity to study since it does not require knowledge of the order parameter but does measure the rigidity of the ordered phase against fluctuations. Our results are consistent with the picture of a continuous transition belonging to a new chiral universality class.

6.2 Model and Methods

The model is described by the following Hamiltonian

$$H = -\sum_{i<j} J\vec{S}_i \cdot \vec{S}_j - \sum_{k<l} J'\vec{S}_k \cdot \vec{S}_l. \tag{6.1}$$

where $\vec{S}_i$ is a classical three component vector of unit length located at the sites i of a hexagonal lattice. The first sum is over nearest neighbours in the triangular

planes which interact with an antiferromagnetic coupling $J < 0$ and the second sum is over inter-plane nearest neighbours which are taken to have a ferromagnetic coupling $J' > 0$ with $|J'| = |J| = 1$. Hence all energies and temperatures are measured in units of $|J|$.

We study the response of the system to a virtual twist of the spin system. The spin stiffness , or helicity modulus[28] , measures the increase in free energy associated with twisting the order parameter in spin space by imposing a gradient of the twist angle about some axis $\hat{n}$ in spin space along some direction $\hat{u}$ in the lattice. The spin stiffness can be written as a second derivative of the free energy with respect to the strength of the gradient and can be calculated as an equilibrium response function[34]. Finite size scaling theory predicts that the spin stiffness should vanish at the critical point with an exponent related to the correlation length exponent.

We calculate the diagonal elements of the spin stiffness tensor corresponding to twists about three principal directions in spin space. If we divide the lattice sites into three equivalent sublattices A, B and C corresponding to the vertices of the elementary triangles, then a chirality vector can be defined to characterize the non-collinear ordering of the spins. The chirality is defined locally for each upward (downward) triangle by the following expression

$$\vec{K}_{\triangle} = \vec{S}_A \times \vec{S}_B + \vec{S}_B \times \vec{S}_C + \vec{S}_C \times \vec{S}_A \tag{6.2}$$

In the ground state, the chirality is uniform and perpendicular to the spin planes. This symmetry of the order parameter suggests that the average chirality direction $(\hat{K})$ be chosen for one of the principal axes and the other two directions $(\hat{\perp}_1, \hat{\perp}_2)$ are chosen to be in the spin plane perpendicular to the average chirality vector such that the three vectors form an orthonormal triad. The spin stiffness component ρ_α at temperature T can be written as (see Appendix A)

$$\rho_\alpha = \frac{1}{N}\sum_{i<j} J_{ij}(\hat{e}_{ij}\cdot\hat{u})^2 \left\langle S_i^\beta S_j^\beta + S_i^\gamma S_j^\gamma \right\rangle - \frac{1}{NT}\left\langle \left(\sum_{i<j} J_{ij}(\hat{e}_{ij}\cdot\hat{u}) \left[S_i^\beta S_j^\gamma - S_i^\gamma S_j^\beta \right] \right)^2 \right\rangle \tag{6.3}$$

where $\alpha, \beta, \gamma = \hat{K}, \hat{\perp}_1, \hat{\perp}_2$ and the indices are taken in cyclic order. The twist is taken to be along the $\hat{u}$ direction in the lattice and $\hat{e}_{ij}$ is a unit vector directed along the nearest neighbour bond from site i to j . The angular brackets indicate a thermal average in the canonical ensemble. Since the ground state is a planar spin arrangement, the stiffnesses satisfy a perpendicular axis theorem $\rho_{\hat{K}} = \rho_{\hat{\perp}_1} + \rho_{\hat{\perp}_2}$ at zero temperature. Deviations from this relationship are a measure of fluctuations of spins from the planar order.

We perform numerical simulations using both a conventional Monte Carlo (MC) heat bath method and the more recent broad histogram method (BHM) introduced by Oliveira et.al.[48] A detailed disscusion of these methods was given in section 3.5. The BHM method[48, 49, 51] is based on the microcanonical ensemble approach to statistical sampling at fixed energy and allows an accurate estimate of the energy density of states $g(E)$. By knowing the density of states $g(E)$ and the microcanonical averages of various quantities $< Q >_E$, their temperature dependence can be determined by using the following expression for the canonical averages

$$< Q >_T = \frac{\sum_E < Q >_E g(E) e^{-E/T}}{\sum_E g(E) e^{-E/T}} \tag{6.4}$$

In the conventional heat bath method temperature is tuned as an external parameter and number of temperature points is limited by number of computer runs. The BHM method allows us to probe the system in a continuous range of T since the microcanonical averages only need to be performed once but this approach requires a large number of energy bins for large system sizes. We simulate spin systems of size $N = L^3$ with $L = 24, 30, 42, 60$ and 66 for the heat bath method and only up to $L = 60$ for the BHM method. We find excellent agreement between these two

numerical methods. Periodic boundary conditions in all three spatial directions are employed for both methods. This differs from the approach used in the previous chapter where periodic boundary conditions were used for the triangular planes but open boundary conditions were used at the top and bottom layers.

6.3 Results

As discussed in section 3.5, the broad histogram method(BHM) is based on the relation

$$g(E) < N_{up}(E) >= g(E + \Delta E) < N_{dn}(E + \Delta E) > \tag{6.5}$$

where $< N_{up}(E) >, < N_{dn}(E) >$ are microcanonical averages which measure the number of moves which increase (decrease) the energy by the amount ΔE . The original dynamics used by Oliveira et. al.[48] for Ising systems to calculate the microcanonical averages in (6.4,6.5) was criticized because it did not satisfy detailed balance[58, 59] and a refined dynamics was introduced in the flat histogram method[60]. In our case the energy is a continuous variable and the dynamics must be changed accordingly. We follow the ideas of Muñoz and Herrmann[61] for systems with continuous degrees of freedom.

We divide the energy axis into bins of a fixed size $\Delta E = 1.8$ such that $\Delta E << E$, where E is the *total* energy of interest. We employ a simple microcanonical dynamics to sample phase space and the energy density of states $g(E)$ (up to a multiplicative constant) is determined using the BHM relation above. One microcanonical sweep consists of a random sweep through the lattice sites and generating a new configuration of the spins by restricting the choice of a new random orientation of the spin at site i with respect to the local field of the nearest neighbours such that the total energy of the system remains within the energy interval $E, E + \Delta E$. All moves are reversible and satisfy detailed balance. At any given value of E , 75 microcanonical

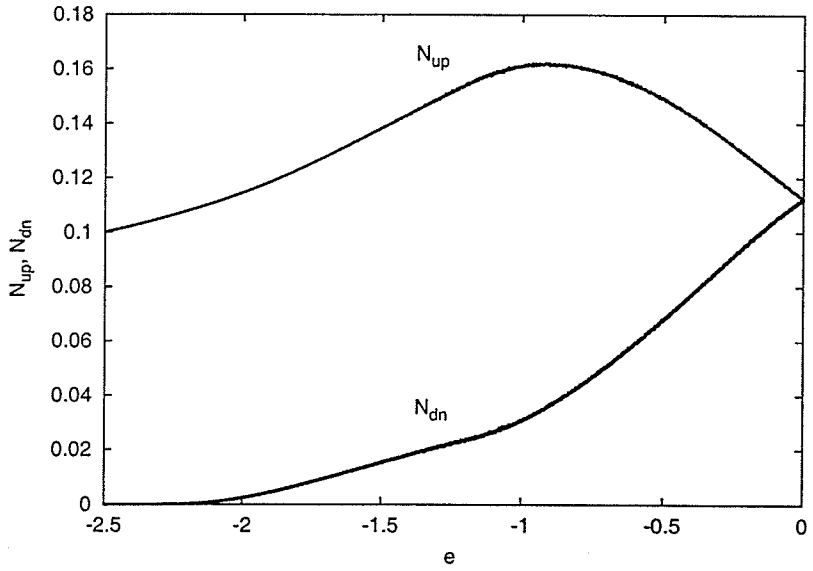

Figure 6.1: $< N_{up}(E) >$ and $< N_{dn}(E) >$ versus energy per site e.

sweeps were performed and 25 sample measurements were taken of various thermodynamic quantities such as the energy, specific heat and spin stiffness. Before sampling the next energy interval, 40 initial microcanonical sweeps were performed to avoid correlations. This procedure was repeated using different seeds for random numbers and errors were determined using the standard deviations for these separate measurements.

Figure 6.1 shows our results for $< N_{up}(E) >$ and $< N_{dn}(E) >$ along the whole energy range of the system. The ground state energy of the system with periodic boundar conditions is $E_g = -2.5N$. As the energy per site, $e = E/N$, tends to its lowest value $< N_{dn}(E) >$ tends to zero as there are no configurations of spins with lower energy, while $< N_{up}(E) >$ is nonzero and both quantities increase with an increase of energy e. There is a noticeable change in both quantities near $e \sim -1$. where $< N_{up}(E) >$ saturates and starts to decrease while $< N_{dn}(E) >$ continues to increase but at a higher rate. As e approaches zero, both quantities attain the same

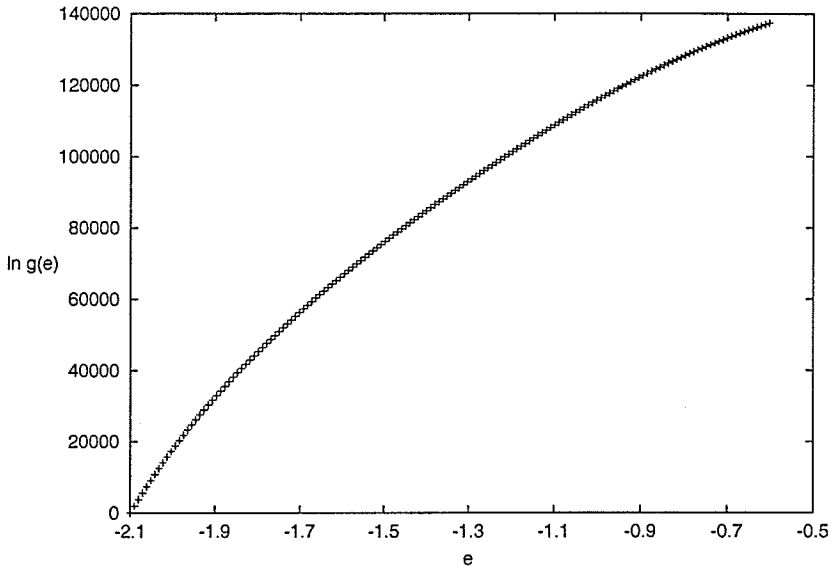

Figure 6.2: Natural logarithm of the energy density of states versus the energy per site e for a $42 \times 42 \times 42$ lattice in the range $-2.1 \leq e \leq -0.5$.

value, as we would expect in the disordered state. We shall see later that a phase transition occurs near the energy where the these quantities exhibit a change in their dependence on e.

Once the microcanonical averages $< N_{up}(E) >$ and $< N_{dn}(E) >$ are known, the microcanonical temperature $T_m(E)$ can be determined from

$$\begin{aligned} 1/T_m(E) &\equiv \frac{d \ln g(E)}{dE} \\ &\simeq \frac{1}{\Delta E} \ln \frac{< N_{up}(E) >}{< N_{dn}(E + \Delta E) >} \end{aligned} \tag{6.6}$$

and we can then integrate this expression in some range of energy to obtain the energy density of states $\ln g(E)$ as a function of E. Figure 6.2 shows our results for $\ln g(e)$ as a function of $e = E/N$ in the case of a $42 \times 42 \times 42$ lattice. The units are arbitrary since we integrate equation (6.6) starting from $e = -2.1$ and not the ground state value $e_0 = -2.5$ .The number of energy bins used for this energy range was 61740. For general values of L, the number of energy bins required to study this

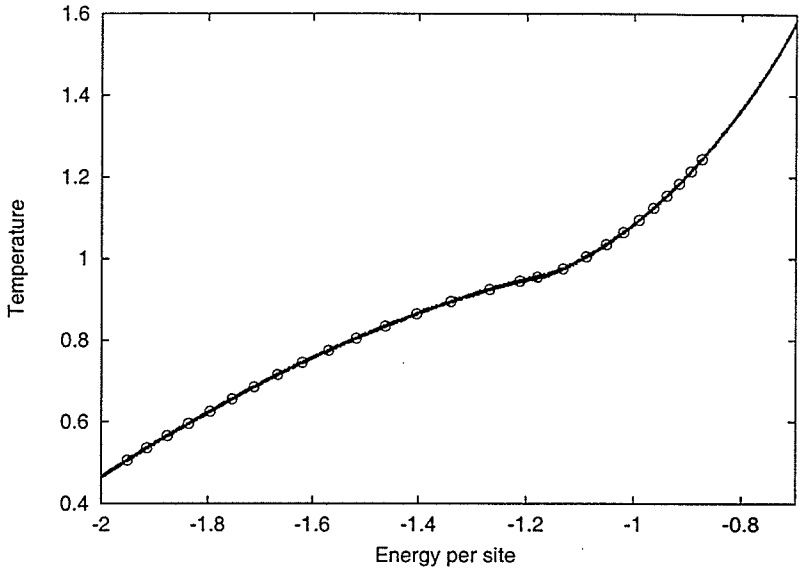

Figure 6.3: The microcanonical and canonical temperatures as a function of the microcanonical and canonical energies repectively. The canonical points correspond to the open circles and the microcanonical points form a dense set.

same range with the same fixed size of energy bin is $5L^3/6$ and is thus of the same order as the number of sites. When the energy density of states is combined with the microcanonical averages $< Q >_E$ for various thermodynamic quantities, we can then plot them as continuous functions of T using equation (6.4).

The microcanonical temperature T_m is an intrinsic property of the system and its change with the microcanonical energy per site, $< E >_E /N$, is plotted in figure 6.3 as the set of dense points that appear as a continuous curve. The density of the points is determined by the size of the energy bins. The overlaping set of points indicated by the circles in figure 6.3 represent the canonical temperature T versus the canonical energy per site, $< E >_T /N$, calculated according to (6.4). Two sets of data are in excellent agreement with each other.

Figure 6.4 shows the energy per site obtained using the BHM method for various linear sizes L. The energy displays strong finite size effects near $T \sim 0.96$ in agreement

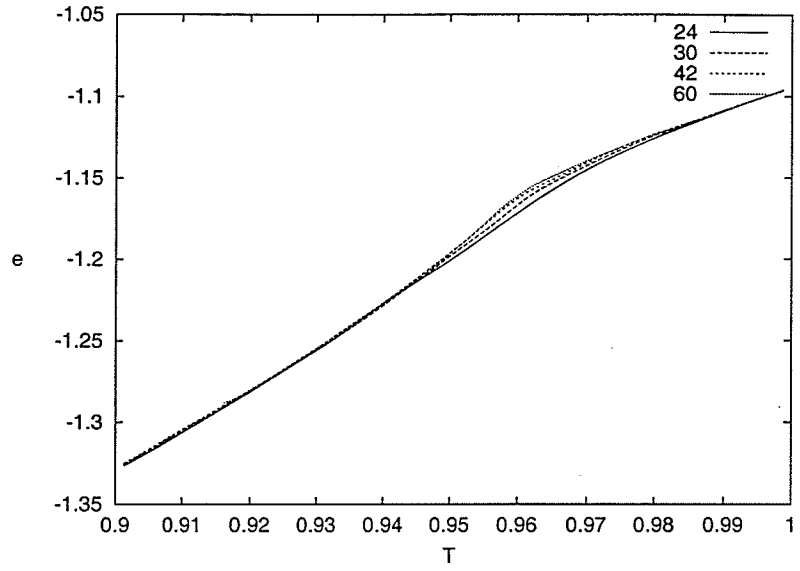

Figure 6.4: Energy per site e obtained using the BHM method for $L = 24, 30, 42, 60$.

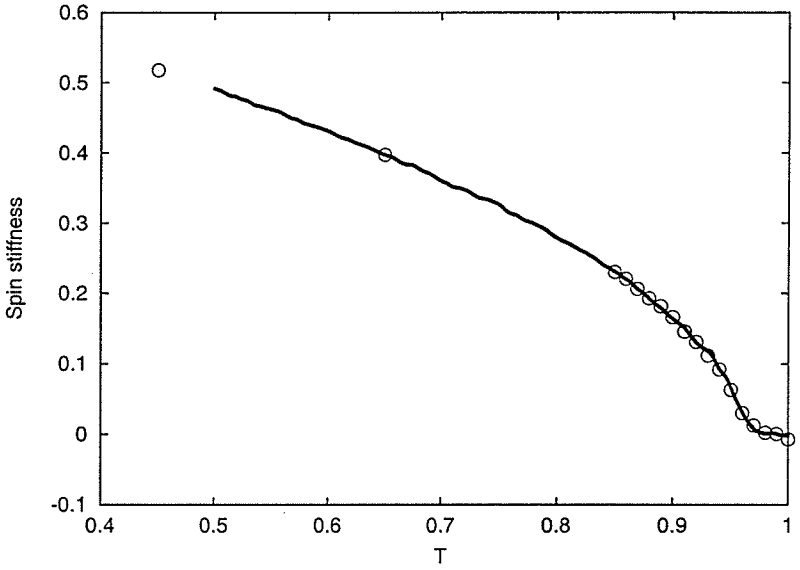

Figure 6.5: The spin stiffness calculated using the BHM(dense set of points) and heat bath(open circles) methods.

with previous MC studies.[10]

We have used both the BHM method and a Monte Carlo heat bath method at fixed values of T to calculate the spin stiffness. In the heat bath method, we discard the first 1000 sweeps and perform 45000 MC steps in each run. Figure 6.5 shows an example of the temperature dependence of the canonical average of the spin stiffness $< \rho >_T$ calculated using the two different methods. The dense set of points are the results obtained using the BHM method and the discrete points indicated by open circles are results obtained using a heat bath simulation.

Figure 6.6(a) shows both our heat bath results, indicated by points, and the BHM results, indicated by lines, for the three stiffnesses for various lattice sizes L as a function of the temperature T. The relation $\rho_{\hat{K}} = \rho_{\hat{1}_1} + \rho_{\hat{1}_2}$ is well satisfied for all values of $T < 0.95$ indicating that there is a relatively small deviation from the planar spin configuration. All three stiffnesses are nonzero at low T and vanish near $T \sim .96$ which corresponds to the same temperature where strong finite size effects occur in the energy (figure 6.4). Figure 6.6(b) shows the heat bath data for $\rho_{\hat{K}}$ on an enlarged temperature scale. The stiffnesses clearly show large finite size effects and approach zero near $T \sim .96$. The points labelled infinity are obtained by plotting $\rho_{\hat{K}}$ versus $1/L$ at various values of T and extrapolating to the large L limit as shown in figure 6.7.

These finite size effects can be used to determine the correlation length exponent ν directly. Finite size scaling considerations for $\rho(T, L)$ predict

$$\rho(T, L) = \frac{1}{L} f(L/\xi) = \frac{1}{L} f(L^{1/\nu}|t|) \tag{6.7}$$

where t is the reduced temperature. This form suggests that we can plot $L\rho(T, L)$ versus T to identify T_c as the temperature where the curves for different values of L intersect. Figure 6.8 shows our heat bath results for $L\rho_K$ as a function of T for lattice sizes $L = 24, 30, 42, 60, 66$. Linear interpolations of neighbouring temperature points indicate that the curves intersect at a value of $T_c = 0.958 \pm 0.002$. We have also used

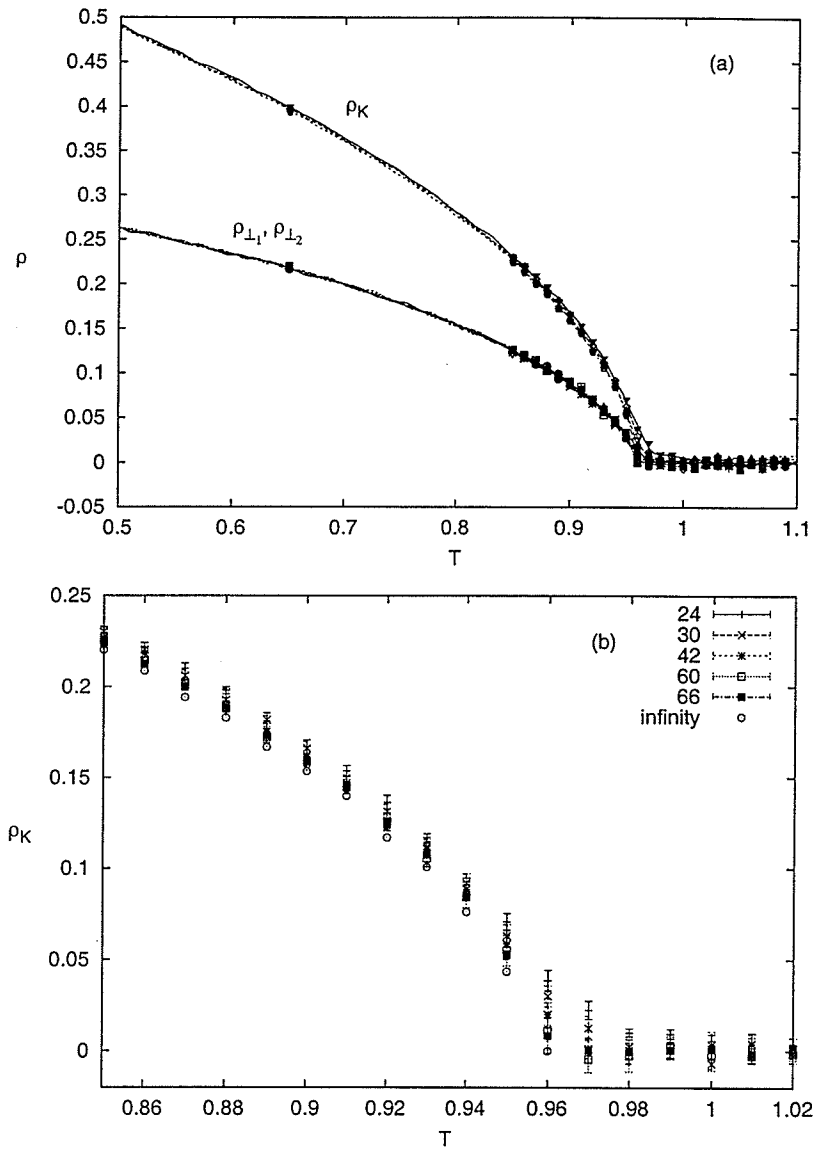

Figure 6.6: Spin stiffnesses as a function of T. a) the points indicate the heat bath results and the lines correspond to the BHM results. All three stiffnesses vanish at the same finite temperature near $T \sim .96$. b) the heat bath results for ρ_K in a smaller temperature range show significant finite size effects near T_c.

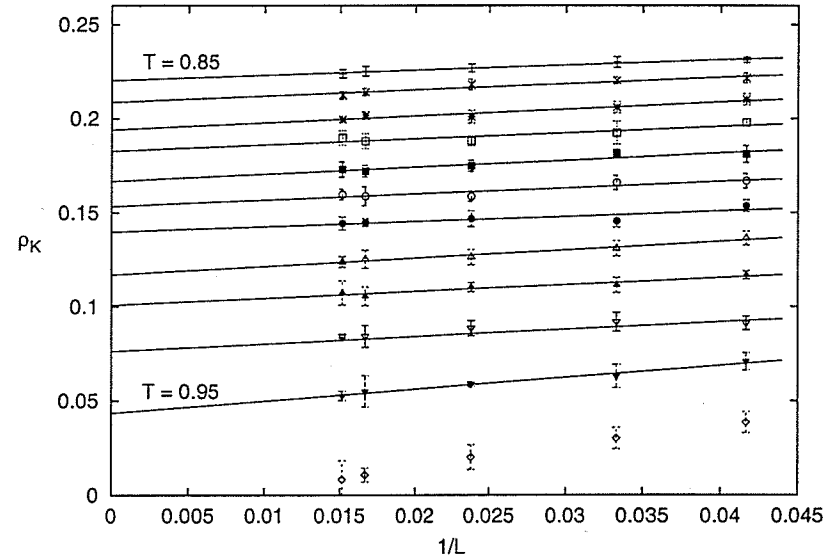

Figure 6.7: The same data as in figure 6.6(b) is plotted as a function of $1/L$ for a set of equally spaced temperatures in the range $.85 \leq T \leq .95$. Extrapolation to the large L limit yields estimates for ρ_K for an infinite lattice.

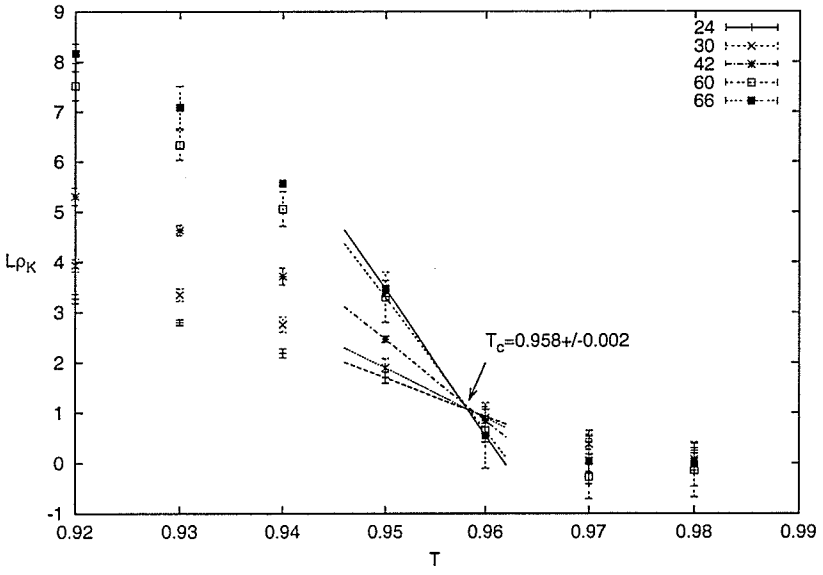

Figure 6.8: $L\rho_K$ versus T for various lattice sizes are indicated by the points. The lines are linear interpolations which indicate a unique crossing point at $T_c = 0.958 \pm 0.002$

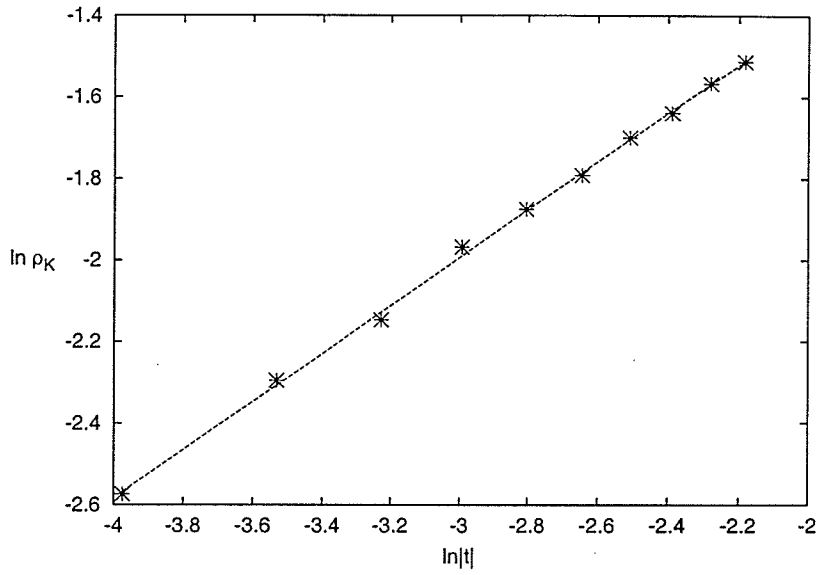

Figure 6.9: A ln-ln plot of ρ_K as $L \to \infty$ versus $|t|$ using the estimated value of T_c yields a value of $\nu = .589 \pm .007$.

our BHM results in the same temperature range and we obtain the same estimate for T_c.

In the limit as $L \to \infty$, the scaling form predicts $\rho \sim |t|^{\nu}$. Using the values of the stiffness obtained by extrapolating to large values of L as in figure 6.7 and then plotting these versus $|t|$ on a ln-ln scale, we can obtain an estimate of ν. Figure 6.9 shows our results for ρ_K which yields the value $\nu = .589 \pm .007$. This value agrees very well with previous Monte Carlo estimates[10] but is slightly larger than the value found by the recent six loop renormalization group calculations in three dimensions.[52, 53]

Figure 6.10 shows a finite size scaling plot of our stiffness results using the values of T_c and ν quoted above. The data obtained from both the heat bath MC method for sizes $L = 24, 30, 42, 60, 66$ and the BHM method for $L = 24, 30, 42$ collapse very well to a universal function for temperatures below T_c. The value $\nu = .589 \pm .007$ is cer-

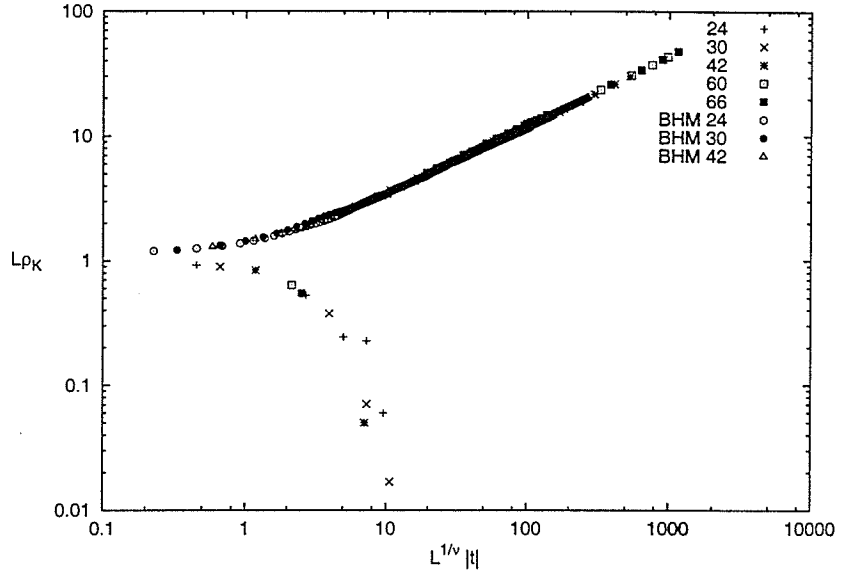

Figure 6.10: Finite-size scaling plot of $L\rho_K$ versus $L^{1/\nu}|t|$ produces a universal curve

tainly very different from the value $\nu = 0.7113$ which describes the three dimensional Heisenberg universality class.[55]

The BHM method can also be used to provide some information about the canonical energy distribution $P(E) = g(E)e^{-E/T}/Z(T)$ where $Z(T)$ is a normalization factor. Figure 6.11 shows a plot of the logarithm of the unnormalized distribution at T_c for lattice sizes $L = 24, 30, 42$ and 60. The results indicate a single peak which sharpens as the number of sites increases. We have found no evidence of multiple peaks in the distribution which would indicate a first order transition. Itakura[16] has recently studied both the antiferromagnetic Heisenberg and XY models on the stacked triangular geometry and concludes that the transition is first order. He studied both the RG flow of an effective LGW Hamiltonian as well as energy histograms of the lattice models. In the case of the XY model, he finds a double peak structure in the energy histogram for very large sizes. However, no such structure was observed in the Heisenberg case. Itakura estimated that for Heisenberg models, a system of

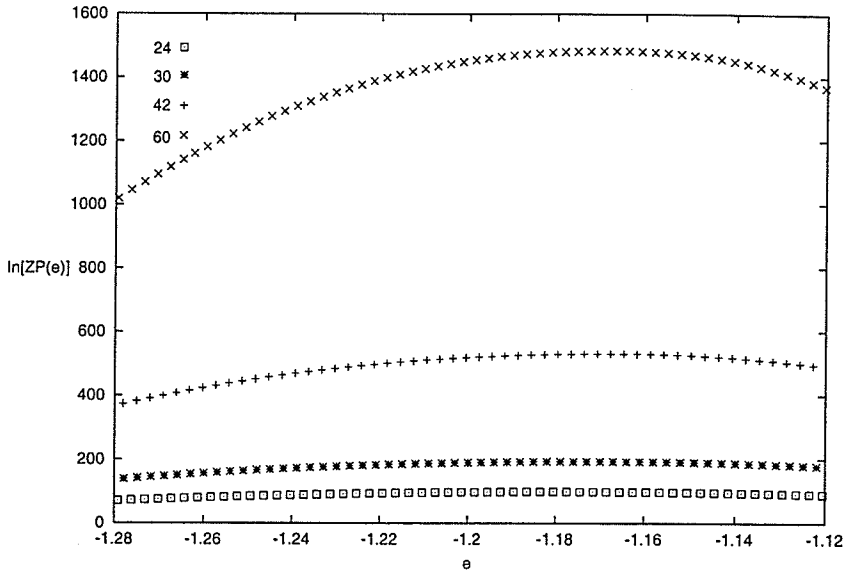

Figure 6.11: Logarithm of the canonical energy distribution for lattice sizes $L = 24, 30, 42$ and 60.

linear size $L \sim 800$ would be needed. At the present time, the investigation of such large sizes is far beyond our available computational resources.

The nature of the phase transition in stacked triangular antiferromagnets is still controversial. Experiments, numerical and theoretical approaches have not reached a definite conclusion about the critical behaviour in these systems. In this section we have calculated the spin stiffness of the isotropic Heisenberg antiferromagnet on the stacked triangular geometry using both a MC heat bath and BHM method. The spin stiffness has the advantage that it measures the rigidity of the ordered phase in response to a virtual twist of the spin system without having to specify the order parameter. The results obtained from both of our numerical approaches agree and predict a continuous phase transition which belongs to the new chiral universality class proposed by Kawamura.

Chapter 7

GENERALIZED STAR MODEL

7.1 Introduction

During the past twenty five years a great deal of research effort has been put into investigating the nature of the phase transition in Heisenberg and XY frustrated systems in three dimensions [10, 12]. In this chapter we study the question of the order of the transition in the context of the XY antiferromagnet on the stacked triangular geometry $L\times L\times L$. Both the Heisenberg and XY stacked triangular antiferromagnets are commonly referred to as the STA model. A number of materials such as the XY stacked triangular antiferromagnets $CsMnBr_3$, $CsNiCl_3$, $CsMnI_3$ and $CsCuCl_3$ as well as the XY helimagnets Ho, Dy and Tb are expected to be described by the STA XY model Hamiltonian. The Hamiltonian of the STA XY model is simply

$$H = -\sum_{i<j} J_{ij}\mathbf{S}_i.\mathbf{S}_j, \tag{7.1}$$

where the $\mathbf{S}_i$ are *two* component classical vectors of unit length. The interactions are antiferromagnetic within the triangular layers and can be either ferromagnetic or antiferromagnetic between layers. The ground state has a planar spin configuration with the three spins on each elementary triangle forming a 120^0 structure with either a positive or negative chirality. For the XY model the chirality has an Ising-like symmetry [10]. In the ground state the vector sum of the three spins on any triangle is zero

$$\mathbf{S}_A + \mathbf{S}_B + \mathbf{S}_C = 0. \tag{7.2}$$

The experimental results indicate that these materials exhibit second order phase

transitions with the exception of $CsCuCl_3$[112] where the transition is found to be weakly first order. The measured critical exponents exhibit scaling laws but vary from material to material which contradicts the basic idea of a unique set of critical exponents for all materials described by the the same model, i.e. the idea of universal behaviour at a continuous phase transition. In some experiments and also in some numerical simulations, the critical exponent η, also called the anomalous dimension, is negative. This is forbidden if the theory which describes the transition is a unitary *LGW* model.[109, 12] Theoretical investigations using a perturbative RG calculation up to high order predict a second order phase transition [52, 53, 56, 94]. The varying critical exponents in this study are associated with a spiral-like RG flow [94] to a chiral fixed point. Non perturbative RG methods predict a weak first order phase transition and attributes the appearance of scaling by a slowing down of the RG flow in the whole region of the coupling constant space [12, 13, 14]. The first numerical investigation of these STA models using Monte Carlo methods indicated a second order phase transition with set of critical exponents associated with a new chirality universality class [11]. Modifications of this model which do not change the symmetry of the order parameter have also recently been introduced and studied [54]. It was found that the modified model exhibits a first order phase transition and the authors concluded that the new chirality class does not exist. The modified model in which disconnected triangles have the constraint (7.2) imposed rigidly is called the *STAR* model. This constraint has the effect of suppressing local fluctuations within the triangles but fluctuations in the relative orientation of these disconnected triangles, or plaquettes, can still occur. Loison and Schotte[54] used Monte Carlo methods to study this *STAR* model and concluded that the transition is first order. They attribute the local rigidity of the plaquettes with making the true first order behaviour of the non-rigid model visible. A recent numerical study of the RG flow in the *LGW* field theory by Itakura[16] also indicates a first order phase transition for STA *XY* model. In order to examine this effect of local rigidity in more detail, we introduce a

generalized model in which we can continuously tune the local rigidity from the STA to the $STAR$ limits [12].

7.2 Model and Methods

A family of models which vary continuously from the stacked triangular antiferromagnet (STA) to the stacked triangular antiferromagnet with local rigidity (STAR) is described by

$$H(r) = -\sum_{i<j} J_{ij}\vec{S}_i.\vec{S}_j + r \sum_{plaquettes} (\vec{S_A} + \vec{S_B} + \vec{S_C})^2 \tag{7.3}$$

where, for XY spins, the $\vec{S}_i$ is a classical two component vector of unit length. The interactions J_{ij} are anti-ferromagnetic within the triangular layers and ferromagnetic between layers with $|J_{ij}| = J = 1$. The parameter r imposes a constraint on the short wavelength fluctuations of the order parameter. By expanding the last term in (7.3), it is easy to see that the coupling strength on disconnected plaquettes is modified as shown in figure (7.1). The dark solid lines have coupling strength $J + 2r$ whereas the couplings between plaquettes have strength J. Continuous changes in r from zero to infinity correspond to a continuous change from the STA to $STAR$ model.

We have used a classical Monte Carlo Metropolis algorithm to study this generalized model as a function of temperature and the rigidity variable r. A number of thermodynamic quantities have been computed with $r = 0.2, 0.5, 0.8, 1, 2$ and 4 for linear lattice sizes $L = 18, 24, 30, 42$ and in some cases 60. In performing these calculations we found that the spatial correlations that develop as the critical point is approached are also accompanied by rather long temporal correlations. This behaviour becomes more pronounced as the rigidity parameter r is increased. In order to reduce the critical slowing down at the transition, each simulation run starts from a disordered state at temperature well above the critical temperature and is slowly cooled to low temperatures. For each such run we have checked that, as $T \to 0$, the

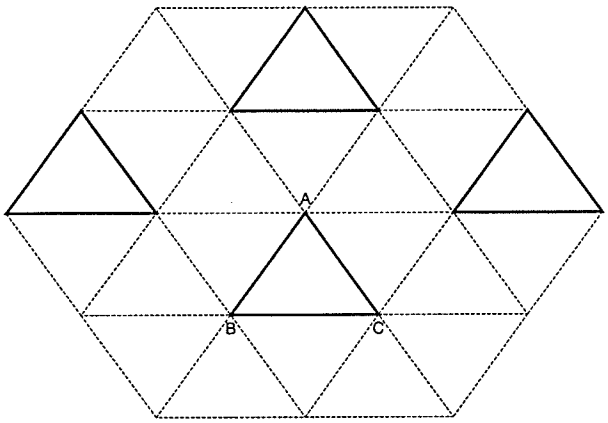

Figure 7.1: A portion of the triangular lattice layer. A, B, and C label different sublattices and the disconnected triangles on which the rigidity constraint is imposed are drawn in full lines. These interactions have strength $J + 2r$.

system is reaching the correct ground state by checking the exactly known energy per site $E_0/N = -\frac{5}{2}J$ of the ground state configuration and, in some cases, the actual configuration of the spins. At high temperatures the ground state energy per site approaches r. The system is allowed to equilibrate for 3×10^5 Monte Carlo sweeps and the averages were performed over 5.5×10^5 steps. In order to avoid correlations between subsequent measurements, $20 - 30$ Monte Carlo sweeps were performed between measurements. In spite of this, for very large values of $r \sim 6$, some initial spin configurations became trapped in metastable states.

7.3 Results and Discussion

The local rigidity constraint introduced in the model (7.3) is varied from $r = 0.0$ to $r = 6.0$ and in this range the system exhibits two basic types of behaviour. In the range $0.0 < r \leq 1.0$ we have studied systems up to sizes $L \leq 42$ and find evidence of a second order phase transition while in the range $r > 1$ studies of systems up to size $L \leq 60$ indicate strong evidence of a first order phase transition. In the following

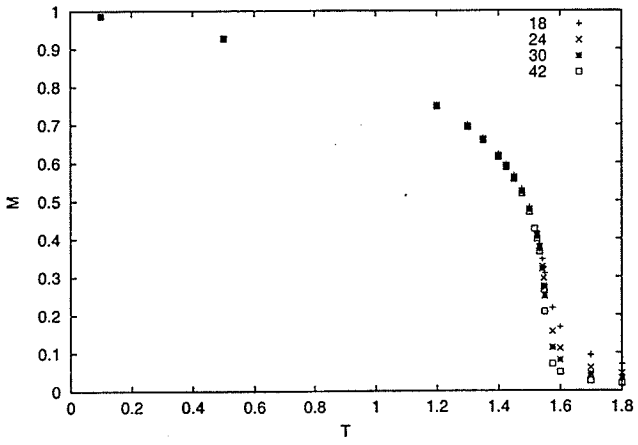

Figure 7.2: Temperature dependence of the order parameter for a number of different sizes of system when $r = 0.2$.

sections we discuss these results in detail.

7.3.1 Order parameter and critical temperature

The model described above has the same ground state symmetry for all positive values of r. There are three sublattices with their spins lying in the xy plane and oriented at 120^0 to each other. The order parameter has been computed using the following expression

$$M = \frac{1}{N}\sum_{i=1}^{3}|M_i| \tag{7.4}$$

where M_i is the total sublattice magnetization of sublattice i and $N = L^3$. An example of the temperature dependence of the order parameter is shown in figure (7.2) for a system with $r = 0.2$ for lattice sizes $L = 18, 24, 30$ and 42. The behaviour indicates that a phase transition occurs near $T \sim 1.6$ where the finite size effects are significant.

A convenient quantity to use to locate the critical temperature is the fourth order

cumulant U_M of the order parameter. It is given by the following expression

$$U_M = 1 - \frac{\langle M^4 \rangle}{3 \langle M^2 \rangle^2}. \tag{7.5}$$

At high temperatures the system is disordered and the probability distribution for M is a single gaussian. For a two-component order parameter the moments satisfy the relation $< M^4 >= 2 < M^2 >^2$ in this limit and the cumulant approaches $1/3$ at high T. At low temperatures we have a perfectly ordered state and the moments $\langle M^{2n} \rangle$ all approach unity. Hence the cumulant approaches the value $2/3$ at low T. Finite size scaling predicts that the cumulant has the scaling form $U_M(L,T) = f_U(L^{1/\nu}t)$ near a second order phase transition where f_U is a universal scaling function. Hence, right at T_c, the cumulants for different lattice size L should all be equal to the universal value $f_U(0) = U_M^*$. The temperature dependence of $U_M(L,T)$ with $r = 0.2$ is shown in figure (7.3) for different lattice sizes L. $U_M(L,T)$ displays behaviour characteristic of a second order phase transition: in the high temperature region ($T > T_c$), $U_M(L,T)$ decreases with increasing size L, while in the low temperature region ($T < T_c$) it approaches the value $2/3$. In both temperature regions, the correlation length ξ is much smaller than the linear size L of the system ($L \gg \xi$). However, close to the transition, where the correlation length ξ is much larger, $U_M(L,T)$ stays more or less constant and independent of system size L with a nontrivial value $U_M^* \sim 0.61$. The critical temperature is estimated to be the value of T where the fourth order cumulants for different sizes L cross. Later in this chapter we will also use a direct measurement of the correlation length to estimate T_c. We find that the critical temperature increases with an increase of the rigidity parameter r as one might expect when some fluctuations are suppressed.

The variation of the critical temperature with the rigidity parameter r is shown in figure (7.4). In the limit of $r \to 0$, $T_c(r)$ approaches the value determined in previous numerical simulations of the XY STA model[11] while, in the limit $r \to \infty$, $T_c(r)$ approaches the value of the $STAR$ model [54]. More discussion on how these critical

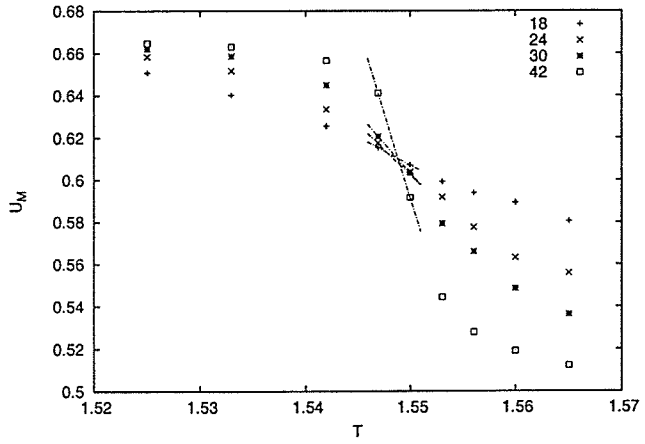

Figure 7.3: Temperature dependence of fourth order cumulant of the order parameter for a system with $r = 0.2$ for different sizes $L = 18, 24, 30, 42$. The crossing point of the curves corresponds to the critical temperature T_c.

temperatures are obtained in the region of first order behaviour will be given later in this chapter. Before presenting our results for small values of r, we first describe our method of estimating critical exponents using the results for $r = 0.2$ as an illustration.

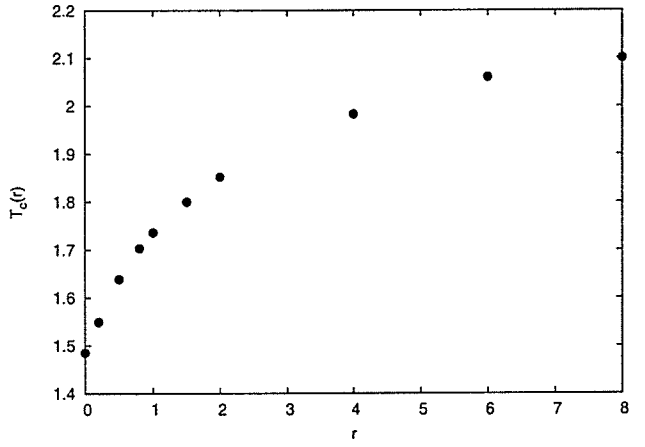

Figure 7.4: Critical temperature as a function of the rigidity parameter r.

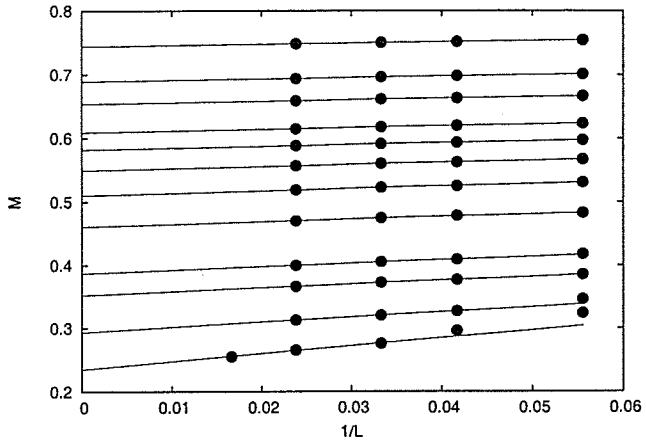

Figure 7.5: Linear extrapolation of the magnetization data to the thermodynamic limit $1/L \to 0$. Lines correspond to T =1.2, 1.3, 1.35, 1.4, 1.425, 1.45, 1.475, 1.5, 1.525, 1.533, 1.542, 1.547 respectively starting from the top of the figure. Solid dots are the Monte Carlo results for each L. The rigidity parameter has the value $r = 0.2$.

7.3.2 Finite size scaling and critical exponents

The behaviour of the system in the vicinity of a critical point where the correlation length ξ becomes large compared to the size of the system can be described in terms of finite size scaling (FSS) theory [108]. If the system exhibits a continuous phase transition, the order parameter is expected to exhibit a power law behaviour close to the critical point in the thermodynamic limit. The asymptotic behaviour of the order parameter for large sizes L can be written as

$$M(L,T) \sim M(\infty,T) + c(T)/L^{d-2} \tag{7.6}$$

where $c(T)$ is a temperature dependent constant and in our case $d = 3$. The last term arises from spin wave contributions[11]. One can use the L dependence given by (7.6) to estimate the thermodynamic limit value $M(\infty,T)$. For a number of fixed temperatures ($T < T_c$), $M(L,T)$ vs $1/L$ plots were analyzed as shown in figure (7.5) for the system with $r = 0.2$. The intercept of the straight line fit to the data points gives a thermodynamic limit estimate of $M(\infty,T)$.

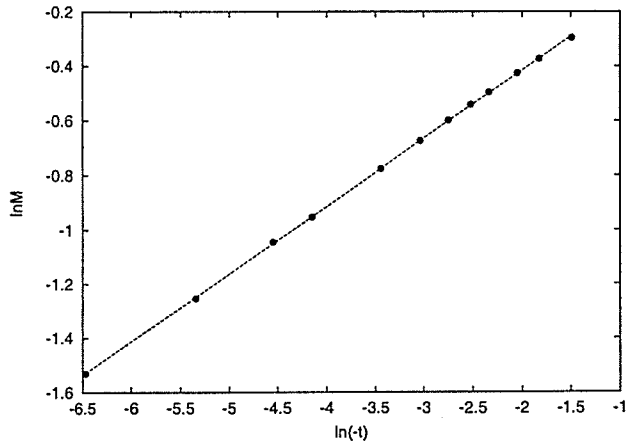

Figure 7.6: The order parameter M is plotted versus reduced temperature t on a log-log scale for a $r = 0.2$ system.

As the critical point is approached from below the magnetization $M(\infty, T)$ is expected to behave as

$$M \sim (-t)^{\beta} \tag{7.7}$$

where $t = (T - T_c)/T_c$ is the reduced temperature which measures the 'distance' from the critical temperature and β is the order parameter critical exponent. This power law behaviour can be tested by plotting the infinite lattice values of M vs t on a log-log scale as shown in figure(7.6).

The critical temperature was first estimated using the fourth order cumulant but is allowed to vary to obtain the best linear fit to the data. In this case we find $T_c = 1.5494 \pm 0.0004$ and the critical exponent is estimated to be $\beta = 0.2494$. The value of β depends sensitively on the value of the critical temperature as illustrated in the following table 7.1 for temperatures in the vicinity of the critical point for which reasonable straight line fits were obtained. These variations allow us to assign errorbars to the value of β . Our estimate is $\beta = 0.249 \pm .006$.

The correlation length exponent ν can be estimated from the finite-size behaviour

T_c	β
1.5490	0.243
1.5491	0.244
1.5492	0.246
1.5493	0.248
1.5495	0.251
1.5496	0.253

Table 7.1: Variation of β for different choices of the critical temperature for which power law behaviour holds when $r = 0.2$.

of the order parameter near $t = 0$ which is given by the following expression

$$M(T, L) = L^{-\beta/\nu} f_M(L^{1/\nu}|t|) \tag{7.8}$$

were f_M is a universal scaling function characteristic of the order parameter M. The asymptotic behaviour of the scaling function $f_M(L^{1/\nu}|t|)$ should agree with the behaviour in the thermodynamic limit (7.7). This yields the following asymptotic forms of $\mathrm{f}_M(\mathrm{L}^{1/\nu}\ |t|)$ both below and above T_c ,

$$\begin{aligned} f_M(L^{1/\nu}|t|) &\sim (L^{1/\nu}|t|)^{\beta} && T < T_c \\ f_M(L^{1/\nu}|t|) &\sim (L^{1/\nu}|t|)^{(\beta - \frac{3\nu}{2})} && T > T_c \end{aligned} \tag{7.9}$$

where the form above T_c is a consequence of a finite susceptibility requirement related to the way order parameter M becomes zero at high temperatures [11, 106].

In order to verify that scaling holds, one can plot $ML^{\beta/\nu}$ versus $L^{1/\nu}|t|$ for various sizes L. For appropriate values of T_c, β and ν the data should collapse onto a single curve f_M which exhibits the asymptotic behaviour given by (7.9) for the argument of scaling function $L^{1/\nu}|t| \gg 1$. The critical temperature T_c and the exponent β were

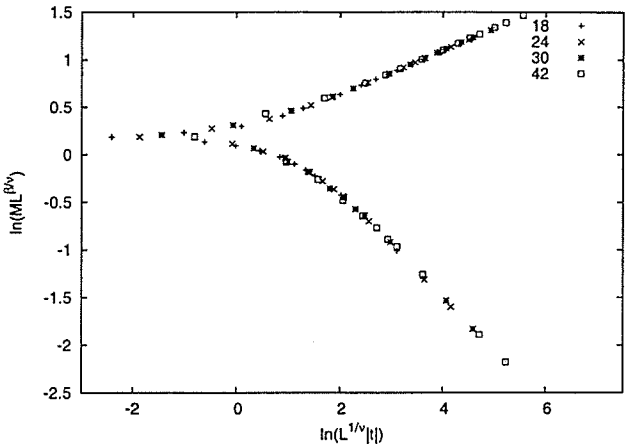

Figure 7.7: Log-log finite size scaling plot of order parameter M for the $r = 0.2$ system. The critical temperature $T_c = 1.5494$ and the exponent $\beta = 0.2494$. The best collapse of data was obtained for $\nu = 0.531$ with asymptotic slopes of 0.2385 for $T < T_c$ and -0.5473 for $T > T_c$.

determined quite independently of the scaling relation (7.8) and this allows us to find an appropriate value for the exponent ν. A sample log-log finite size scaling plot for $r = 0.2$ is shown in figure (7.7). The data collapse for $T < T_c$ holds for a range of values of the exponent ν from 0.51 to 0.54, while above T_c, the value $\nu = 0.5311$ gives the best collapse of data. The asymptotic slope for $T < T_c$ of 0.2385 is less than the previous estimate of $\beta = 0.249 \pm 0.006$ using the thermodynamic limit magnetization data which indicates that the correction terms to the leading term in (7.9) may be important. The value of this asymptotic slope of 0.2385 is insensitive to the variation of the other two parameters, namely T_c and ν. The asymptotic slope for $T > T_c$ of -0.5473 is in good agreement with values of β=0.2494 and ν=0.531 for which the best collapse of data was obtained. The final estimate for correlation length exponent is $\nu = 0.53 \pm 0.02$

The ordering susceptibility has been also calculated from thermal averages of M

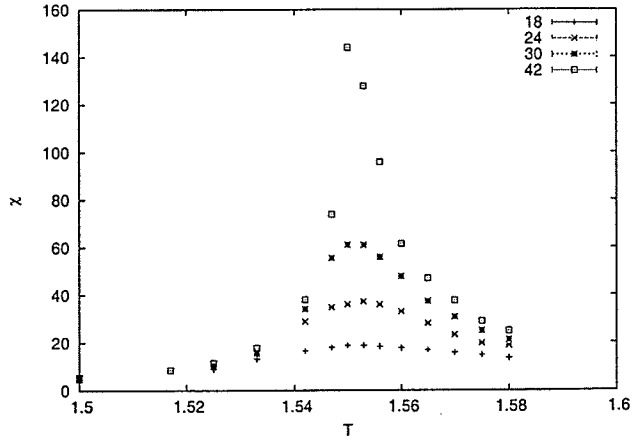

Figure 7.8: Ordering susceptibility for various lattice sizes when $r = 0.2$.

and M^2 using

$$\chi = \frac{(\langle M^2 \rangle - \langle M \rangle^2)}{T}. \tag{7.10}$$

The temperature dependence of the susceptibility for various lattice sizes is shown in figure (7.8) for the $r = 0.2$ system. The finite size scaling prediction for the susceptibility and the asymptotic behavior of the corresponding scaling function are given by the following expressions for $T > T_c$.

$$T\chi = L^{\gamma/\nu} f_\chi(L^{1/\nu}|t|). \tag{7.11}$$

where near T_c the scaling function behaves as $f_\chi(L^{1/\nu}|t|) \sim (L^{1/\nu}|t|)^{-\gamma}$.

A log-log plot of (7.11) using the estimated value of T_c and the exponent ν were analyzed by varying the exponent γ to get the best overlap of data for different sizes L . A value of the exponent γ in the range 1.09 to 1.2 gives a reasonable collapse of the data with an asymptotic slope of the scaling function ~ 1.091. The value $\gamma = 1.1 \pm 0.1$ is chosen as the best estimate from the susceptibility finite size scaling analysis. A finite size scaling plot illustrating this data collapse is shown in figure (7.9).

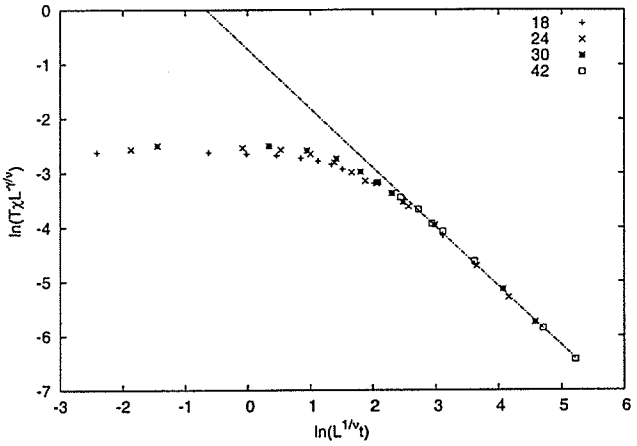

Figure 7.9: Log-log plot of the susceptibility χ above the critical point for $r = 0.2$. We estimate $T_c = 1.5494$, $\nu = 0.531$ and $\gamma = 1.1$, which yields an asymptotic slope of 1.091.

7.3.3 Structure factor and correlation length

Spatial correlations can be studied by considering the spin structure factor $S(\vec{q})$ defined by

$$S(\vec{q}) = \frac{1}{N} \sum_{i,j} \left\langle \vec{S}_i \cdot \vec{S}_j \right\rangle e^{i\vec{q}(\vec{r}_i - \vec{r}_j)} \tag{7.12}$$

where the indices i and j denote lattice sites, $\vec{q}$ is wave vector in the first Brillouin zone and the brackets $< ... >$ denote thermal averages. For wave vectors close to the ordering wave vector $\vec{Q}$ =(4π/3,0,0) one can calculate the antiferromagnetic correlation length ξ using the Ornstein-Zernicke form [23]

$$S(\vec{q}) = \frac{S(\vec{Q})}{1 + \xi^2(\vec{q} - \vec{Q})^2} \tag{7.13}$$

Figure (7.10) shows the structure factor $S(\vec{Q})$ as a function of T. The low temperature limit is proportional to the number of sites N. We compute $S(\vec{q})$ for a number of wavevectors $\vec{q}$ in the vicinity of the ordering vector $\vec{Q}$ =(4π/3,0,0) within the first Brillouin zone. Using (7.13) we then plot $S(\vec{Q})/S(\vec{q}) - 1$ vs $(\vec{q} - \vec{Q})^2$ at each fixed

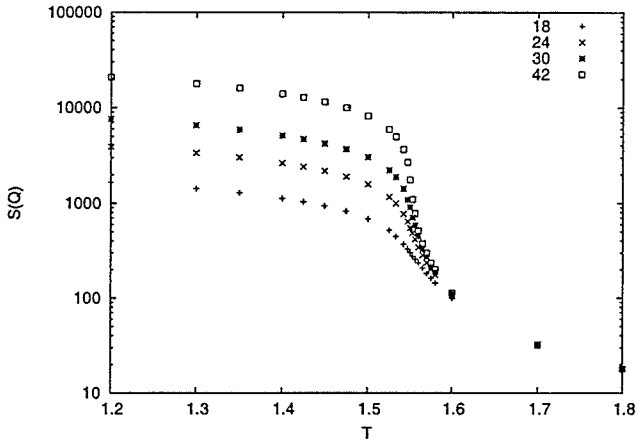

Figure 7.10: Semi-log plot of spin structure factor $S(\vec{Q})$ at the ordering vector $\vec{Q}$.

temperature T and extract ξ^2. In spite of a small anisotropy for some $\vec{q}$ points that tends to become smaller with increased size of the system, a reasonable linear dependence on $(\vec{q}-\vec{Q})^2$ has been found as shown for example in figure (7.11). The correlation length has been computed as the square root of the slope of a linear fit to $S(\vec{Q})/S(\vec{q})-1$ vs $(\vec{q}-\vec{Q})^2$ for each temperature and the temperature dependence of the correlation length is shown in figure (7.12) for $r=0.2$.

The correlation length at a second order transition diverges but it cannot exceed the size of the system. In a finite system the correlation length should have following form according to FSS theory

$$\xi(L,T) \sim L f_\xi(L^{1/\nu}t). \tag{7.14}$$

At the critical point f_ξ is a constant and hence by plotting ξ/L vs T for various sizes L we can identify the critical temperature as illustrated in figure (7.13). The critical temperatures determined in this way are in a good agreement with those found using the fourth order cumulant of the magnetization. Table 7.2 shows a comparison of the critical temperatures found using the two approaches for several values of r.

It has been found that, in the case of XY frustrated materials for which the set of

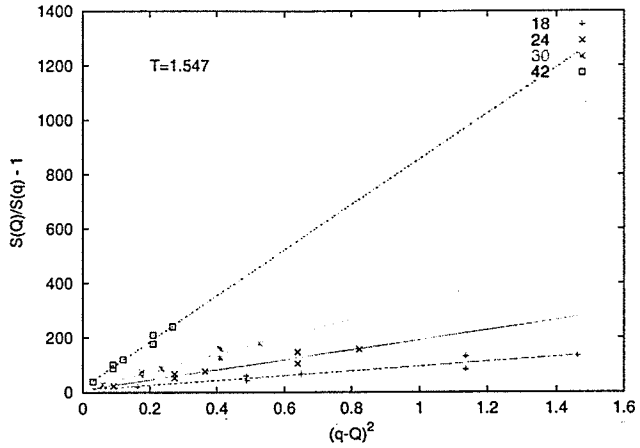

Figure 7.11: $S(\vec{Q})/S(\vec{q}) - 1$ vs $(\vec{q} - \vec{Q})^2$ plot for various sizes L shows a linear dependence at fixed temperature in agreement with the Ornstein-Zernicke expression.

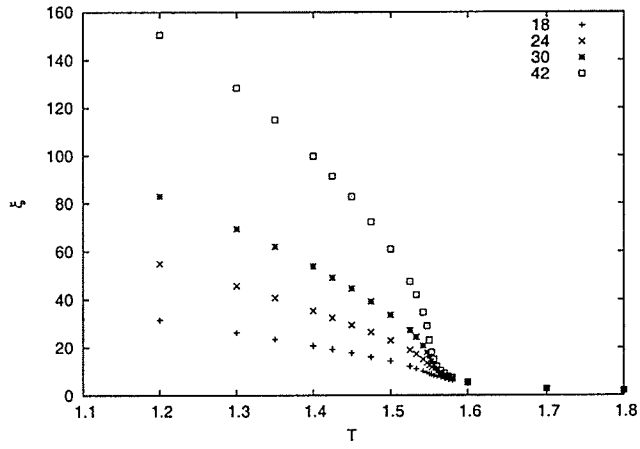

Figure 7.12: Temperature dependence of the correlation length for $r = 0.2$.

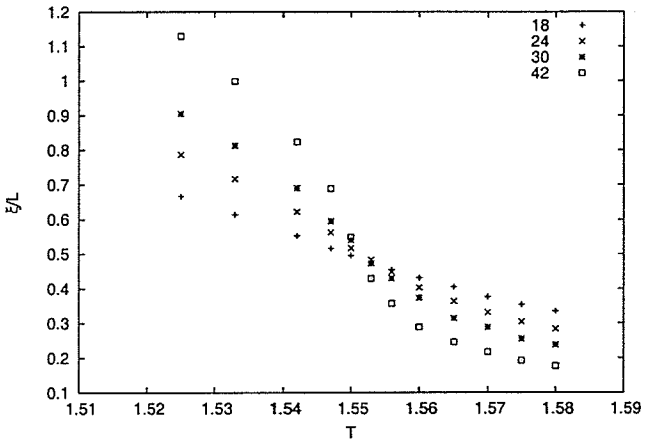

Figure 7.13: Temperature dependence of the scaled correlation length for $r = 0.2$ and sizes of system $L = 18, 24, 30, 42$. The curves cross at a critical temperature $T_c = 1.5494$.

critical exponents has been measured in experiments as well as in numerical studies, that the correlation function critical exponent η is small but negative at the critical point. At T_c, the structure factor depends on system size as follows

$$S(\vec{Q}, L) \sim L^{2-\eta}. \tag{7.15}$$

where the exponent η is often called the anomalous dimension. Although the form (7.15) is only correct at T_c, we will use it to study the size dependence of the structure factor at any temperature. In this way we can obtain some information about the

r	0.2	0.5	0.8	1.0
$T_c(U_M)$	1.5493	1.641	1.704	1.7369
$T_c(\xi)$	1.5494	1.642	1.704	1.739

Table 7.2: Critical temperatures T_c for different values of rigidity parameter r estimated from the fourth order cumulant U_M are given in the first row and those obtained using the correlation length scaling are in the second row.

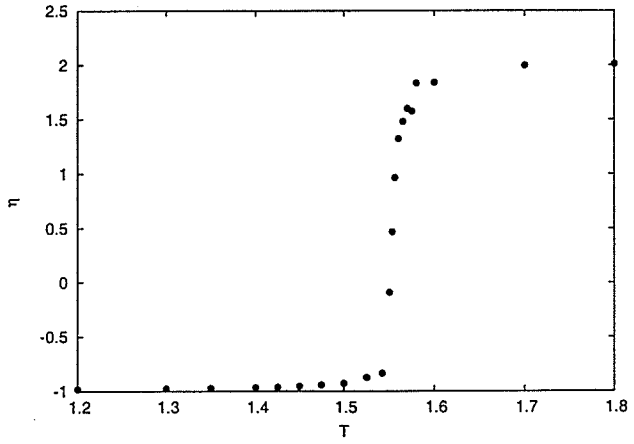

Figure 7.14: Temperature dependence of the critical exponent η for $r = 0.2$. $\eta(T_c) = -0.06 \pm 0.02$.

values of η near T_c. Figure (7.14) shows η as a function of T obtained by studying the structure factor at the ordering wavevector for system sizes $L = 18, 24, 30$ and 42 when $r = 0.2$. At the critical temperature, η has a small negative value. We find that η=-0.06 $\pm$ 0.02.

A negative value of η is puzzling in spite of the fact that we find a reasonable scaling behaviour and a set of exponents that also seem to satisfy scaling relations characteristic of a second order phase transition. The critical exponent η should be strictly positive for a real fixed point corresponding to a true continuous transition [109]. In addition, the exponents associated with a universality class should be independent of the coupling strengths J_{ij} and hence they should be independent of the parameter r that modifes the coupling on disconnected plaquettes. Contrary to this we find that the critical exponents for which finite size scaling holds change with the rigidity parameter r suggesting a 'pseudo-scaling' and possibly 'pseudo critical exponents'. However, it is also possible that there is a tricritical point at non-zero values of r where the transition changes from second order to first order with different exponents right at the tricritical point. In this case one may observe a change in the

exponents due to crossover effects.

7.3.4 Results for $r = 0.5, 0.8$ and 1.0.

The same FSS approach used for $r = 0.2$ was also applied to study $r = 0.5, 0.8$ and 1.0 for system sizes $L \leq 42$. In each case, a pseudo scaling of the critical exponents is found. Figures (7.15)-(7.20) show the results for the case $r = 0.5$. The data collapses very well for these system sizes but the exponent values differ from those obtained for $r = 0.2$. We estimate $\beta = 0.249, \gamma = 1.04$ and $\nu = 0.518$ which are slightly smaller than the values for $r = 0.2$. Figures (7.21)-(7.26) show the corresponding results for $r = 0.8$. Again the data collapses very well but the exponents are somewhat different with $\beta = 0.218, \gamma = 1.0$ and $\nu = 0.490$. Finally figures (7.27)-(7.32) show the results for $r = 1.0$ where we find $\beta = 0.213, \gamma = 1.0$ and $\nu = 0.482$. For all of these values of r, a 'pseudo-scaling' of the exponents is observed. However, in each case the exponent η is small and negative.

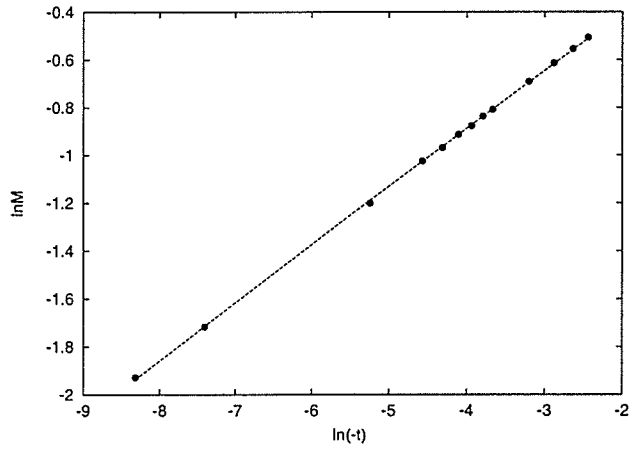

Figure 7.15: Order parameter $M(\infty, T)$ plotted versus reduced temperature t on log-log scale for $r = 0.5$.

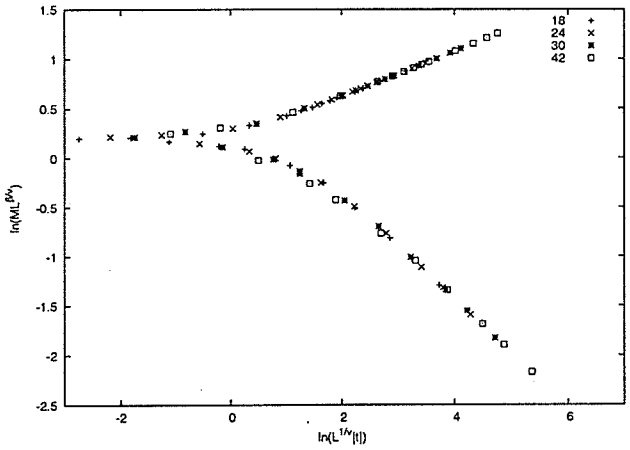

Figure 7.16: Log-log finite size scaling plot of order parameter M for $r = 0.5$ The critical temperature $T_c = 1.642$ and the exponent β =0.243. The best collapse of the data was obtained for ν=0.5177 with asymptotic slopes of 0.231 for $T < T_c$ and -0.5327 for $T > T_c$.

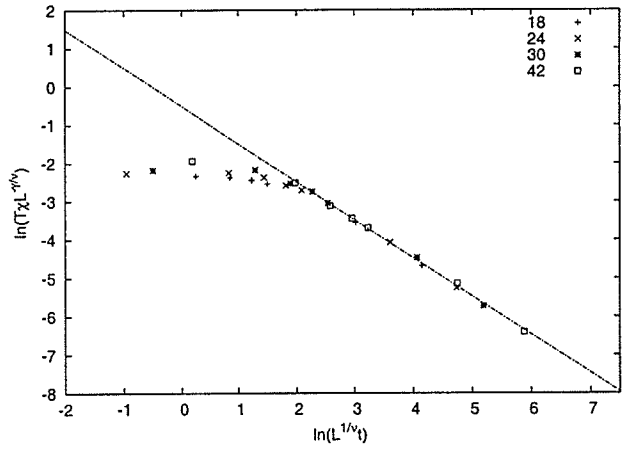

Figure 7.17: Log-log finite size scaling plot for the susceptibility χ above the critical point for $r = 0.5$. Here T_c=1.642, ν=0.518 and γ=1.04, while the asymptotic slope of f_χ has a value of 1.028.

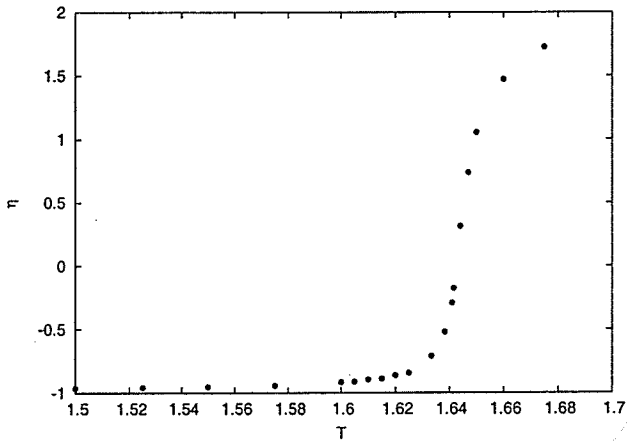

Figure 7.18: Temperature dependence of the critical exponent η for$r = 0.5$. $\eta(T_c)$=-0.08 $\pm$ 0.03

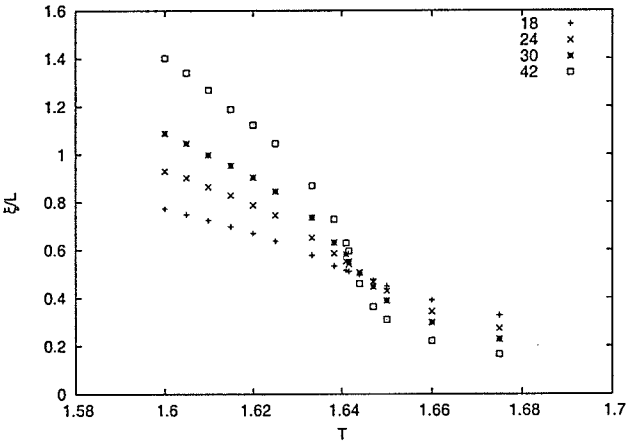

Figure 7.19: Temperature dependence of the scaled correlation length for $r = 0.5$ and sizes $L = 18, 24, 30$ and 42. Curves cross at the critical temperature T_c=1.642.

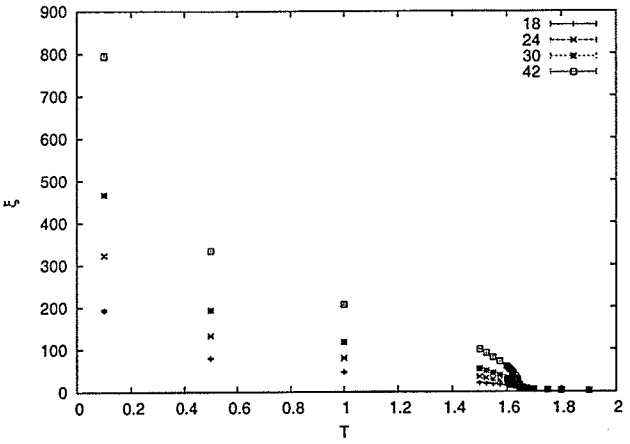

Figure 7.20: Temperature dependence of correlation length for $r = 0.5$.

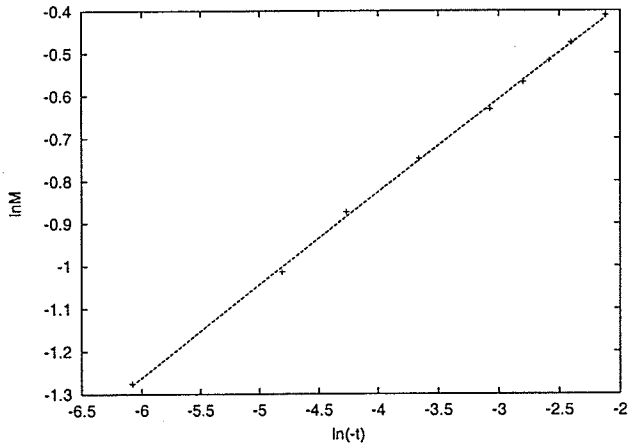

Figure 7.21: Order parameter $M(\infty, T)$ plotted versus reduced temperature t on log-log scale for a $r = 0.8$ system.

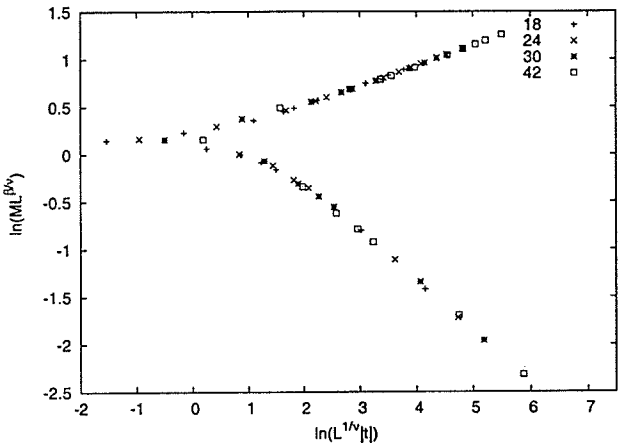

Figure 7.22: Log-log finite size scaling plot of order parameter M for $r = 0.8$ system. The critical temperature $T_c = 1.7039$ and the exponent β =0.218. The best collapse of data was obtained for ν=0.49 with an asymptotic slope of 0.216 for $T < T_c$ and -0.508 for $T > T_c$.

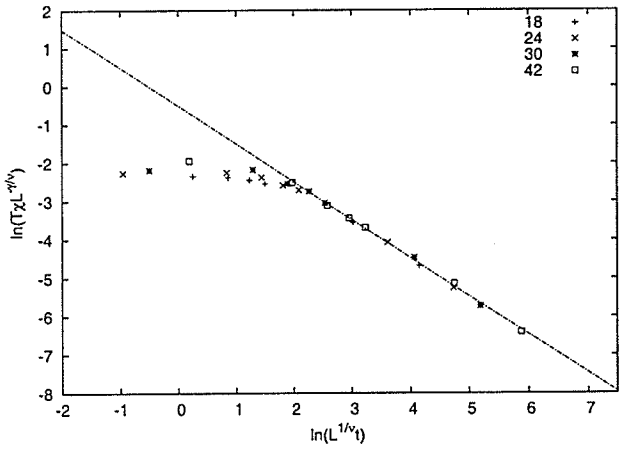

Figure 7.23: Log-log scale finite size scaling plot for the susceptibility χ above critical point for $r = 0.8$. In this case T_c=1.7039, ν=0.49 and γ=1.0, while the asymptotic slope of f_χ has a value of 0.9946.

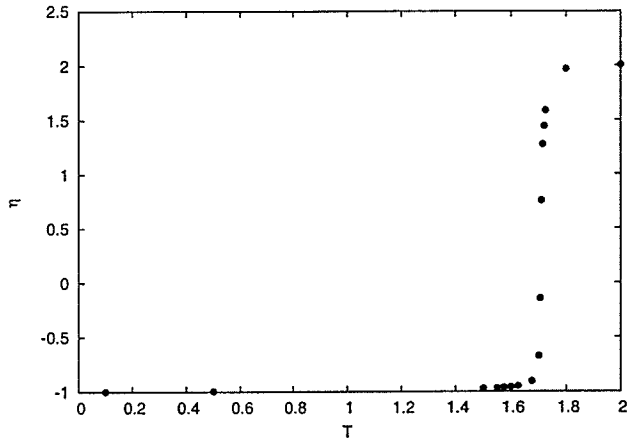

Figure 7.24: Temperature dependence of critical exponent η for r=0.5. $\eta(T_c)$=-0.04 $\pm$ 0.02

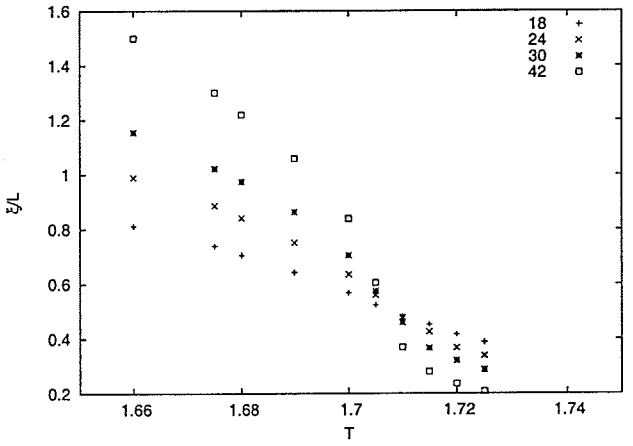

Figure 7.25: Temperature dependence of scaled correlation length for $r = 0.8$ and system sizes $18, 24, 30$ and 42. Curves cross at the critical temperature T_c=1.704.

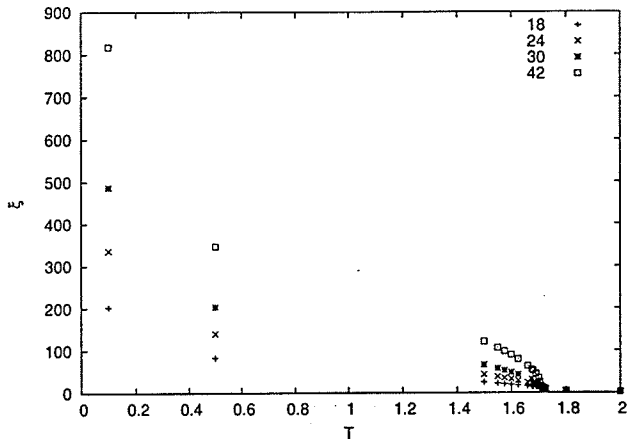

Figure 7.26: Temperature dependence of the correlation length for $r = 0.8$.

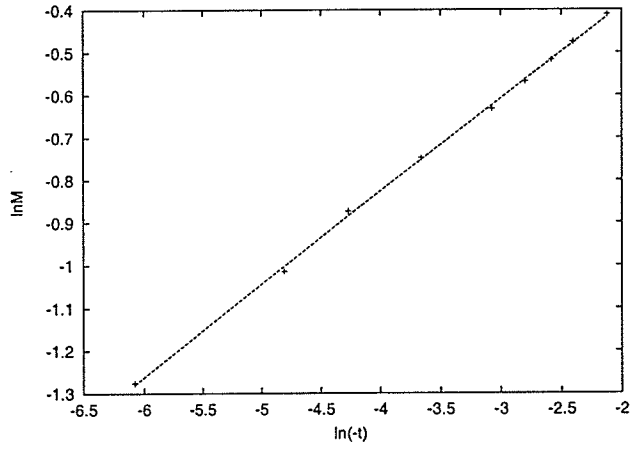

Figure 7.27: Order parameter $M(\infty, T)$ plotted versus reduced temperature t on log-log scale for a $r = 1.0$ system. Here Tc =1.7369.

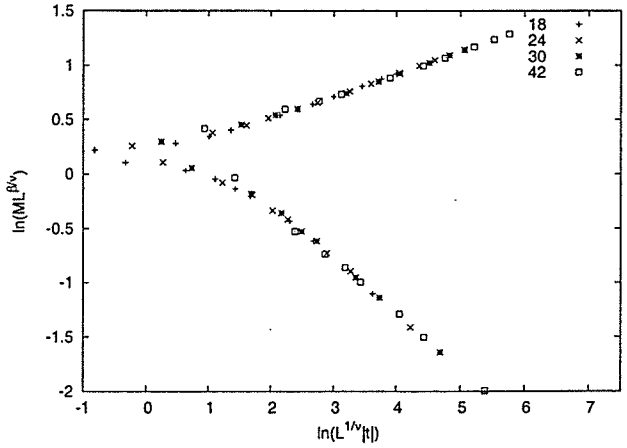

Figure 7.28: Log-log finite size scaling plot of order parameter M for a $r = 1.0$ system. The critical temperature $T_c = 1.7369$ and the exponent β =0.2134. The best collapse of data was obtained for ν=0.4817 with an asymptotic slope of 0.199 for $T < T_c$ and -0.5096 for $T > T_c$.

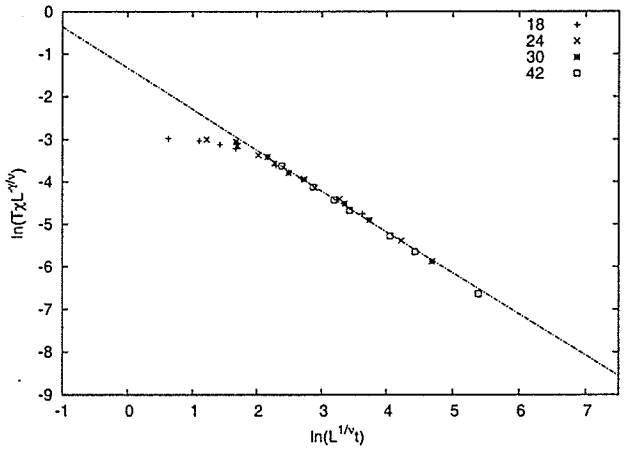

Figure 7.29: Log-log scale finite size scaling plot for the susceptibility χ above the critical point for $r = 1.0$. Here T_c=1.7369, ν=0.482 and γ=1.0, while the asymptotic slope of f_χ has a value of 0.9637.

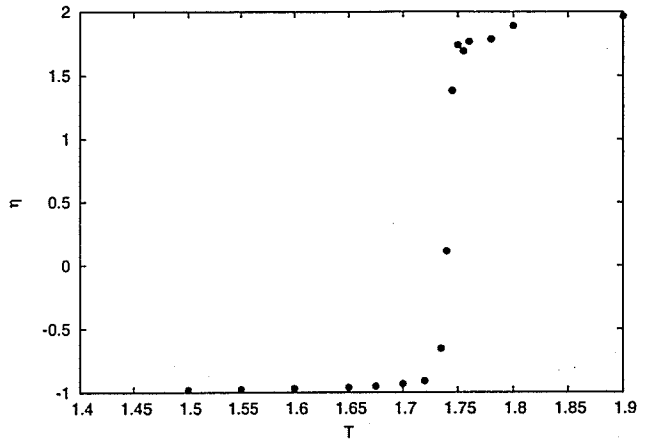

Figure 7.30: Temperature dependence of the critical exponent η for $r = 1.0$. $\eta(T_c)$=-0.07 $\pm$ 0.03

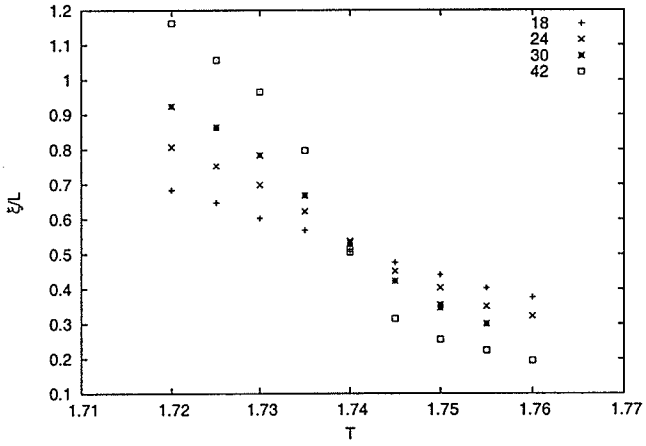

Figure 7.31: Temperature dependence of the scaled correlation length for $r = 1.0$ and system sizes $18, 24, 30$ and 42. Curves cross at the critical temperature T_c=1.739.

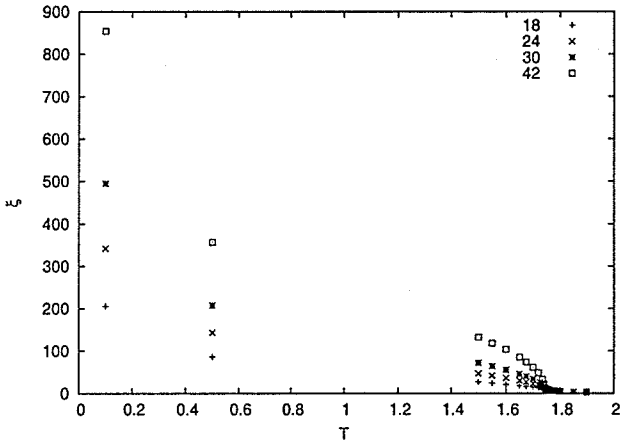

Figure 7.32: Temperature dependence of the correlation length for $r = 1.0$.

critical exponents	β	γ	ν	η
r=0.0 T_c=1.458(2)	0.253(10)	1.13(5)	0.54(2)	-
r=0.2 T_c=1.5494(4)	0.249(6)	1.1(1)	0.531(20)	-0.06(2)
r=0.5 T_c=1.6420(3)	0.243(9)	1.04(10)	0.518(20)	-0.08(4)
r=0.8 T_c=1.7039(7)	0.218(10)	1.0(1)	0.490(20)	-0.04(3)
r=1.0 T_c=1.737(1)	0.213(9)	1.0(2)	0.482(25)	-0.07(3)

Table 7.3: Summary of critical exponents for various rigidity parameters r. The results for $r = 0$ were obtained by Kawamura[1].

The critical exponents found for $r = 0.2, 0.5, 0.8$ and 1.0 are within the range of experimentally determined critical exponents for ABX_3 compounds and Tb. A summary of the critical exponents is given in table 7.3. The specific heat critical exponent α was rather difficult to obtain as the specific heat has a significant nonsingular part.

A verification of scaling and hyperscaling relations are given in table 7.4 as well as values for α and η that follow from these relations. We find that the critical exponent η determined directly from the structure factor calculation as well as by using the scaling relations is consistently negative.

7.3.5 First order phase transition for $r \geq 1.0$

For larger values of the rigidity parameter r our results indicate that a first order transition occurs. The probability distribution for the energy $P(E)$ is a useful quantity to study to locate first order transitions. Away from the critical point one expects a Gaussian distribution in energy while at the critical point a double peak in $P(E)$ occurs. The transition point can be located by finding the temperature where the weights under the peaks in $P(E)$ become equal. However distinguishing between a

scaling relation	r=0.2	r=0.5	r=0.8	r=1.0
$2\beta+\gamma-3\nu=(0)$	0.005	0.028	0.034	0.02
α=2-3ν	0.407	0.446	0.53	0.554
α=2-2β-γ	0.402	0.474	0.564	0.574
η=2β/ν-1	-0.062	-0.0618	-0.11	-0.116
η=2-γ/ν	-0.072	-0.0077	-0.04	-0.075

Table 7.4: Verification of scaling/hyperscaling relations and critical exponents α and η determined by using scaling/hyperscaling relations.

weak first order transition and a second order transition is rather delicate especially in case of a possible tricritical point. In order to make sure what type of phase transition the double peak structure represents, it is necessary to study the size dependence of the probability distribution $P(E)$. In the region of a second order transition the two peak structure gets closer in energy with an increase in the size of system and at large enough size the double peak structure disappears completely. In the region of the first order transition, the two peaks remain separated and become sharper with increased size L [35]. A double peaked structure of $P(E)$ has been found for rigidity parameters $r = 1.0, 1.5, 2.0, 4.0, 6.0$ and 8.0. As the value of the rigidity parameter r decreases the size of the system where the double peak structure starts to appear increases. Figure (7.33) shows a probability distribution for $r = 4$ that has been reweighted in order to identify the critical point. The double peaked $P(E)$ becomes evident in this case at a system size $L = 24$ and it is easy to see that for $L = 60$ the two peaks are separated by a zero probability region, indicating a discontinuous behavior of energy as shown in figure (7.34). The critical temperature of a first order transition as well as the energy difference between the peak maxima (or latent heat)

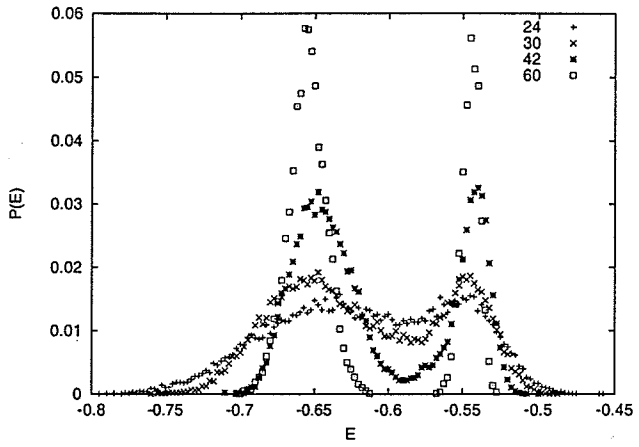

Figure 7.33: Size dependence of the energy probability distribution function for $r = 4.0$. A double peaked structure is apparent for sizes $L = 24, 30, 42$ and 60.

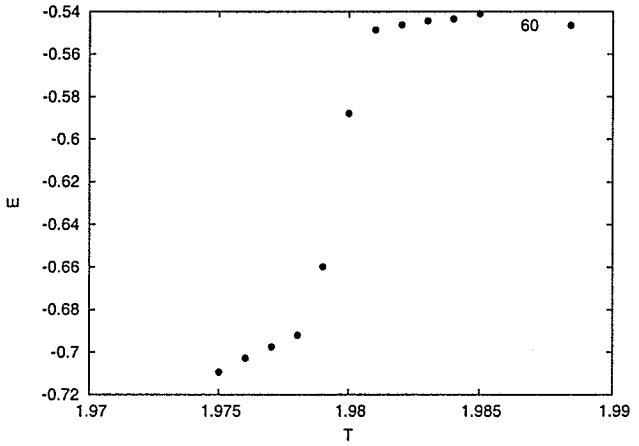

Figure 7.34: Temperature dependence of energy for $r = 4.0$ and $L = 60$ shows discontinuous behaviour at the critical temperature.

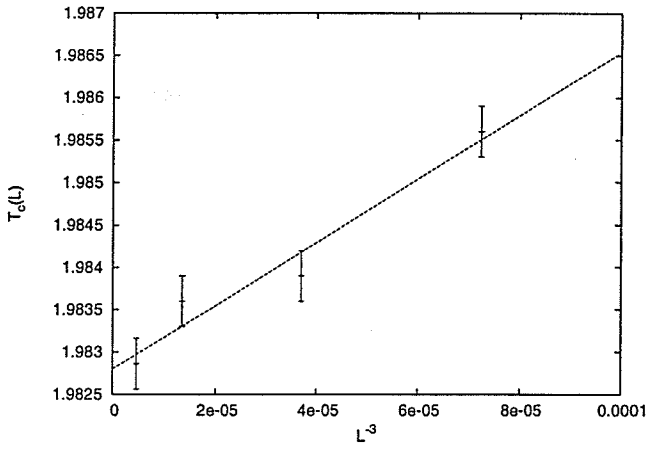

Figure 7.35: Extrapolation of a size dependent critical temperature $T_c(L)$ to the thermodynamic limit for r=4.0. $T_c(\infty) = 1.9828$

can be obtained using the finite size scaling theory developed by Lee and Kosterlitz [50]. The thermodynamic discontinuities at a first order transition become rounded in finite systems as in the continuous phase transition case. However the finite size scaling behaviour at the first order transition is different. The size dependent critical temperature $T_c(L)$ in a system exhibiting a first order transition scales as

$$T_c(L) \sim L^{-d} \tag{7.16}$$

where d is the dimension of the system. By plotting $T_c(L)$ vs L^{-3} it is possible to estimate the value of the critical temperature of the infinite system as shown in figure 7.35 for $r = 4.0$. The finite size scaling theory predicts that the positions of the peak energies scale as $1/L$ if the system exhibits a strong first order transition. In figure 7.36 we plot the energies per site, E_1 and E_2, of the peak maxima versus $1/L$ and extrapolate to the thermodynamic limit. This approach allows us to estimate $\Delta E = |E_1 - E_2|$ which is the latent heat at the transition.

We have repeated this analysis for other values of r and we find similar behaviour. In particular we have reexamined the value r=1.0 and the results for the energy

histograms are shown in figure 7.37 for L=48, 60 and 72. Again we see a double peak structure which is evidence of a first order phase transition but which is much weaker then for r=4.0. The evidence for the first order transition at r=1.0 occurs at a larger value of L than in the previous case r=4.0. In addition, the latent heat ΔE is significantly smaller.

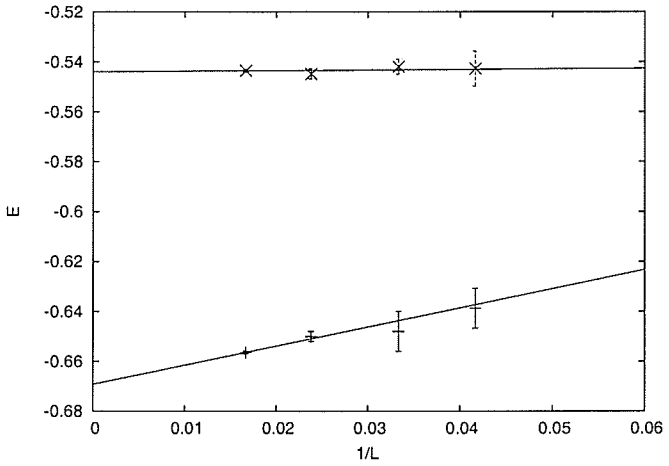

Figure 7.36: Extrapolation of the energies of the peak maxima to the thermodynamic limit according to FSS predictions at a first order transition.

In figure 7.38 we plot ΔE vs r and find that it extrapolates linearly to the physically interesting case $r = 0.0$. In this extrapolation ΔE at $r = 0.0$ remains nonzero with the estimated value 0.010 ± 0.007. This behaviour suggests that the phase transition at $r = 0$ might be weakly first order. Since ΔE does not extrapolate to zero for $r > 0$, there does not seem to be a tricritical point separating the two regions of 'pseudo-scaling' and first order behaviour. If the system exhibits a first order phase transition for all values of the rigidity parameter r (including the $r = 0.0$ - STA XY model), the reason that we are not able to identify it may be that the system sizes we used previously are too small. In order to confirm our result of a non-zero latent heat at $r = 0.0$, we have also studied the energy probability distribution for the $r = 0.0$ case using system sizes $L = 96$ and $L = 138$.

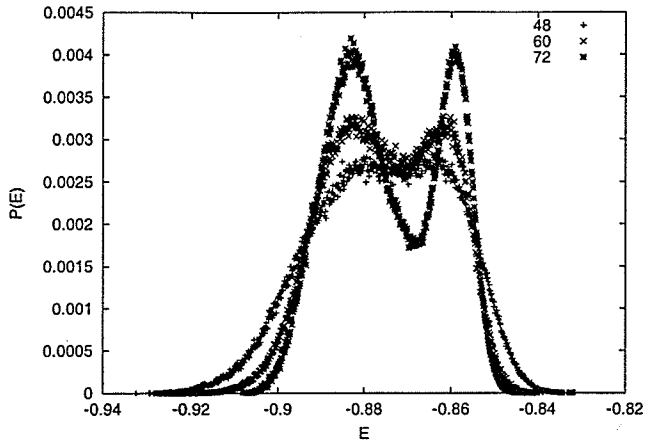

Figure 7.37: Size dependence of the energy probability distribution for r=1.0. A double peak structure appears for sizes L=48, 60 and 72.

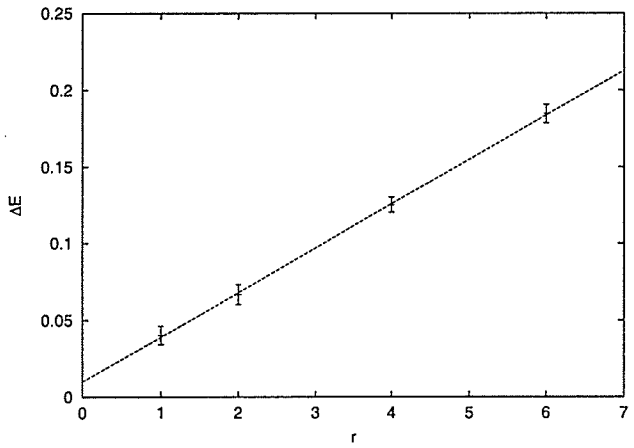

Figure 7.38: Extrapolation of the energy difference of peak maxima to $r = 0$.

Figure 7.39 shows $P(E)$ at the critical temperature for the two system sizes. A double peak structure characteristic of a first order phase transition is evident. As the size of the system is increased, the peaks sharpen and the depth of the minimum between the peaks also increases. The value of $\Delta E \sim 0.011$ for $r = 0.0$ estimated from figure 7.39 is in excellent agreement with the estimate of 0.010 ± 0.007 obtained from the extrapolation of $\Delta E(r)$ to $r = 0.0$.

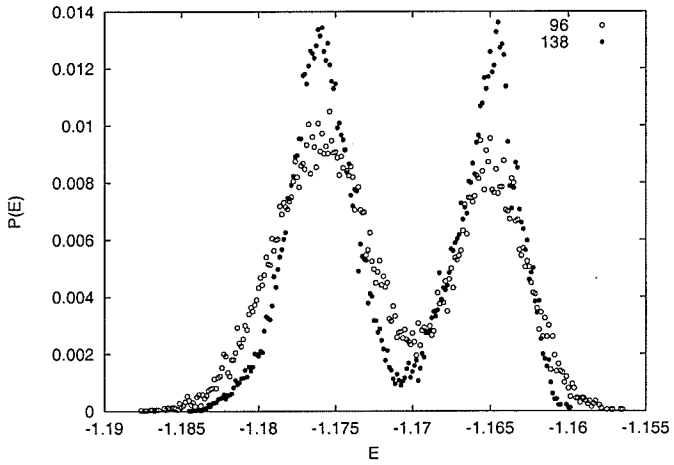

Figure 7.39: P(E) for STA XY model ($r = 0$) for $L = 96$ and $L = 138$ at T_c.

7.4 Conclusion

We have studied a generalized STAR model (7.3) which allows us to move continuously from the STA to STAR XY models. Using system sizes $L \leq 60$ we found two different types of behaviour. For $r \leq 1.0$ the system exhibits a 'pseudo-critical' behaviour whereas, for $r \geq 1.0$, a first order phase transition occurs. The critical exponents obtained in the $r \leq 1.0$ range appear to vary with the rigidity parameter r. This nonuniversal behaviour is inconsistent with true critical behaviour at a continuous phase transition for systems having the same symmetry of the order parameter. We conclude that the critical exponents are really 'pseudocritical' exponents and the

observed scaling is 'pseudoscaling'. Using FSS to study the first order transitions in the range $r > 1.0$ we were able to estimate the value of latent heat $\Delta E(r)$ for several values of r. We extrapolated the values of the latent heat $\Delta E(r)$ to $r = 0$ and we found a small but nonzero latent heat for the XY STA model which indicated a very weak first order phase transition. We have confirmed this behaviour by studying the energy probability distribution for $r = 0$ using the much larger systems sizes $L = 96$ and $L = 138$. In these cases we find unambiguous evidence that the phase transition in the XY STA model is of the first order.

The estimated values of critical exponents are within the range of the experimentally observed critical exponents for ABX_3 compounds and Tb. The 'pseudocriticality' explains as well the negative value of the critical exponent η. Our simulations are consistent with the predictions of the non perturbative RG (NPRG) theoretical approach [17, 20, 107]. In the NPRG theory the appearance of incompatible sets of critical exponents in the XY STA was explained in terms of a very slow RG flow in coupling space and a very weak first order phase transition is predicted for both XY and Heisenberg model.

It has been observed by Itakura[18] that clear evidence of a first order in XY STA only becomes evident for larger sizes of the system L. Hence previous studies that used smaller sizes $L \leq 60$ were not able to detect any first order behaviour. We also find that systems larger than $L > 72$ are needed to see the double peak structure in the energy probability distribution. There are several cases in the literature [51] of effective exponents being measured if a system is not close enough to its critical point $t = (T - Tc)/Tc = 0$. In our case we have a similar situation except that the systems we study are not always large enough in size and we observe effective exponents. The true behaviour only appears for sufficiently large sizes. The finite size scaling approach involves both quantities, the reduced temperature t and the size L of the system, in the scaling functions $F(t, L)$ and it is equally important to study the system close to T_c and also for large L.

Chapter 8

SUMMARY AND FUTURE OUTLOOK

8.1 Summary

The behaviour of antiferromagnets on triangular geometries remains controversial even after more than 25 years of research. Real experiments, numerical simulations and field theories have all provided a variety of different results for both Heisenberg and XY models. The main focus has been on the order of the phase transition which occurs on the hexagonal lattice geometry. Some results provide strong evidence that the transition in both models is continuous but with exponents that belong to a new chiral universality class. Other results point towards an interpretation in terms of a weak first order transition. The antiferromagnetic Heisenberg model on triangular geometries has rather different properties from the usual Néel antiferromagnets. The ordered state is noncollinear and the order parameter is essentially a rotation matrix with SO(3) symmetry. Homotopy theory considerations in $d = 2$ admit the existence of a Z_2 topological defect, or vortex, in this model. This type of topological excitation also plays an important role in the superfluid phase of He^3 which has the same order parameter symmetry. Previous studies[3, 4, 12, 13, 16] in $d = 2$ have shown that the Heisenberg system undergoes a purely topological phase transition. In this thesis, Monte Carlo methods have been used to consider two basic questions: i) how does the two dimensional behaviour of the Heisenberg model cross over to the three dimensional behaviour? and ii) what is the nature of the transition in three dimensions?

Detailed Monte Carlo simulations were performed in chapter 5 to study the crossover from two dimensional to three dimensional behaviour. We calculated a number of

physical quantities paying special attention to study of the spin wave excitations through the spin stiffness. In addition, topological excitations were probed directly using the response of the system to the presence of a virtual vortex that we call vorticity. A phase transition of purely topological character was found for the stacked triangular lattice with layer thicknesses $H = 2, 3, 4, 6, 8, 14, 20$ and 24. The systems show no rigidity with respect to spin wave excitations at any finite temperature in accord with the predictions of Peierls[26], Mermin and Wagner[28] and Hohenberg[29]. The spin stiffness is zero at all finite temperatures indicating exponentially decaying correlations. However, the system has rigidity at low temperatures to the formation of isolated vortices. Our vorticity data indicates that there is a finite temperature below which there are no free vortices and above which a proliferation of vortices occurs. At sufficiently low temperature we find very good agreement with the predictions of the nonlinear sigma model (NLσ) which predicts the vanishing spin stiffness at all finite temperatures [10]. As the number of layers increases, the spin wave stiffness approaches a finite value at low T in the $3d$ limit. The NLσ model approach does not include any vortex degrees of freedom and predicts that the system orders only at zero temperature. The role of vortex degrees of freedom in our study becomes apparent through the study of the vorticity or the related quantity called vorticity modulus. The vorticity moduli shows a universal jump at the critical temperature which is inversely proportional to number of layers H and hence, in the limit of a three dimensional system, approaches zero.

The topological phase transition is characterized by exponentially decaying correlations in the regions both above and below the critical temperature. This differs from the very well known Kosterlitz - Thouless vortex unbinding phase transition observed in the studies of He^4 superfluid films and the ferromagnetic XY model. The Kosterlitz - Thouless transition is a classic example of the appearance of quasi long range order in the form of tightly bound vortex pairs. However the vortices in this case are associated with a two component order parameter described either as a two

component vector or a complex number and they differ from Z_2 vortices associated with an order parameter with SO(3) symmetry. The correlations in the Kosterlitz - Thouless transition decay exponentially in the high temperature phase but show a power law decay in the low temperature phase.

Analyzing the vorticity moduli data using the predictions of finite size scaling theory (FSS), we have found that the expected collapse of the data to a universal curve is only possible for a slightly modified scaling form. Due to the free boundary conditions at the surface layers, we find that the thickness H of the layers is not the only important length scale and it is modified for systems with $H \leq 8$ where an effective layer thickness must be used. Similar effects of surface boundary conditions has been also been observed in a numerical study of He^4 thin films [91, 92]. The same considerations apply to the finite size scaling description of the thickness dependent critical temperature. Our results indicate that the $2d$ behaviour approaches the $3d$ behaviour in a continuous way and that topological excitations play an important role between the two limits.

Chapter 6 was dedicated to a study of the spin stiffness in the $3d$ Heisenberg model on a stacked triangular lattice. The order of the phase transition of this model is a highly debated question. Based on the numerical observation of the scaling characteristic for continuous phase transitions and also on the fact that the symmetry of order parameter (SO(3)) differs from that found in the Heisenberg antiferromagnet on a bipartite lattice (O(3)), Kawamura[52] conjectured that the phase transition belongs to a new 'chirality universality' class. In our study we used both a heat bath Monte Carlo algorithm and a broad histogram method to study the spin stiffness. We find excellent agreement between two methods. The spin stiffness can be used to directly measure the correlation length critical exponent ν. We used finite size scaling theory (FSS) to extract the value of critical exponent ν and find that the spin wave stiffness scales according to the FSS predictions which are characteristic of a continuous phase transition with a value of the critical exponent ν that belongs to

the proposed 'chirality universality' class. Our numerical value of exponent $\nu = 0.59$ agrees very well with the value found by indirect methods in the numerical simulations in reference [1].

In chapter 7 we addressed the controversy regarding the order of the phase transition in XY stacked triangular antiferromagnets (STA). The chiral degree of freedom in this latter model is discrete and the order parameter symmetry can be described as $S_1 \times Z_2$. Here S_1 describes the unit circle of all possible orientations of a two dimensional unit vector and Z_2 describes the two possible realizations of the chirality. Early Monte Carlo studies of this model indicated a continuous phase transition, while slightly modified models that do not change the symmetry of the order parameter but impose rigid constraints that suppress local fluctuations of the order parameter (STAR model) find a first order phase transition. We introduced a generalized STAR model [17] in which we can continuously tune the local rigidity from the STA limit (no rigidity) to the STAR limit (infinite rigidity).

We find two types of behaviour in systems of size $L \leq 60$. A detailed analysis in the region where weak rigidity constraints are imposed (rigidity parameter r$\leq$ 1) suggests that the system undergoes a phase transition which exhibits 'effective scaling' and 'effective critical exponents'. The observed critical exponents are different for different values of rigidity parameter r and this fact is inconsistent with a true universal behaviour of systems that have the same order parameter and spatial dimension. However the estimated values of critical exponents agree well with the values of critical exponents found in experimental studies of materials that can be described by the XY STA model. The scaling relations and our direct estimate of the critical exponent η from a calculation of the structure factor yield a negative value. A negative value of the exponent η is forbidden by first principles in the continuum Φ^4 LGW theory used to describe these systems.

As the strength of the rigidity constraint is increased (rigidity parameter r$\geq$ 1.0) the phase transition becomes first order. Although this change in the order of the

transition with an increase in the rigidity parameter r was suggestive of a possible tricritical point, our study of systems of larger size than previously considered have revealed unambiguous evidence for a first order phase transition even in the limit when no rigidity is imposed (XY STA model). An extrapolation of our estimates of the latent heat for values of r where we find a first order transition to the $r = 0$ limit suggests a small but finite latent heat in the XY STA model and consequently a weak first order transition. Our findings are consistent with the non perturbative RG theoretical approach which also suggests very weak first order transition [17, 20, 107]. The weak first order transition in the XY model is associated with a slowing down of RG flow and there is no fixed point or minimum in the flow in this approach.

The same theoretical approach suggests a weak first order phase transition for the Heisenberg model as well. However the NPRG picture of the Heisenberg STA differs from that of the XY STA. Pseudoscaling and pseudocritical exponents are also predicted but they are related to presence of a complex fixed point with small imaginary parts called a pseudofixed point. Furthermore, the predicted pseudocritical exponents are very close to those predicted by the high order perturbative RG approach [98, 21, 100, 88] and from the experimental point of view the two approaches are indistinguishable. Numerical studies of the STAR model [99] as well as a numerical study of the RG flow [18] do not find any direct evidence of a first order transition in the Heisenberg STA. It has been suggested that a system of linear size $L \sim 800$ is needed to detect the first order behaviour which is computationally unachievable at present.

8.2 Future Outlook

Our studies indicate that topological excitations in the Heisenberg antiferromagnet on triangular geometries play an important role between $d = 2$ and $d = 3$. This suggests that it is necessary to include topological degrees of freedom in the field theoretical

studies of this model in order to reach a better understanding of the underlying physics. It is also possible that topological excitations play an important role in the $3d$ system and hence further investigations are desirable.

One possible extension of the studies presented here is to allow for some exchange anisotropy in the Hamiltonian. This anisotropy could favour either an easy plane (XY-like) or an easy axis (Ising-like). Watarai and Miyahita[109, 110] have made some preliminary investigations of the easy axis case. However, it would also be interesting study the role of topological excitations in this system.

The variation in the results reported by different investigators, specifically related to the order of the phase transition in both XY and Heisenberg STA models in $3d$, clearly indicate that further theoretical work and experimental measurements are required before the properties of these frustrated materials are completely understood. Although our findings related to the XY STA unambiguously show that the system undergoes a first order phase transition further numerical work for both the XY and the Heisenberg STA are desirable to reveal the underlying physics. Of particular interest would be a study of the generalized STAR model introduced in chapter 7 for the Heisenberg case where it has also been predicted that local rigidity constraints imposed on the order parameter might be responsible for possible 'pseudo critical' behaviour. This study would require consideration of much larger system sizes. Another approach that could be used to identify a possible first order phase transition is the short time dynamics approach [111, 112] . The advantage of this approach is that much shorter Monte Carlo runs are needed and larger system sizes can be studied with the same computational resources .

BIBLIOGRAPHY

[1] Hikaru Kawamura. *J. Phys. Soc. Japan*, **61**:1299, 1992.

[2] M. E. Fisher. *Rev. Mod. Phys.*, **46**:597, 1974.

[3] H. Kawamura and S. Miyashita. *J. Phys. Soc. Japan*, **53**:4138, 1984.

[4] H. Kawamura and M. Kikuchi. *Phys. Rev. B*, **47**:1134, 1993.

[5] J. M. Kosterlitz and D. J. Thouless. *J. Phys. C*, **6**:1181, 1973.

[6] J. M. Kosterlitz. *J. Phys. C*, **7**:1046, 1974.

[7] T. Dombre and N. Read. *Phys. Rev. B*, **39**:6797, 1989.

[8] P. Azaria, B. Delamotte, and T. Jolicoeur. *Phys. Rev. Lett.*, **64**:3175, 1990.

[9] P. Azaria, B. Delamotte, and D. Mouhanna. *Phys. Rev. Lett.*, **68**:1762, 1992.

[10] P. Azaria, B. Delamotte, T. Jolicoeur, and D. Mouhanna. *Phys. Rev. B*, **45**:12612, 1992.

[11] B. W. Southern and A. P. Young. *Phys. Rev. B*, **48**:13170, 1993.

[12] B. W. Southern and H-J Xu. *Phys. Rev. B*, **52**:R3836, 1995.

[13] W. Stephan and B. W. Southern. *Phys. Rev. B*, **61**:11514, 2000.

[14] H-J Xu and B. W. Southern. *J. Phys. A: Math. Gen.*, **29**:L133, 1996.

[15] L. Capriotti, R. Vaia, A. Cuccoli, and V. Tognetti. *Phys. Rev. B*, **58**:273, 1998.

[16] W. Stephan and B. W. Southern. *Can. J. Phys.*, **79**:1459, 2001.

[17] B. Delamotte, D. Mouhanna, and M. Tissier. *cond-mat/0309101, submitted to Phys. Rev. B*, 2003.

[18] M. Itakura. *J. Phys. Soc. Jpn.*, **72**:74, 2003.

[19] M. F. Collins and O. A. Petrenko. *Can. J. Phys.*, **75**:605, 1997.

[20] M. Tissier, B. Delamotte, and D. Mouhanna. *Phys. Rev. Lett.*, **84**:5208, 2000.

[21] A. Pelissetto, P. Rossi, and E. Vicari. *Phys. Rev. B*, **63**:140414(R), 2001.

[22] P. W. Anderson. *Basic Notions of Condensed Matter Physics.* The Benjamin/Cummings Publishing Company, Inc., 1984.

[23] James P. Sethna. In *1991 Lectures in Complex Systems, SFI Studies in the Sciences of Complexity*, volume **XV**, page 243. Addison Wesley, 1992.

[24] R. E. Peierls. *Proc. Cambridge Philos. Soc.*, **32**:477, 1936.

[25] L. Onsager. *Phys. Rev.*, **65**:117, 1944.

[26] R. Peierls. *Surprises in Theoretical Physics.* Princeton University Press, 1979.

[27] R. Peierls. *Helv. Phys. Acta*, Suppl. 2, **7**:81, 1934.

[28] N. D. Mermin and H. Wagner. *Phys. Rev. Lett.*, **17**:1133, 1966.

[29] P. C. Hohenberg. *Phys. Rev.*, **158**:383, 1967.

[30] P. M. Chaikin and T. C. Lubensky. *Principles of Condensed Matter Physics.* Cambridge University Press, 1997.

[31] J. Goldstone. *Nuovo Cimento*, **19**:155, 1961.

[32] G. Toulouse and M. Kléman. *Journal de Physique*, **37**:L149, 1976.

[33] M. E. Fisher, M. N. Barber, and D. Jasnow. *Phys. Rev. A*, **8**:1111, 1973.

[34] K. Binder and D. Stauffer. In K. Binder, editor, *Applications of the Monte Carlo Method in Statistical Physics*, page 1. Springer-Verlag, 1987.

[35] D. P. Landau and Kurt Binder. *A Guide to Monte Carlo Simulations in Statistical Physics.* Cambridge University Press, 2000.

[36] M. N. Barber. In C. Domb and J. L. Lebowitz, editors, *Phase Transitions and Critical Phenomena*, page 146. Academic Press, 1983.

[37] J. A. Olive, A. P. Young, and D. Sherrington. *Phys. Rev. B*, **34**:6341, 1986.

[38] P. M. C. de Oliveira, T. J. P. Penna, and H. J. Herrmann. *Braz. J. Phys.*, **26**:677, 1996.

[39] Jose D. Muñoz and Hans J. Herrmann. In D. Landau, editor, *Computer Simulation Studies in Condensed-Matter Physics XII.* Springer, Berlin, 1999.

[40] Jose D. Muñoz and Hans J. Herrmann. *International Journal of Modern Physics C*, **10**:95, 1999.

[41] P. M. C. de Oliveira. *Eur. Phys. J. B*, **6**:111, 1998.

[42] N. Metropolis et al. *J. Chem Phys.*, **21**:1087, 1953.

[43] J. D. Muñoz and H. J. Herrmann. Basis and applications of the broad histogram method for continuous systems. In *Monte Carlo and Structure Optimization Methods for Biology, Chemistry and Physics, electronic proceedings, www.scri.fsu.edu/workshops/MCworkshop.html*, 1999.

[44] A. Papoulis. *Probability, Random Variables, and Stochastic Processes.* McGraw-Hill, 1965.

[45] M. E. Fisher. In M. S. Green, editor, *Critical Phenomena, Proceedings of the 51st Enrico Fermi School.* Academic Press, 1971.

[46] M. E. Fisher and M. N. Barber. *Phys. Rev. Lett.*, **28**:1516, 1972.

[47] John Cardy. *Scaling and Renormalization in Statistical Physics.* Cambridge University Press, 1996.

[48] L. P. Kadanoff and F. J. Wegner. *Phys. Rev. B*, **4**:3989, 1971.

[49] K. Binder. *Z. Physik*, **43**:119, 1981.

[50] J. Lee and J. M. Kosterlitz. *Phys. Rev. B*, **43**:3265, 1991.

[51] B.D. Gaulin. In H.T. Diep, editor, *Magnetic Systems with Competing Interactions*, page 286. World Scientific, 1994.

[52] Hikaru Kawamura. *J. Phys.: Condens. Matter*, **10**:4707, 1998.

[53] A. Pelissetto and E. Vicari. *Phys. Rep.*, **368**:549, 2002.

[54] N. W. Ashcroft and N. D. Mermin. *Solid State Physics.* Holt, Rinehart and Winston, 1976.

[55] A. P. Ramirez. Strongly geometrically frustrated magnets. *Ann. Rev. Mater. Sci.*, **24**:453, 1994.

[56] G. Toulouse. *Commun. Phys.*, **2**:115, 1977.

[57] G. H. Wannier. *Phys. Rev.*, **79**:357, 1950.

[58] J. Villain. *Journal de Physique*, **38**:385, 1977.

[59] T. E. Mason, M. F. Collins, and B. D. Gaulin. *J. Phys. C*, **20**:L945, 1987.

[60] Y. Ajiro, T. Nakashima, Y. Unno, H. Kadowaki, M. Mekata, and N. Achiwa. *J. Phys. Soc. Japan*, **57**:2648, 1988.

[61] B. D. Gaulin, T. E. Mason, M.F. Collins, and J. F. Larese. *Phys. Rev. Lett.*, **62**:1380, 1989.

[62] T. E. Mason, B. D. Gaulin, and M. F. Collins. *Phys. Rev. B*, **39**:586, 1989.

[63] H. Kadowaki, S. M. Shapiro, T. Inami, and Y. Ajiro. *J. Phys. Soc. Japan*, **57**:2640, 1988.

[64] J. Wang, D. P. Belanger, and B. D. Gaulin. *Phys. Rev. Lett.*, **66**:3195, 1991.

[65] R. Deutshmann, H. van Löhneysen, J. Wosnitza, R. K. Kremer, and D. Visser. *Euro. Phys. Lett.*, **17**:637, 1992.

[66] T. Kato, T. Asano, Y. Ajiro, S. Kawano, T. Ihii, and K. Iio. *Physica B*, **213-214**:182, 1995.

[67] T. Kato, K. Iio, T. Hoshimo, T. Mitsui, and H. Tanaka. *J. Phys. Soc. Japan*, **61**:275, 1992.

[68] K. Adachi, N. Achiwa, and M. Mekata. *J. Phys. Soc. Japan*, **49**:545, 1980.

[69] U. Schotte, N. Stüsser, K. D. Schotte, H. Weinfurter, H. M. Mayer, and M. Winkelman. *J. Phys.: Condens. Matter*, **46**:10105, 1994.

[70] M. Campostrini, M. Hasenbusch, A. Pelissetto, P. Rossi, and E. Vicari. *Phys. Rev. B*, **63**:214503, 2001.

[71] H. Kadowaki, K. Ubokoshi, K. Hirakawa, J. L. Martinez, and G. Shirane. *J. Phys. Soc. Japan*, **56**:4027, 1987.

[72] J. Wosnitza, R. Deutschmann, H. von Löhneysen, and R. K. Kremer. *J. Phys.: Condens. Matter*, **6**:8045, 1994.

[73] H. Weber, D. Beckmann, J. Wosnitza, H. von Löhneysen, and D. Visser. *Int. J. Mod. Phys. B*, **9**:1387, 1995.

[74] D. Beckmann, J. Wosnitza, H. von Löhneysen, and D. Visser. *Phys. Rev. Lett.*, **71**:2829, 1993.

[75] M. Enderle, G. Fortuna, and M. Steiner. *J. Phys.: Condens. Matter*, **6**:L385, 1994.

[76] M. Enderle, R. Schneider, Y. Matsuoka, and K. Kakurai. *Physica B*, **234-236**:554, 1997.

[77] Y. Oohara, H. Kadowaki, and K. Iio. *J. Phys. Soc. Japan*, **60**:393, 1991.

[78] M. Campostrini, M. Hasenbusch, A. Pelissetto, P. Rossi, and E. Vicari. *Phys. Rev. B*, **65**:144520, 2002.

[79] H. Kawamura. *J. Phys. Soc. Japan*, **54**:3220, 1985.

[80] H. Kawamura. *J. Phys. Soc. Japan*, **55**:2095, 1986.

[81] H. Kawamura. *J. Phys. Soc. Japan*, **56**:474, 1987.

[82] M. L. Plummer and A. Mailhot. *Phys. Rev. B*, **50**:16113, 1994.

[83] E. H. Boubcheur, D. Loison, and H. T. Diep. *Phys. Rev. B*, **54**:4165, 1996.

[84] A. Mailhot, M. L. Plummer, and A. Caillé. *Phys. Rev. B*, **50**:6854, 1994.

[85] T. Bhattacharya, A. Billoire, R. Lacaze, and T. Jolicoeur. *J. Phys. I (Paris)*, **4**:181, 1994.

[86] D. Loison and H. T. Diep. *Phys. Rev. B*, **50**:16453, 1994.

[87] A. Peles and B. W. Southern. *Phys. Rev. B*, **67**:184407, 2003.

[88] P. Calabrese, P. Parruccini, and A. I. Sokolov. *Phys. Rev. B*, **68**:094415, 2003.

[89] N. D. Mermin. *Phys. Rev.*, **176**:250, 1996.

[90] V. Ambegaokar, B. I. Halperin, D. R. Nelson, and E. D. Siggia. *Phys. Rev. B*, **21**:1806, 1980.

[91] N. Schultka and E. Manousakis. *Phys. Rev. B*, **51**:11712, 1995.

[92] N. Schultka and E. Manousakis. *J. Low Temp. Phys.*, **109**:733, 1997.

[93] D. J. Thouless. *Topological Quantum Numbers in Nonrelavistic Physics.* World Scientific, 1998.

[94] H. Kawamura. *Can. J. Phys.*, **79**:1447, 2001.

[95] A. Mailhot, M. L. Plumer, and A. Caillé. *Phys. Rev. B*, **50**:6854, 1994.

[96] S. A. Antonenko and A. I. Sokolov. *Phys. Rev. B*, **49**:15901, 1994.

[97] S. A. Antonenko, A. I. Sokolov, and K. B. Varnashev. *Phys. Lett.*, **208A**:161, 1995.

[98] A. Pelissetto, P. Rossi, and E. Vicari. *Phys. Rev. B*, **65**:020403(R), 2001.

[99] D. Loison and K. D. Schotte. *Eur. Phys. J. B*, **14**:125, 2000.

[100] P. Calabrese, P. Parruccini, and A. I. Sokolov. *Phys. Rev. B*, **66**:180403R, 2002.

[101] J. S. Wang. *Eur. Phys. J. B*, 8:287, 1998.

[102] B. A. Berg and U. H. E. Hansmann. *Eur. Phys. J. B*, **6**:395, 1998.

[103] J. S. Wang. *Physica A*, **281**:147, 2000.

[104] M. Campostrini, M. Hasenbusch, A. Pelissetto, P. Rossi, and E. Vicari. *Phys. Rev. B*, **65**:144520, 2002.

[105] H. B. Weber, T. Werner, J. Wosnitza, H. v. Löhneysen, and U. Schotte. *Phys. Rev. B*, **54**:15924, 1996.

[106] J. Zinn-Justin. *Quantum Field Theory and Critical Phenomena.* Oxford University Press, New York, 3rd ed., 1989.

[107] M. Tissier, D. Mouhanna, and B. Delamotte. *Phys. Rev. B*, **61**:15327, 2000.

[108] D. P. Landau. *Phys. Rev. B*, **13**:2997, 1976.

[109] S. Watarai and S. Miyashita. *J. Phys. Soc. Japan*, **63**:1916, 1994.

[110] S. Watarai and S. Miyashita. *J. Phys. Soc. Japan*, **67**:816, 1998.

[111] B. Zheng. *Int. J. Mod. Phys. B*, **12**:1419, 1998.

[112] L. Schülke and B. Zheng. *Phys. Rev. E*, **62**:7482, 2000.

[113] H. Goldstein. *Classical Mechanics.* Addison-Wesley Publishing Company, 2nd ed., 1981.

Appendix A

SPIN STIFFNESS

In order to compute the spin stiffness numerically we use the following approach. Consider a virtual twist of the spin system about an arbitrary axis $\hat{n}$ in the spin space. Each spin vector $\vec{S}_j$ is rotated by a different angle $\theta_j = (\vec{r}_j \cdot \hat{u})\frac{\Theta}{L}$ which is equivalent to imposing a gradient $\hat{u}\frac{\Theta}{L}$ on the system. Here $\vec{r}_j$ is the position vector of site j and $\hat{u}$ is a unit vector along the direction of the gradient in the lattice. In the presence of the twist, each spin transforms as

$$\vec{S}_j \rightarrow \vec{S}'_j = \mathbf{R}(\theta_j)\vec{S}_j \tag{A.1}$$

where $\vec{S}_j$ and $\vec{S}'_j$ are regarded as column vectors and $\mathbf{R}(\theta_j)$ is rotation matrix.

Consider the Euler parameterization of the rotation matrix in terms of the quaternion $(e_0, \vec{e})$ which satisfies $e_0^2 + \vec{e}\cdot\vec{e} = 1$ where

$$e_0 = \cos(\frac{\theta_j}{2}) \tag{A.2}$$

$$\vec{e} = \hat{n}\sin(\frac{\theta_j}{2}). \tag{A.3}$$

The axis of rotation is $\hat{n}$ and the rotation angle is θ_j. A clockwise rotation of the spin $\vec{S}_j$ by an angle θ_j can be written as[113]

$$\vec{S}'_j = (e_0^2 - \vec{e}\cdot\vec{e})\vec{S}_j + 2(\vec{e}\cdot\vec{S}_j)\vec{e} + (\vec{S}_j \times \hat{n})\sin(\theta_j). \tag{A.4}$$

In the presence of the twist, the original Hamiltonian $H = -\sum_{<ij>} J_{ij}\vec{S}_i^T \cdot \vec{S}_j$ is transformed and depends on the strength of the gradient $\alpha = \Theta/L$ implicitly through rotation matrix $\mathbf{R}$ as follows

$$H \rightarrow H(\alpha) = -\sum_{<ij>} J_{ij}\vec{S'}_i^T \cdot \vec{S'}_j$$

$$
\begin{aligned}
&= -\sum_{<ij>} J_{ij}\vec{S}_i^T\mathbf{R}^T(\theta_i)\mathbf{R}(\theta_j)\vec{S}_j \\
&= -\sum_{<ij>} J_{ij}\vec{S}_i^T\mathbf{R}(-\theta_i)\mathbf{R}(\theta_j)\vec{S}_j \\
&= -\sum_{<ij>} J_{ij}\vec{S}_i^T\mathbf{R}(\theta_j-\theta_i)\vec{S}_j \qquad \text{(A.5)}
\end{aligned}
$$

where in each case the superscript ^{T} denotes the transpose. The relative angle $(\theta_j-\theta_i)$ can be written as

$$
\begin{aligned}
\theta_{ij} &= \theta_j-\theta_i = (\vec{r_j}-\vec{r_i})\cdot\hat{u}\frac{\Theta}{L} \\
&= (\hat{e_{ij}}\cdot\hat{u})\alpha \qquad \text{(A.6)}
\end{aligned}
$$

where $\hat{e_{ij}}$ is a unit vector from site i to site j and the lattice constant is set equal to unity.

The final expression for the Hamiltonian in the twisted state is

$$
H(\alpha) = -\sum_{<ij>} J_{ij}\vec{S}_i^T\mathbf{R}(\theta_{ij})\vec{S}_j \qquad \text{(A.7)}
$$

with θ_{ij} defined in (A.6) and the elements of the rotation matrix given explicitly by

$$
\begin{aligned}
R_{11} &= \cos^2(\frac{\theta_{ij}}{2}) + (n_x^2-n_y^2-n_z^2)\sin^2(\frac{\theta_{ij}}{2}) \\
R_{12} &= 2(n_xn_y\sin^2(\frac{\theta_{ij}}{2}) + n_z\sin(\frac{\theta_{ij}}{2})\cos(\frac{\theta_{ij}}{2})) \\
R_{13} &= 2(n_xn_z\sin^2(\frac{\theta_{ij}}{2}) - n_y\sin(\frac{\theta_{ij}}{2})\cos(\frac{\theta_{ij}}{2})) \\
R_{21} &= 2(n_xn_y\sin^2(\frac{\theta_{ij}}{2}) - n_z\sin(\frac{\theta_{ij}}{2})\cos(\frac{\theta_{ij}}{2})) \\
R_{22} &= \cos^2(\frac{\theta_{ij}}{2}) - (n_x^2-n_y^2+n_z^2)\sin^2(\frac{\theta_{ij}}{2}) \\
R_{23} &= 2(n_yn_z\sin^2(\frac{\theta_{ij}}{2}) + n_x\sin(\frac{\theta_{ij}}{2})\cos(\frac{\theta_{ij}}{2})) \\
R_{31} &= 2(n_xn_z\sin^2(\frac{\theta_{ij}}{2}) + n_y\sin(\frac{\theta_{ij}}{2})\cos(\frac{\theta_{ij}}{2})) \\
R_{32} &= 2(n_yn_z\sin^2(\frac{\theta_{ij}}{2}) - n_x\sin(\frac{\theta_{ij}}{2})\cos(\frac{\theta_{ij}}{2})) \\
R_{33} &= \cos^2(\frac{\theta_{ij}}{2}) - (n_x^2+n_y^2-n_z^2)\sin^2(\frac{\theta_{ij}}{2}) \qquad \text{(A.8)}
\end{aligned}
$$

The equilibrium properties of system are determined from the partition function and the free energy density. In the presence of the twist, these quantities become

$$f' = F'/L^d = -\frac{kT}{L^d}\ln(Z') \tag{A.9}$$

$$Z' = \mathrm{Tr} e^{-H(\Theta)/kT} = e^{\sum_{ij} J_{ij}\vec{S}_i^T \mathbf{R}\vec{S}_j/kT} \tag{A.10}$$

The spin stiffness is related to the free energy cost of the twist as follows

$$f' = f + \frac{1}{2}\rho_{\hat{n}}\,(\Theta/L)^2 \tag{A.11}$$

and is thus given by $\rho_{\hat{n}} = \frac{d^2 f'}{d(\alpha)^2}|_{\alpha=0}$ where $\alpha = \Theta/L$ is the gradient magnitude. The second derivative of the twisted free energy with respect to the gradient strength α can be written as

$$\frac{d^2 f'}{d\alpha^2} = kT\left(\frac{1}{Z'^2}\left(\frac{dZ'}{d\alpha}\right)^2 - \frac{1}{Z'}\left(\frac{d^2 Z'}{d\alpha^2}\right)\right). \tag{A.12}$$

Substituting Z' from (A.10), the spin stiffness becomes

$$\rho_{\hat{n}} = \frac{d^2 f'}{d\alpha^2}\,|_{\alpha=0} = \frac{1}{L^d}\left[\left\langle\frac{d^2 H(\alpha)}{d\alpha^2}\right\rangle_T - \frac{1}{T}\left\langle\left(\frac{dH(\alpha)}{d\alpha}\right)^2\right\rangle_T + \frac{1}{T}\left(\left\langle\frac{dH(\alpha)}{d\alpha}\right\rangle_T\right)^2\right]_{\alpha=0} \tag{A.13}$$

where the notation $\langle ... \rangle_T$ indicates a thermal average. Since H is even in α, the average value of $dH(\alpha)/d\alpha$ in equation A.13 is equal to zero and only the first two terms contribute to the spin stiffness in equibibrium. Note that

$$\frac{dH(\alpha)}{d\alpha} = -\sum_{<i,j>} J_{ij}\vec{S}_i\frac{d\mathbf{R}}{d\alpha}\vec{S}_j \tag{A.14}$$

$$\frac{d^2 H(\alpha)}{d\alpha^2} = -\sum_{<i,j>} J_{ij}\vec{S}_i\frac{d^2\mathbf{R}}{d\alpha^2}\vec{S}_j. \tag{A.15}$$

Calculating the first and second derivatives of the rotation matrix $\mathbf{R}$ with respect to α in the limit $\alpha = 0$ yields

$$\frac{\partial\mathbf{R}}{\partial\alpha}|_{\alpha=0} = (\hat{e}_{ij}\cdot\hat{u})\begin{bmatrix} 0 & n_z & -n_y \\ -nz & 0 & n_x \\ n_y & -n_x & 0 \end{bmatrix} \tag{A.16}$$

and

$$\frac{d^2\mathbf{R}}{d\alpha^2}|_{\alpha=0} = (\hat{e}_{ij}\cdot\hat{u})^2 \begin{bmatrix} \frac{1}{2}(-1+n_x^2-n_y^2-n_z^2) & n_xn_y & n_xn_z \\ n_xn_y & -\frac{1}{2}(1+n_x^2-n_y^2+n_z^2) & n_yn_z \\ n_xn_z & n_yn_z & -\frac{1}{2}(1+n_x^2+n_y^2-n_z^2) \end{bmatrix} \tag{A.17}$$

These results can be used to write the following expression for the spin stiffness of the system when a virtual twist is imposed about an arbitrary direction $\hat{n}$ in spin space

$$\begin{aligned} \rho_{\hat{n}} = -\frac{1}{L^d}\sum_{<ij>} J_{ij}(\hat{e_{ij}}\cdot\hat{u})^2\langle S_{ix}[(n_x^2-1)S_{jx}+n_xn_yS_{jy}+n_xn_zS_{jz}]+ \\ S_{iy}[n_xn_yS_{jx}+(n_y^2-1)S_{jy}+n_yn_zS_{jz}]+ \\ S_{iz}[n_xn_zS_{jx}+n_yn_zS_{jy}+(n_z^2-1)S_{jz}]\rangle \\ -\frac{1}{TL^d}\langle(\sum_{<ij>} J_{ij}(\hat{e_{ij}}\cdot\hat{u})[S_{ix}(n_zS_{jy}-n_yS_{jz})+ \\ S_{iy}(-n_zS_{jx}+n_xS_{jz})+S_{iz}(n_yS_{jx}-n_xS_{jy})])^2\rangle \end{aligned} \tag{A.18}$$

which can also be expressed in the following compact form

$$\begin{aligned} \rho_{\hat{n}} = -\frac{1}{L^d}\sum_{i<j} J_{ij}(\hat{e}_{ij}\cdot\hat{u})^2\left\langle(\vec{S}_i\cdot\hat{n})(\vec{S}_j\cdot\hat{n})-\vec{S}_i\cdot\vec{S}_j\right\rangle \\ -\frac{1}{L^dT}\left\langle\left[\sum_{i<j} J_{ij}(\hat{e}_{ij}\cdot\hat{u})\hat{n}\cdot(\vec{S}_i\times\vec{S}_j)\right]^2\right\rangle. \end{aligned} \tag{A.19}$$

Appendix B

VORTICITY

The expression for the vorticity can be derived in much the same way as the spin stiffness. Instead of a virtual gradient $\hat{u}\Theta/L$ being imposed on the spin system with strength Θ/L, a virtual curl is imposed. Imposing a virtual curl on the system is the same as creating a virtual vortex. The axis of the curl (vortex) is again an arbitrary direction $\hat{n}$ in spin space and the components of the curl at the position of the spin $\vec{S}_j$ are $m\hat{\phi}_j/r_j$. The strength of the curl is measured in terms of the winding number m of the vortex and must be an integer. The unit vector $\hat{\phi}_j$ is tangent to the perpendicular line connecting the axis of the vortex and the position of the spin at site j and r_j is the distance of the spin from the axis of the vortex(see figure (2.6)).

The free energy cost of creating a virtual vortex is proportional to the square of the winding number

$$f' = f + \frac{1}{2}V_{\hat{n}} \ m^2 \tag{B.1}$$

The expression for the free energy f' is the same as for the twist in appendix A with the relative angle now given by $\theta_{ij} = m\hat{e_{ij}} \cdot \hat{\phi}_i/r_i$. Although the winding number m is discrete, we treat it as a continuous variable and take the second derivative with respect to m evaluated at $m = 0$. In reality, the vorticity is related to the finite difference $[f'(1) + f'(-1) - 2f'(0)]$ which is a measure of having a vortex ($m = \pm 1$) and not having a vortex ($m = 0$) but this reduces to the same final expression for the vorticity as the second derivative

$$V_{\hat{n}} = -\frac{1}{L^{d-2}}\frac{\sqrt{3}}{4\pi}\sum_{i<j} J_{ij}(\frac{\hat{e}_{ij}\cdot\hat{\phi}_i}{r_i})^2 \left\langle (\vec{S}_i\cdot\hat{n})(\vec{S}_j\cdot\hat{n}) - \vec{S}_i\cdot\vec{S}_j \right\rangle$$
$$- \frac{1}{L^{d-2}}\frac{\sqrt{3}}{4\pi}\left\langle \left[\sum_{i<j} J_{ij}(\frac{\hat{e}_{ij}\cdot\hat{\phi}_i}{r_i})\hat{n}\cdot(\vec{S}_i\times\vec{S}_j)\right]^2 \right\rangle \qquad \text{(B.2)}$$

The factor $\sqrt{3}/4\pi$ has been introduced as a normalization factor since it is convenient for comparing the vorticity with the stiffness. The sums in (B.2) diverge logarithmically with the system size and the vorticity can be written in the form

$$V_{\hat{n}} = C_{\hat{n}} + v_{\hat{n}} \ln L \qquad \text{(B.3)}$$

where $C_{\hat{n}}$ is a core term which should be independent of the system size and $v_{\hat{n}}$ is the vorticity modulus which plays a similar role to the stiffness.